UNIVERSITÉ DE MONTRÉAL

DEVELOPMENT OF SUBSTRATE INTEGRATED WAVEGUIDE FILTERS

YU TANG

DÉPARTEMENT DE GÉNIE ÉLECTRIQUE

ÉCOLE POLYTECHNIQUE DE MONTRÉAL

MÉMOIRE PRÉSENTÉ EN VUE DE L'OBTENTION

DU DIPLÔME DE MAÎTRISE ÉS SCIENCES APPLIQUÉES (M. Sc. A.)

(GÉNIE ÉLECTRIQUE)

AVRIL 2006

Your file Votre référence
ISBN: 978-0-494-19336-5
Our file Notre référence
ISBN: 978-0-494-19336-5

UNIVERSITÉ DE MONTRÉAL

ÉCOLE POLYTECHNIQUE DE MONTRÉAL

Ce mémoire intitulé:

DEVELOPMENT OF SUBSTRATE INTEGRATED WAVEGUIDE FILTERS

présenté par : TANG, Yu

en vue de l'obtention du diplôme de : Maîtrise ès sciences appliquées

a été dûment accepté par le jury d'examen constitué de :

M. Jean Conan, Ph. D., président

M. Wu Ke, Ph. D., membre et directeur de recherche

M. Christophe Caloz, Ph. D., membre

To my parents

To my Lord and Savior, Christ Jesus

ACKNOWLEDGEMENTS

I would like to express my gratitude to Dr. Ke Wu, for giving me the chance to pursue this master studying, for bringing me into this interesting and challenging field, as well as his support during the project research period.

I would like to give my thanks to Mr. Roch Brassard for his fabricating the circuits, Mr. René Archambault and Mr. Jean-Sabastien Décarie for their software support, and Mr. Marsan Eric for his support on measurement.

I would also like to thank Mr. Ping Yang, Dr. Dominic Deslandes, Mr. Xiaoma Jiang for helpful discussions and suggestions and to all the researchers at POLY-GRAMES.

A special thank is also extended to Dr. Thomas Sieverding and his company Mician for their generous trial supplying of the software u-Wave Wizard.

Finally I would like to express my gratitude to my Lord and personal Savior, Who gives me peace, strength and courage in frustration and difficulties. His love and salvation have comforted me always.

ABSTRACT

The purpose of the research project in this thesis is to design and develop substrate integrated waveguide (SIW) band-pass filters. A variety of design scenarios implementing filtering structure in H-plane can be integrated onto substrates. In this thesis, two design approaches are presented. The first approach is to develop the conventional direct-coupled cavity filters, which are synthesized and designed with Levy's method and numerical analysis based on mode matching of the waveguide's H-plane discontinuities. The second approach is to connect dual mode resonant cavities with apertures, whose coupling routings are based on the understanding of general synthesis theory, and the methods to produce transmission zeros in stopbands.

A procedure of making metallized grooves/slots or metallized via holes on dielectric substrates, then plating both top and bottom of the dielectric with metal is employed to form a structure similar to rectangular waveguide. Such a structure exhibits solid mechanical strength and can be conveniently fabricated with PCB processes. In the structure, rectangular waveguide modes without current in z direction on the narrow wall can propagate without obvious radiation loss when slots and via holes are arrayed with small distance. This structure supports all H_{m0} modes ($m = 1, 2, 3, \ldots$), and is called a substrate integrated waveguide (SIW).

The attenuation properties of a SIW guide with Roger RT/duroid and alumina coated with copper are investigated. The attenuation constant due to conductor loss

significantly decreases with the increasing substrate thickness. From a dielectric loss aspect, the loss tangent of the material plays a key role.

Three different discontinuities, working as coupling parts, are employed for direct-coupled cavity filter design. In order to determine the dimensions of the coupling parts, the mode matching technique was used. Numerical codes were developed based on Wexler's model so as to get the parameters of the T type equivalent circuit of the coupling parts.

Quarter-wave transformer prototype circuits and Levy's modified formula are used for the synthesis, which can be applied to filters with moderate band-width ($\geq$ 20%). Three filters are fabricated with Rogers RT/duroid 6002 for the direct-coupled cavity filter designs. The measurement results demonstrate a good agreement with the design theory. Tolerance analysis was done on one of the filters. The power flow of SIW guides of 10 mil thickness and filter pulse power capability are given.

Full-wave simulation is used for design of the dual mode filters. The frequency responses of a dual mode cavity in different mode combinations are investigated. The behaviors of two cascaded cavities in the H_{102} & H_{201}, H_{301} & H_{102} and H_{203} & H_{104} mode combinations, connected by aperture and coupled to the input/output port, are also studied. Tuning properties of the H_{203} & H_{104} mode combination in a single cavity with coupling apertures and an

input/output port are investigated in HFSS. If symmetrical couplings are required for the filter synthesis, one H_{203} & H_{104} cavity may supply one transmission zero (TZ) at a finite frequency. An asymmetrical coupling scenario has the potential to supply two TZs from one cavity.

A 2-cavity filter with two TZs and a 3-cavity filter with four TZs were synthesized based on the general synthesis theory and the properties of H_{203} & H_{104} resonance. Measurements on the 3-cavity filter integrated on 20 mil Rogers TMM3 demonstrate a 4.58 dB insertion loss at the center frequency, with a bandwidth of 760 MHz and better than 20 dB return loss in the passband. Measurements agree well with the simulation results.

RÉSUMÉ

Les tendances courantes dans le développement des circuits RF et micro-ondes, incluant les circuits à ondes millimétriques, sont orientées vers une intégration à faible coût et haute densité des composantes et de ces circuits. Ceci est surtout poussé par l'invention et le développement du concept des circuits à substrat intégré (substrate integrated circuits ou SIC), en particulier, le guide d'ondes à substrat intégré, ce qui permet la conception de guide d'ondes planaires qui normalement auraient été tridimensionnels. Ceci permet une intégration complète de circuits planaires et non planaires fait d'un seul substrat avec un simple procédé de fabrication.

Dans cette thèse, deux méthodes seront présentées pour la conception de filtres à guide d'ondes avec substrat intégré, et quatre pieces de filtres SIW avec différentes structures seront démontrées. Les filtres SIW sont intégrés sur du Rogers RT/duroid 6002 et un matériel laminé TMM3, qui opèrent en mode de résonance simple d'une cavité directement couplée et en mode de résonance double pour les cavités dégénérées, respectivement.

Cette dissertation comporte trois parties:

1. L'étude générale des propriétes du guide SIW
2. Conception de filtre SIW à cavité directement couplée en mode simple et fabrication sur substrat Rogers RT/duroid 6002
3. Conception de filtre SIW en mode double et fabrication sur substrat Rogers TMM3

CONDENSÉ EN FRANÇAIS

DÉVELOPPEMENT DE FILTRES EN GUIDES D'ONDES INTÉGRÉS AU SUSTRAT

0.1. Étude des propriétés des guides SIW

Basé sur le calcul des constants d'atténuation, l'influence des propriétés du substrat diélectrique RT/duroid 6002 et de l'alumine sur les pertes d'insertion du guide SIW est étudiée. Les facteurs de qualité Q_d et Q_c correspondant aux pertes diélectriques (α_d) et aux pertes par conductivité (α_c) pour la cavité SIW à demi-onde sont donnés. Donc, le facteur de qualité sans charge Q_u de la cavité SIW à demi-onde SIW pour intégration sur le RT/duroid 6002 et l'alumine sont démontrés. La relation de chaque facteur de qualité (Q_d, Q_c et Q_u) avec l'épaisseur de SIW et le facteur de dissipation diélectrique du substrat dans différentes conditions de recouvrement sont illustrés dans des diagrammes. Ces diagrammes donnent une ligne directrice dans la sélection du matériel pour la conception de composants/filtres SIW. Les calculs démontrent que, sous la même condition de recouvrement métallique, le facteur de dissipation diélectrique et l'épaisseur du substrat jouent des rôles importants pour déterminer les pertes d'un guide d'onde SIW d'une certaine longueur.

0.2. DISCONTINUITÉS INDUCTIVES ET MODÈLE D'ADAPTATION MODALE POUR LE COUPLAGE DE FILTRES

La première méthode de design emploie une synthèse conventionnelle du filtre à cavité couplée directement basée sur le prototype passe-bas à impédance distribuée par échelons. Les discontinuités inductives carrées sont employées en tant que parties de couplage des filtres.

La technique d'adaptation modale est employée pour la résolution des discontinuités du guide d'ondes. Afin de sauver du temps de programmation, le modèle de Wexler pour les discontinuités de type échelon est employée, ce qui procure la possibilité d'employer des parties de couplage de formes différentes. La symétrie des parties de couplage est utilisée afin d'obtenir les paramètres de circuit équivalent des parties de couplage en bande étroite, ce qui évite la recherche de la solution complète des discontinuités à double plan. En traitant les intégrales des équations linéaires du modèle de Wexler, les solutions analytiques sont disponibles pour les cas opérant en mode H_{10} d'un guide d'onde rectangulaire et la symétrie simplifie les termes de l'intégrale de manière considérable. Le code donne l'amplitude et la phase du coefficient de réflexion des parties de couplage de dimensions données. Inversement, le coefficient de réflexion requis peut être produit en choisissant les dimensions des parties de couplage. L'analyse numérique et le codage sont effectués à l'aide de l'environnement Matlab. La convergence des solutions est atteinte en obéissant la règle que le ratio du numéro de mode dans chaque guide d'onde est égal à la propagation de la section transversale des guides d'ondes.

Les inverseurs K sont calculés à partir de la procédure de synthèse de filtre avec la formule modifiée de Levy, qui peut être étendue au design de filtre à largeur de bande intermédiaire. Chaque inverseur K correspond à une valeur du coefficient de réflexion. L'amplitude et la phase du coefficient de réflexion d'une partie de couplage spécifique sont obtenues à l'aide des codes bases sur le modèle de Wexler pour l'adaptation modale. Il s'ensuit que, inversement, les dimensions de la partie de couplage carrée sont obtenues à l'aide de l'amplitude requise du coefficient de réflexion. Une partie de couplage de la cavité de filtre directement couplée procure un déphasage négatif du coefficient de réflexion, ce qui mène à une réduction de la longueur de la cavité. La valeur de la compensation de la phase de la cavité résonante due aux parties de couplage est aussi obtenue par la phase de réflexion calculée à partir de codes lors de l'étape de design de filtres.

La transition guide d'ondes à ligne microruban est employée dans ce projet. Une extension de la ligne micro ruban large du guide SIW avec impédance équivalente du guide SIW, définie par la relation puissance-courant dans HFSS, est employée pour agir en tant que pont entre le guide SIW et la ligne microruban 50 Ohm. Le pont entre le guide SIW et la ligne microruban peut être conçu en tant que défilement de la ligne micro ruban ou un transformateur à quart d'onde. Le premier offre une excellente fréquence en large bande. Le second démontre une perte d'insertion faible à la fréquence centrale de la bande étroite.

0.3. Filtres à substrat integré avec cavité directement couplée en cascade

En analyse de discontinuité, les résultats numériques pour des discontinuités bifurquées et à iris asymétrique démontrent une adaptation parfaite du point de vue

électrique et magnétique dans le voisinage des fonctions du guide d'ondes. Ces résultats valident le code. Dans le design de filtres, les paramètres structuraux obtenus de la synthèse de filtre sont optimisés à l'aide de l'environnement u-Wave Wizard. Les résultats d'optimisation sont confirmés à l'aide d'Ansoft HFSS.

Trois pièces de filtres à 4 cavités avec partie de couplage de formes différentes ont été conçus, construits et mesurés. Tous ont été réalisés à l'aide du matériel laminé micro-ondes Rogers RT/duroid 6002 de 10 mil. Ils ont une structure de filtre d'insertion métallique, à bifurcation symétrique large et à iris asymétrique, respectivement.

Le décalage de la fréquence centrale à 24.36 GHz, 24.32 GHz, 24.38 GHz respectivement, est dû à l'erreur de la permittivité relative. La permittivité relative actuelle du substrat laminé Rogers RT/duroid 6002 employé est de 2.86. Les comparaisons entre les résultats de simulation employant une telle valeur et les résultats des tests du filtre sont donnés. Les pertes d'insertion du filtre à 4 cavités avec iris asymétrique posé sur 10 mil de RT/duroid 6002 atteint 3.4 dB à la fréquence centrale de 24 GHz tout en gardant un affaiblissement de réflexion dans toute la bande passante meilleur que 17 dB. Aux fréquences centrales, les pertes d'insertion du filtre à insert métallique et du filtre large symétrique à bifurcation sont de 4.9 dB et 4.0 dB, respectivement.

L'analyse des tolerances est implantée pour le filtre à iris asymétrique. La largeur du mur du guide SIW, l'épaisseur de l'iris inductive en longueur et la largeur de l'iris dans la direction transversale furent devise avec une erreur de $\pm\Delta$. Les longueurs de la cavité résonante furent déviées en conséquence des épaisseurs changeantes des iris. Les nombres aléatoires distribués uniformément furent produits pour 20 combinaisons des dimensions des filtres. Les résultats démontrent que une

tolérance de fabrication de 0.4 mil peut assurer la performance requise du filtre du composant intégré sur le RT/duroid 6002. Les résultats des mesures sont en bon accord avec les résultats simulés dans la bande passante et la bande d'arrêt.

Les pertes d'insertion des filtres sont relativement hautes en raison du matériel à haute perte tangentielle du matériel employé. Ceci pourrait être amélioré en employant du matériel céramique à haute pureté dont la perte tangentielle est le dixième de celle du RT/duroid 6002. Augmenter l'épaisseur du substrat peut réduire la perte. Par contre, l'épaisseur supérieure à 20 mil peut détériorer la performance de la transition. Une raison peut être la radiation de la ligne micro ruban relativement large de la ligne de transmission 50 Ohm.

0.4. Couplages croisés, Résonance de guides d'onde en mode dual

La deuxième méthode de design, basé sur la résonance en mode dual de la cavité résonante rectangulaire dégénérée, emploie d'abord les apertures de couplage afin de cascader ces cavités ensemble. Les coefficients de couplage entre les modes peuvent être calculés. Ils sont une fonction de ses paramètres géométriques. Les dimensions requises de la structure de filtre proposée peuvent être obtenues par l'entremise d'approches conventionnelles. Deuxièmement, la compréhension de la théorie générale de la synthèse de filtres et la production de zéros de transmission (TZ) en filtres donnent une base à la construction d'un filtre.

Quelques exemples d'amélioration de sélectivité de filtres et de la production de TZ sont listés dans la documentation. Les deux modes d'opération, simple et double, sont couverts. Un exemple classique détaillé démontre la réalisation physique et la

manière de calculer les coefficients de couplage est incluse afin de bien comprendre les procédures de design. Il fut démontré que la forme générale des fonctions de transfert de la bande passante des réseaux symétriques peut être réalisés soit en cavités de guides d'ondes couplés en mode simple ou en mode double.

M. Guglielmi propose une nouvelle famille de scénarios en mode double entièrement inductifs, ou la nouveauté apportée est que chaque cavité de la structure produit deux pôles de transmission et au moins un zéro de transmission et le couplage entièrement inductif de l'entre-cavité permet l'implantation de filtres simples planaires en mode dual sur le substrat. Le mécanisme de résonance en mode dual et la condition contraignante sont décrits.

Afin d'éviter les procédés compliqués pour obtenir la représentation des paramètres de réseau de la jonction du guide d'ondes à double plan formé par les apertures, la simulation électromagnétique (EM) à onde pleine est employé pour la conception, après l'étude des propriétés de chaque cavité en mode dual dans une combinaison de modes spécifiques. Chaque cavité en mode dual exhibe une réponse fréquentielle sous la condition d'une injection d'onde à travers l'aperture connectée au port d'entrée et l'aperture asymétrique au port de sortie. Les combinaisons en mode dual telles que H_{102} & H_{201}, H_{102} & H_{301} et H_{203} & H_{104} qui exhibent deux pôles résonants dans la bande passant et des TZ(s) dans la bande d'arrêt sont démontrés.

Quand deux cavités à mode dual sont combinées, on s'attend à ce qu'ils produisent deux zéros de transmission. Lorsque deux cavités sont reliées à travers une aperture, les valeurs des coefficients de couplage pour un filtre à cavité directement couplé peut être référencé afin de décider des dimensions de l'ouverture. Puisque les coefficients de couplage inter-cavité au milieu sont habituellement plus petits à

comparer à ceux entre la cavité et l'entrée/sortie du guide d'ondes, la longueur de l'ouverture au milieu est plus longue afin de produire un plus petit couplage. Par opposition, l'entrée/sortie de l'aperture de couplage est petite de manière à procurer de plus larges coefficients de couplage. Les performances obtenues en cascadant deux cavités H_{102} & H_{201}, deux cavités H_{301} & H_{102} et deux cavités H_{203} & H_{104} sont démontrées, respectivement.

Afin d'employer la combinaison H_{203} & H_{104} pour construire le filtre, les propriétés d'ajustement d'une cavité simple H_{203} & H_{104} sont étudiés avec attention et illustrés aux figures. a). Lorsque la largeur et la longueur de la cavité est proprement ajustée, le mode de résonance dual peut être maintenu. Le ratio de la longueur de la cavité à sa largeur est $l/a \approx 1.53$; c'est la clé pour maintenir la réponse mode dual. b). Plus l'aperture est épaisse, plus l'onde se dégrade. Il s'ensuit que le couplage devient faible lorsque l'épaisseur est augmentée. Deux pôles résonants peuvent être séparés davantage lorsque le couplage s'affaiblit avec une épaisseur d'aperture croissante. Ceci peut alimenter un mécanisme afin d'ajuster la largeur de bande de la cavité résonante. c). La réponse fréquentielle de la cavité simple H_{203} & H_{104} cavity est sensible à l'influence de la largeur d'aperture. Les deux pôles se séparent davantage lorsque la largeur de l'aperture augmente, produisant ainsi un mécanisme efficace pour contrôler la largeur de bande. d). Des ports entrée/sortie plus larges changent aussi le pôle résonant. Ceci permet au mécanisme de changer la largeur de bande et le facteur de qualité Q. Par contre, la tendance du changement est dans la direction opposée de celle qui survient lors du changement de la largeur de l'aperture. Des dimensions optimales doivent exister lorsque la largeur de l'aperture et la largeur du port sont changées simultanément.

En un mot, toutes les dimensions structurales telles que la **longueur de la cavité**, **la largeur de la cavité**, **l'épaisseur de l'aperture**, **la largeur de** l'**aperture**

et **la largeur de l'entrée/sortie du guide d'ondes** de la cavité H_{203} & H_{104} peuvent être employées afin d'ajuster les lieux résonants, le déplacement des deux pôles, le facteur de qualité Q de la cavité et la largeur de bande.

0.5. Filtres SIW à mode dual basés sur la résonance H_{203} & H_{104}

Basé sur les simulations EM à onde pleine et les propriétés d'ajustement des cavités H_{203} & H_{104}, les configurations des filtres à deux et trois cavités furent construits. Les structures à deux cavités et trois cavités procurent deux ZT et quatre ZT respectivement, puisque les filtres sont géométriquement symétriques avec un offset symétrique de l'ouverture. Les scénarios de couplage des configurations de filtres à 2-cavités et 3-cavités employant la résonance H_{203} & H_{104} sont expliqués par des diagrammes.

Un filtre à 3-cavités de 6-pôles et 4-TZs basé sur la résonance H_{203} & H_{104} et intégré sur du Rogers TMM3 20 mil est optimisé, fabriqué et mesuré. Les pertes d'insertion de la bande passante ont atteint 4.58 dB à la fréquence centrale et 5.3 dB à ses extrémités, tandis que l'affaiblissement de réflexion fut meilleur que 20 dB sur l'entité de la bande passante. La perte de rejet à la basse fréquence de 22 GHz dans la bande d'arrêt est de -65 dB, ce qui est 20 dB plus grand que la valeur simulée. La perte de rejet à 25 GHz dans la partie supérieure de la bande d'arrêt est de -65 dB. La largeur de bande est de 760 MHz. Les résultats des mesures et des simulations sont comparés. Les tests concordent bien avec la théorie de conception.

En résumé, deux méthodes de conception furent employées dans ce projet. Il y a plusieurs méthodes pour le design de guides d'ondes à cavité qui peuvent être employées à cette fin. Quelques structures de guides d'ondes de filtrage, par exemple

ceux de [10] dans le Chapitre 3 et ceux de [17] dans le Chapitre 5, qui ont des changements en deux dimensions dans le plan-H et sont opérés en mode H_{n0} (n = 1, 2, 3, ...) peuvent être adoptés pour l'intégration et le développement de filtres SIW.

Le développement est surtout limité au procédé de fabrication. Dans le cas de substrats minces tels ceux de 10 mil et 20 mil, une tolérance de fabrication de 0.4 mil sur un substrat à faible permittivité diélectrique tel le RT/duroid 6002 peut rencontrer la condition de filtrage. Les SIW sur substrats plus épais sont attendus en raison de leur Q élevé (faibles pertes d'insertion). Malgré ceci, une nouvelle transition en design qui règle le problème de radiation de la transition guide d'ondes - microruban devrait être adoptée. Dans cette situation, le nombre de cavités peut aussi accroître en vue d'améliorer la performance du filtre.

TABLE OF CONTENTS

LIST OF FIGURES

LIST OF TABLES

LIST OF SIGNS AND ABBREVIATIONS

IL	Insertion Loss
RL	Return Loss
SIW	Substrate Integrated Waveguide
TZ	Transmission Zero
ε_r	Relative Permittivity
$\tan\delta_l$	Loss Tangent
σ	Conductivtity
Q_c	Quality Factor due to Conductor Loss
Q_d	Quality Factor due to Dielectric Loss
Q_u	Unloaded Quality Factor
$K_{r,r+1}$	K Inverter of Filter
$(S_{11})_{r-1,r}$	Reflection Coefficient of Coupling Part
ε_{re}	Effective Relative Permittivity
P_{qk}	Power Flow of SIW
$(P_{qk})_0$	Power Capacity of Filter
M_{ij}	Element of Coupling Matrix

Chapter 1 FUNDAMENTALS OF FILTERS AND SIW TECHNIQUE

1.1 Basic Concepts and Filter Theory

RF/microwave filters as well as filter components can be represented by two-port network. The synthesis of such two-port networks with filtering function of prescribed insertion loss characteristics was first given by S. Darlington [1]. Before the insertion loss theory was proposed, the image parameter theory was developed. However, many filters have been designed and developed on the basis of the insertion loss theory since then [2, 3, 4].

The transfer function of two-port filter is a mathematical description of the network response characteristics, which is simply a mathematical expression of $S_{21}(\omega)$. In many cases, an amplitude-squared transfer function for a lossless passive filter network is defined as

$$|S_{21}(j\omega)|^2 = \frac{1}{1+\varepsilon^2 F_n^2(\omega)} \tag{1.1.1}$$

where ε is the ripple constant, $F_n(\omega)$ represents a filtering or characteristic function, and ω is the angular frequency.

For a linear, time-invariant network, the transfer function may be defined as a rational function,

$$S_{21}(p) = \frac{N(p)}{D(p)} \tag{1.1.2}$$

where $N(p)$ and $D(p)$ are polynomials in terms of a complex frequency variable $p=\sigma+j\omega$. For a lossless passive network, the **neper** frequency $\delta=0$ and $p=j\omega$. Finding a realizable rational transfer function that produces response characteristics approximating the required response is the starting point of a filter synthesis. In many cases, the rational transfer function of (1.1.2) can be constructed from the amplitude-squared transfer function of (1.1.1).

Function $F_n(\omega)$ allows classifying filters into three main categories: 1. Butterworth response; 2. Chebyshev response; and 3. Elliptic response.

The conventional waveguide filters have the advantages of low loss and high quality factor etc. Most of them need tuning screws to adjust the frequency response to the designed specifications. Filters can also be realized with conventional planar structure, such as microstrip, strip line and CPW etc. However, when frequencies go up to the higher end in the microwave spectrum, especially in millimeter-wave range, the conventional structures cannot realize the required filtering function due to the radiation of the open or semi-open system. Furthermore, even at lower frequencies, both loss and power handling capability present a problem for designing a high performance filter.

The substrate integrated waveguide (SIW) technique was proposed [5] to realize a variety of waveguide/rectangular cavities in thin dielectric substrate, which have the following features:

1. Because the relative permittivity is larger than 1, the wavelength shrinks in the dielectric. The component size can be much smaller if integrated on a relative high permittivity dielectric substrate.

2. The loss tangent of the dielectric plays a key role in the component insertion loss.

3. Thin substrates may result in high conductivity loss due to the metal wall.

1.2 Why SIW Is Employed and What Is SIW?

Conventional waveguide filters are with high cost, heavy weighed, hard to fabricate and they need tuning. But they have small loss (high Q). Conventional planar filters realized with microstrip, strip-line and CPW, due to their open structure, are with high loss, and hard to fabricate when frequency goes higher and up to millimeter wave range.

To integrate waveguide structure on dielectric substrate can be implemented by coating the top and bottom of the substrate while replacing the side wall with metalized via holes or slots. Such kind of structure supports all TM mode in which there is no current of z direction on the side wall. When the distance of via holes, or the gap due to cutting slots are small, radiation is very small and the performance of such structure is exactly the same as dielectric-filled waveguide.

SIW technique supplies a method to fabricate filters with ordinary PCB process. So it is in low cost, light weight, small size, easy to integrate with other planar circuit and it does not need tuning.

1.3 Properties of Substrate Integrated Waveguide

In the following, attenuations and **influence of the SIW length** on the insertion loss of SIW guide are analyzed.

If the surface roughness is ignored, the loss results from two mechanisms, namely imperfect conductor wall and dielectric loss.

The attenuation constants due to conductor and dielectric losses in rectangular waveguide, respectively, are [6]

$$\alpha_c = \frac{2R_m}{bZ_0'\left(1-k_c^2/k_0'^2\right)^{1/2}}\left[\left(1+\frac{b}{a}\right)\frac{k_c^2}{k_0'^2}+\frac{b}{a}\left(\frac{1}{2}-\frac{k_c^2}{k_0'^2}\right)\left(\frac{ab}{a^2+b^2}\right)\right] \tag{1.3.1}$$

$$\alpha_d = \frac{k_0'^2 \tan\delta_l}{2\beta_{10}'} \tag{1.3.2}$$

where $R_m = (\omega\mu/2\delta)^{1/2}$ is the surface resistance, δ is the skin depth, $k_0 = k_0\sqrt{\varepsilon_r}$ is the wave number in the dielectric, $k_c = \frac{\pi}{a}$ is the cut-off wave number, β_{10} is the phase constant, $Z_0 = \sqrt{\frac{\mu}{\varepsilon}} = \sqrt{\frac{\mu_0}{\varepsilon_0}} / \sqrt{\varepsilon_r}$ is the intrinsic wave impedance of the dielectric medium, ε_r is the relative permittivity of dielectric material, $\tan\delta_l$ is the loss tangent, a and b are SIW width and thickness (height), respectively. The units of α_c in (1.3.1) and α_d in (1.3.2) are nepers.

The insertion loss IL of an SIW waveguide of length L is,

$$IL = 10\log_{10}\frac{P}{P_0} = -8.69\alpha_L L \text{ (dB)} \tag{1.3.3}$$

where $P = P_0 e^{-2\alpha_L z}$, $\alpha_L = \alpha_c + \alpha_d$ and $P_0 = P|_{z=0}$. Here z is the direction of wave propagation, and L the length of the SIW guide.

Since losses on the wall of coupling components in the filter are not considered, equations (1.3.1), (1.3.2) and (1.3.3) give the minimum loss of the SIW filter of length L, which can be an approximation for our purpose. Since the waveguide cavities are formed by inserting coupling parts in SIW, there are more conducting walls for surface current flowing, on which **loss integration should be carried out**. Furthermore, the current distribution in a filter resonant cavity is quite different from that of a dielectric filled transmission waveguide (SIW). For the above reasons, the exact computation of the loss is much more complicated, which needs a solution to the field distribution, and integration on the waveguide wall of each cavity.

Equations (1.3.1) and (1.3.2) yield a good perspective viewing on the comparison of conductive loss and dielectric loss in an SIW waveguide. Table 1.3.1 lists the values of losses due to the two kinds of mechanism in a dielectric ($\varepsilon_r = \varepsilon_r' - j\varepsilon_r'' = \varepsilon_r'(1 - j\tan\delta_l) = 2.94(1 - j0.0012)$, $\tan\delta_l = 0.0012$) filled copper

(conductivity $\sigma = 5.8\times10^7$ S/m) waveguide of width of a=252 mil working at f=24GHz. We may see that the conductor loss decreases with the increase in waveguide height b. The values for unloaded quality factor $Q_u = \frac{\beta}{2(\alpha_c + \alpha_d)} = \frac{Q_c Q_d}{(Q_c + Q_d)}$ of the half wavelength cavity of a given waveguide width (a=252 mil) are also shown. Here, $Q_c = \frac{\beta}{2\alpha_c}$ and $Q_d = \frac{\beta}{2\alpha_d}$. The relationship of the quality factors with substrate thickness, and with tangent loss are shown in Fig. 1.3.1- Fig. 1.3.4.

The design point of the SIW guide in this project is in the first column of Table. 1.3.1, where the unloaded Q is 289. If 10 mil thick ceramic is used, the unloaded Q may increase to 524. This may be seen in Table 1.3.2.

Increasing the thickness of substrate may decrease the conductive loss which results in increase of unloaded Q. This may be seen in Table 1.3.1 and 1.3.2.

Table 1.3.1 Attenuations of H_{10} mode in a RT/duroid 6002 SIW & Q of half-wave cavity

thickness of SIW dielectric b (mil)	10	20	30	60
dielectric attenuation constant $\alpha_d\,(neper/m)$	0.6291	0.6291	0.6291	0.6291
conductive attenuation constant $\alpha_c\,(neper/m)$	0.5945	0.3093	0.2145	0.1207
total attenuation constant $\alpha_L\,(neper/m)$	1.224	0.9384	0.8436	0.7498
Quality factor Q_c	595.9	1145	1651	2935
Quality factor Q_d	563.0	563.0	563.0	563.0
unloaded cavity Q_u	289.5	377.5	419.9	472.4

$f_0 = 24GHz$, $a = 252mil = 6.4mm$, $\varepsilon_r = 2.94$, $\lambda_0' = \lambda_0/\sqrt{\varepsilon_r} = 7.29mm$,

$\lambda_g' = \lambda_0'/\sqrt{1-(\frac{\lambda_0'}{2a})^2} = 8.87mm$, $\beta_{10}' = 708.47 \quad rad/M$

$\varepsilon_r = \varepsilon_r'(1 - j\tan\delta_l) = 2.94(1 - j0.0012)$, $\sigma = 5.8\times10^7 S/M$

Table 1.3.2 Attenuations of H_{10} mode in a ceramic-filled SIW & Q of half-wave cavity

thickness of SIW dielectric b (mil)	10	20	30	60
dielectric attenuation constant $\alpha_d\,(neper/m)$	0.0963	0.0963	0.0963	0.0963
conductive attenuation constant $\alpha_c\,(neper/m)$	1.134	0.6099	0.4369	0.2678
total attenuation constant $\alpha_L\,(neper/m)$	1.230	0.7062	0.5332	0.3641
Quality factor Q_c	568.9	1058	1477	2409
Quality factor Q_d	6699	6699	6699	6699
unloaded cavity Q_u	524.5	913.5	1210	1772

$f_0 = 24GHz$, $a = 137mil = 3.48mm$, $\varepsilon_r = 9.9$, $\lambda_0' = \lambda_0/\sqrt{\varepsilon_r} = 3.97mm$,

$\lambda_g' = \lambda_0'/\sqrt{1-(\frac{\lambda_0'}{2a})^2} = 4.83mm$, β_{10}=1290.2 rad/M,

$\varepsilon_r' = \varepsilon_r'(1-j\tan\delta_l) = 9.9(1-j0.0001)$, $\sigma = 5.8\times10^7\,S/M$

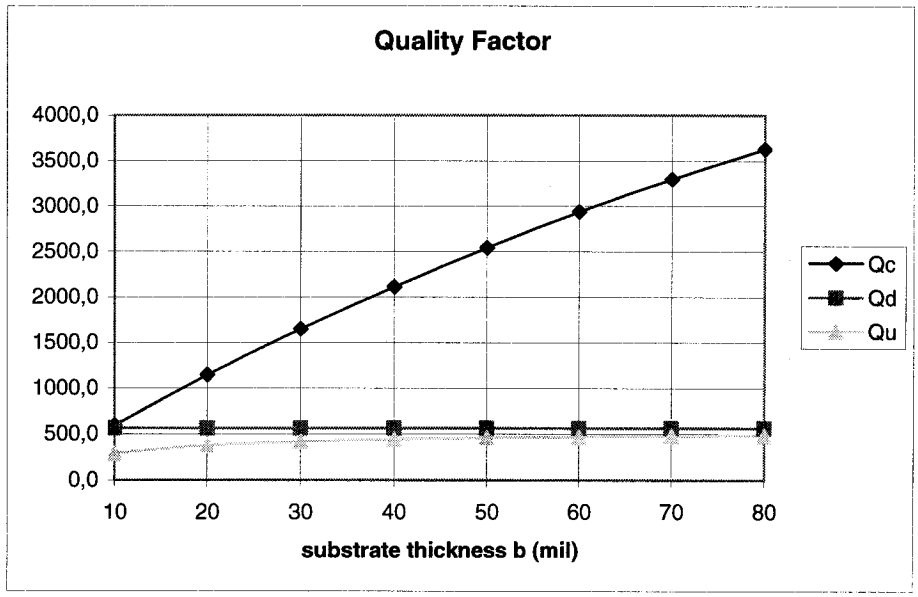

Fig 1.3.1 Quality factors versus b: a=252 mil, $\varepsilon_r = 2.94(1-j0.0012)$, $\sigma = 5.8\times10^7\,S/M$

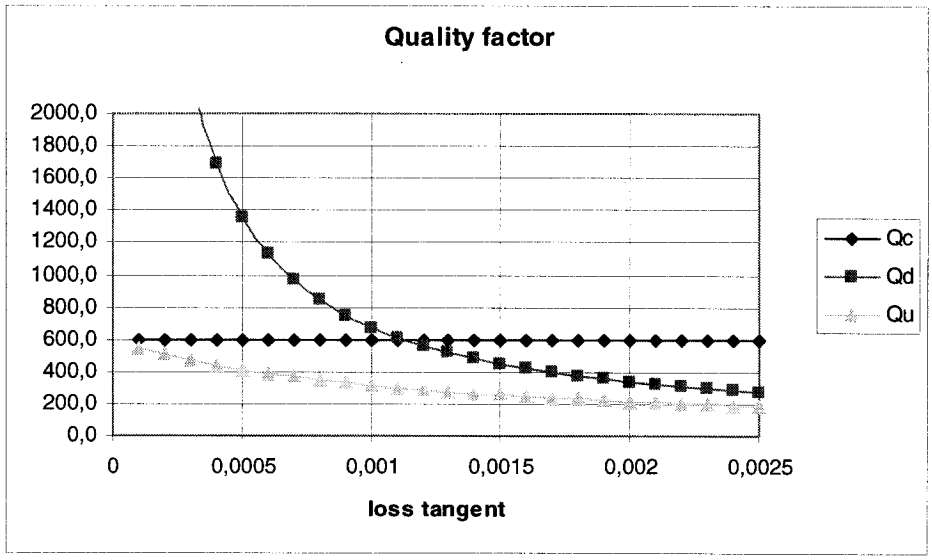

Fig 1.3.2 Quality factors versus $\tan\delta_l$: a=252 mil, b=10 mil, $\varepsilon_r = 2.94$, $\sigma = 5.8\times10^7 S/M$

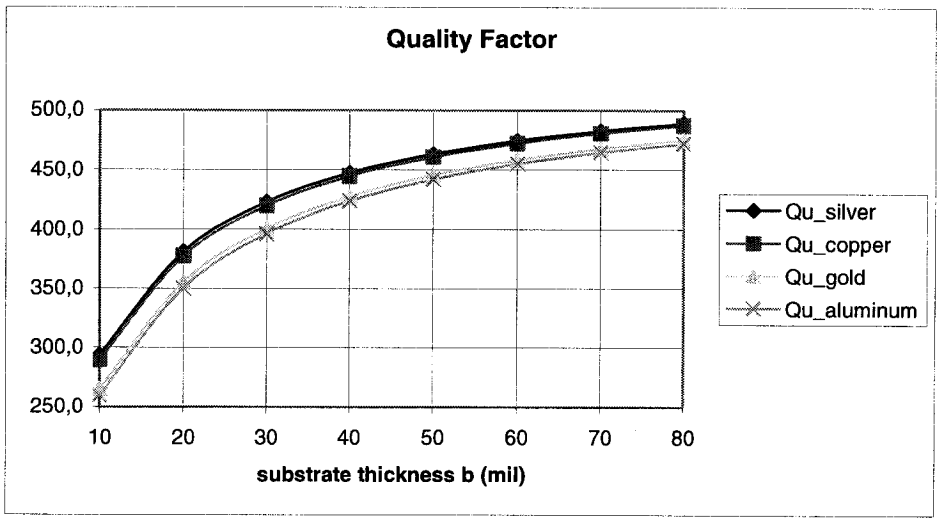

Fig. 1.3.3 Unloaded Q versus substrate thickness b: a=252 mil,

$\varepsilon_r = 2.94(1 - j0.0012)$

$\sigma_{silver} = 6.14\times10^7 \quad S/M, \sigma_{copper} = 5.8\times10^7 \quad S/M, \sigma_{gold} = 4.1\times10^7 \quad S/M,$

$\sigma_{aluminum} = 3.8\times10^7 \quad S/M$

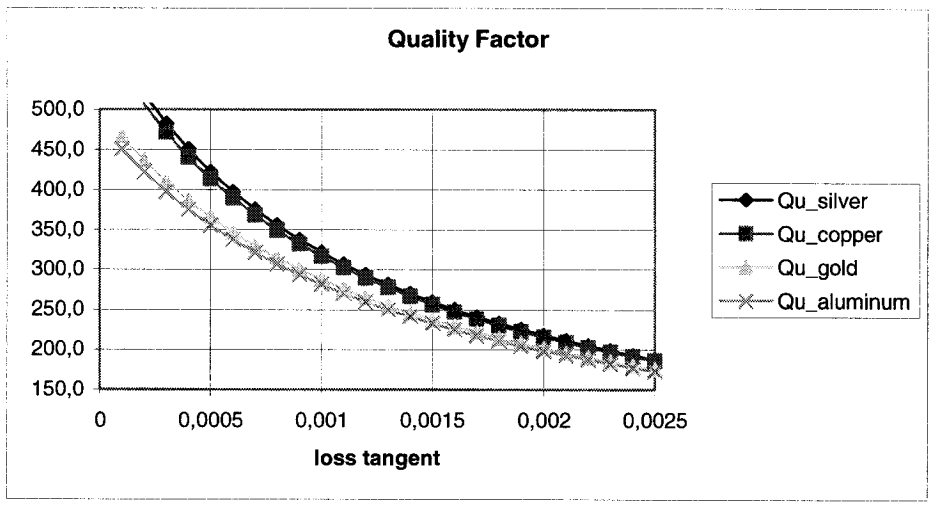

Fig. 1.3.4 Unloaded Q versus $\tan\delta_l$: a=252 mil, b=10 mil, $\varepsilon_r = 2.94$

$\sigma_{silver} = 6.14\times10^7 \quad S/M, \sigma_{copper} = 5.8\times10^7 \quad S/M, \sigma_{gold} = 4.1\times10^7 \quad S/M,$

$\sigma_{aluminum} = 3.8\times10^7 \quad S/M$

REFERENCES

[1] S. Darlington, "Synthesis of reactance four poles which produce prescribed insertion loss characteristics," J. Math. Phys., vol. 18, pp. 257-353, Sept. 1939.

[2] G. L. Matthaei, L. Young and E. M. T. Jones, Microwave filters, impedance-matching networks, and coupling structures, McGraw-Hill Book Company, New York

[3] R. Levy, "Theory of direct-coupled-cavity filters," IEEE Trans. Microwave Theory Tech., vol. MTT-15, pp. 340-348, June. 1967.

[4] J. D. Rhodes, "Design formulas for stepped impedance distributed and digital wave maximally flat and Chebyshev low-pass prototype filters," IEEE Trans. Circuits Syst., vol CAS-22, pp. 866-874, Nov. 1975

[5] Ku Wu, D. Deslandes, Y. Cassivi, Telecommunications in Modern Satellite, Cable and Broadcasting Service, 2003, TELSIKS, 6th International Conference on, Volume 1, 1-3 Oct. 2003 Page(s) : P-III-P-X vol.1

[6] R. E. Collin, Field Theory of Guided Waves. IEEE Press, New York, 1991

Chapter 2 INDUCTIVE DISCONTINUITIES AND MODE MATCHING MODEL FOR FILTER COUPLING

2.1 Introduction

The design theory for various types of microwave band-pass filters are described in Chapers 8, 9, 10 and 11 of G. L. Matthaei, L. Young and E. M. T. Jones' book [1]. The design procedure which employs a design point of view with narrow-band approximations is given in Chapter 8. This approach is only useful to designs having fractional bandwidth of typically around 20% or less. The design procedure which makes use of step transformers as a prototype for the filters is given in Chapter 9, an approach which can be used in the design of band-pass filters of moderate bandwidth. The design procedures in Chapter 10 deal with either narrow- or wide-bandwidth designs since their method fixes various filter parameters at both band-edge and mid-band frequencies.

With respect to waveguide band-pass filters, utilizing a low-pass prototype, the design principles and procedure are given in Sections 8.02, 8.03, 8.04 and 8.06 of [1]. In the generalized equations used for the design of such filters, the impedance (K) or inductance (J) inverters represent the couplings while the half wavelength resonant cavities are series or cascaded in a line. The shunt inductive discontinuities of a waveguide are employed in the configuration to represent the coupling part. The capacitive discontinuities of the waveguide are not applied to this 2-dimensional H-plane problem.

From an electromagnetic field perspective, the K or J inverter of the waveguide filter can be physically realized by either electric coupling or magnetic coupling between the resonant cavities.

Substrate integrated waveguide (SIW) filters have two main features that distinguish them from conventional waveguide filters.

1. They are realized on dielectric substrates, i.e. the filtering response is obtained via dielectric-filled waveguides or similar structures. Due to the presence of the dielectric, the dielectric loss ($\tan\delta$) is brought about;

2. They are fabricated in thin substrates. In practical applications, they need to couple with other planar components.

2.2 Some Inductive Discontinuities

A couple of discontinuities are commonly used to perform the role of K (or J) inverters between cavities for design purposes. The simplest one is an inductive post in the waveguide. Such a discontinuity was calculated by a few authors [2, 3, 4]. The application of such a discontinuity to an SIW filter design has been done in a prototype filter [5]. A symmetric iris, an asymmetric iris and a bifurcation are shown in (a), (b) and (c) of Fig. 2.2.1.

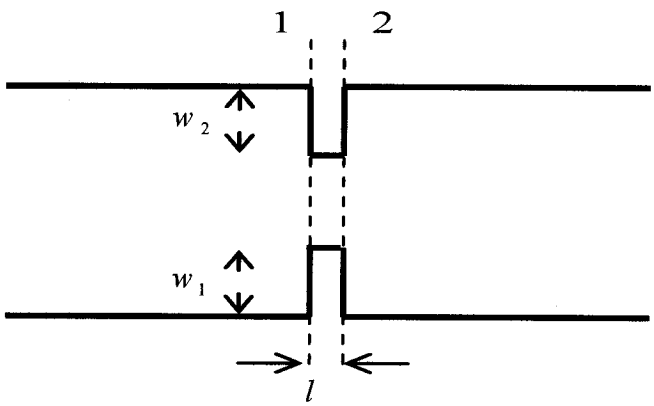

$w_1 \neq 0, w_2 \neq 0, w_1 = w_2$ *or* $w_1 \neq w_2$

(a) Iris

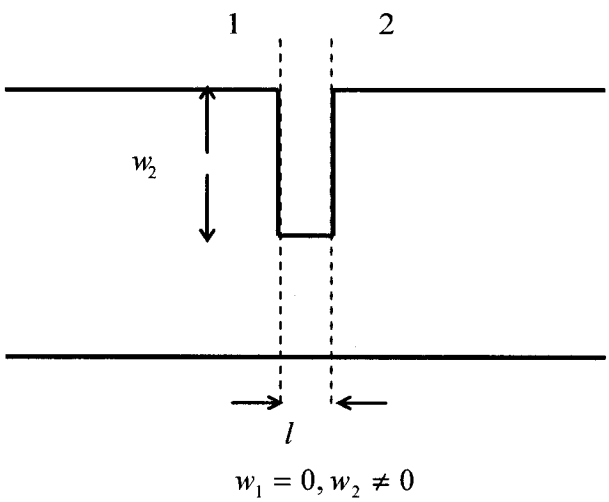

(b) Asymmetric iris

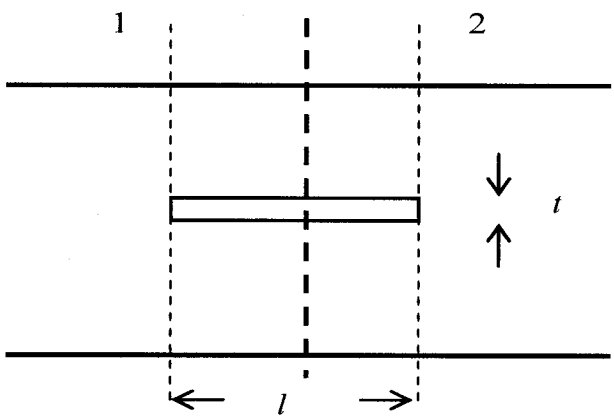

(c) Centrally located bifurcation (axial strip)

Fig.2.2.1: Top views: a couple of inductive discontinuities employed as planar filter coupling parts

2.3 General Description of Mode Matching Technique for solving discontinuities

The mode matching method is widely used for solving waveguide discontinuity problems [6, 7, 8, 9]. With regards to the discontinuity types in Fig. 2.2.1, the efforts are made in seeking the solutions for the step-type waveguide discontinuity (junction) and the waveguide bifurcation.

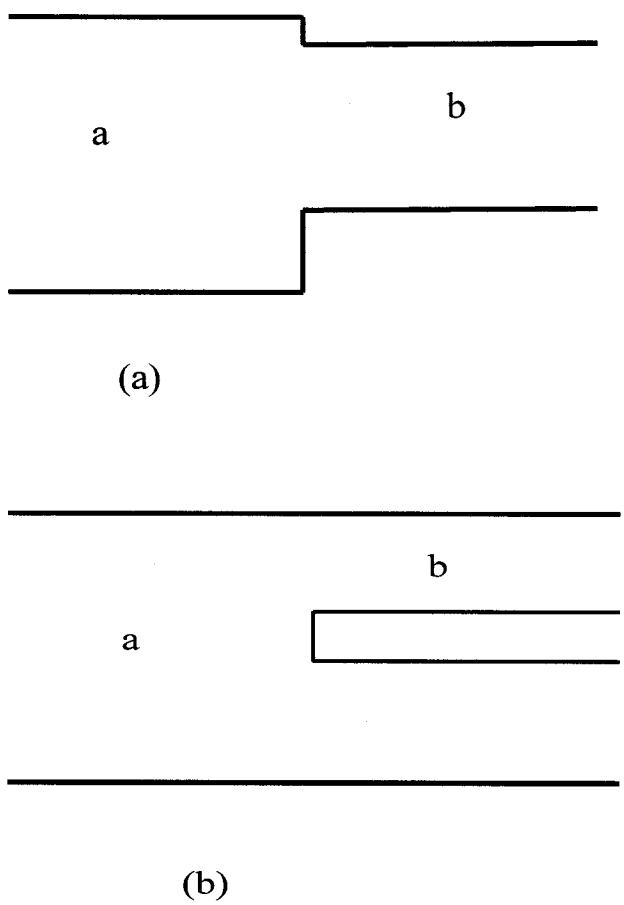

Fig. 2.3.1: (a) single waveguide step and (b) waveguide bifurcation

A single waveguide step discontinuity and an infinitely long waveguide bifurcation are shown in Fig. 2.3.1. Let us suppose that an incident H_{10} wave is injected from the left into waveguide a. Forward- and backward-scattering occur at the discontinuity. To satisfy the boundary conditions, higher modes are produced in the vicinity of the discontinuity. The scattering matrix representation of a waveguide with a single step or bifurcation shown in Fig. 2.3.1 can be obtained by a mode matching technique. In practical applications, if the wave becomes cutoff in waveguide b and the length of guide b is more than a few times the wavelength, the incident H_{10} wave is completely reflected.

In Fig. 2.2.1, since the irises are of finite thickness and the bifurcation is of finite length, they are actually two discontinuities combined together, called double-plane steps [9]. In the situation, the wave interaction between the two steps (junctions) has to be taken into account. In the situation of single mode propagation, the incident H_{10} wave from the left is scattered at junction 1. A fraction of the incident wave is reflected back to the input port on the left and some fraction is transmitted over the junction. Hence, the solution to the configuration in Fig. 2.2.1 requires more complicated calculations. When the waveguide junction and the waveguide portion between junctions 1 and 2 are represented by a scattering matrix (ABCD matrix) the overall scattering matrix can be represented as the multiplicity of three ABCD matrices as described in [8, 9]. Facing the same discontinuity, the calculation of thick rectangular windows with modal analysis was done previously in [10]. In applying inductive discontinuities to filter design, a new method for controlling the location of zero transmission was also proposed in [11].

In this project, the Wexler model [7] was adopted for calculating the discontinuities. Instead of calculating the scattering parameters of the discontinuities, the equivalent circuit for the double-plane discontinuities at the band-pass filter central frequency is obtained by making use of the symmetry in Fig. 2.2.1(a), (b) and (c). This will be described in detail in Section 2.4.

The obvious advantage in using the Wexler Model is that the geometry of the discontinuity can be changed so as to easily obtain the T-shape equivalent circuit description for a couple of different continuities (coupling parts) by modifying the computer code slightly. This reduces the computational work and can be done easily.

2.4 Wexler Model for Double-plane Step-type Discontinuities

2.4.1 Wexler Model

The discontinuity in Fig. 2.3.1(a) belongs to a general form which consists of two uniform cylindrical waveguides having different cross sections and distributions of enclosed electrical properties. The rectangular waveguide is one of the specific situations to form such a junction. The junction can be described as a function of two transverse coordinates u_1 and u_2. Boundary conditions, the continuity of transverse fields through all the apertures and a zero tangential electric field at the conducting surface, all are satisfied by a suitable infinite series of modes that are appropriate to each side of the junction. If the modes of propagation in both guides and the scattering coefficients of succeeding discontinuities are known, the properties of the junction may be computed. The problem is to find how power is apportioned between the various scattered modes.

A more general situation than those configurations in Fig. 2.2.1, is sketched in Fig. 2.4.1 where the system consists of three dissimilar guides a, b and c. The junctions are noted as 1 and 2 in the figure.

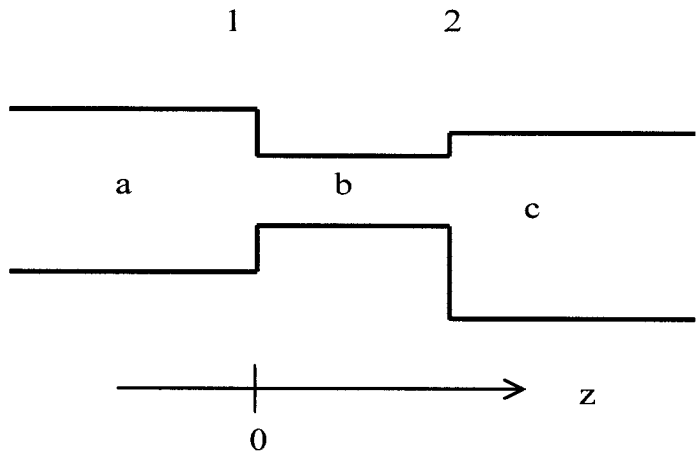

Fig. 2.4.1: General waveguide double-plane steps

When a mode $i=1$ with mode coefficient a_1 is emitting from a matched source in a and encountering waveguide b at $z=0$, those for the back-scattered modes are a_2, a_3, ..., a_i, ..., and ρa_1 is the reflected. Taking $\bar{E}$ to be the total transverse electric-field vector function within the aperture at the discontinuity, the field expanded in terms of modes just to the left of junction 1 is

$$\bar{E} = (1+\rho)a_1\bar{e}_{a1} + \sum_{i=2}^{\infty} a_i\bar{e}_{ai} \tag{2.4.1}$$

Subscript a denotes quantities relative to the first waveguide. Similarly, the total magnetic field can be expressed by

$$\bar{H} = (1-\rho)a_1\bar{h}_{a1} - \sum_{i=2}^{\infty} a_i\bar{h}_{ai} \tag{2.4.2}$$

The aperture fields at $z=0$ in Fig. 2.4.1 can be expressed in terms of the modes in b. If waveguide b is matched, the transverse electric-field pattern of mode j is given by $b_j\bar{e}_{bj}$. Each transmitted evanescent or propagating mode j reaching junction 2 partially

reflects and scatters power into other modes k with some of the modes returning to junction 1 . Therefore, it is necessary to account for these returned waves, as well as for the positively directed ones, when summing modes.

In waveguide b, scattering coefficients are used to relate the amplitudes and phases of modes transmitted past junction 1 to those reflected from junction 2. Consider waveguide b to be excited from junction 1 by a single forward wave j whose amplitude is unity, i.e. $b_j = 1$ at junction 1 . Then scattering coefficients s_{jk} are defined as being equal to mode coefficients b_k of the k back-scattered waves, transformed in amplitude and phase to junction 1 from 2. This is repeated for all j. Obviously, junction 2 must be solved before junction 1 .

Multiplying b_j by s_{jk} gives the contribution of j to k as seen at junction 1 . Because each forward-propagating mode j has an infinity of back-scattered modes k of the form $s_{jk} b_j \vec{e}_{bk}$ associated with it, the total transverse electric and magnetic fields just to the right of junction 1 are found as a result of the summation over all j and k. This gives

$$\vec{E} = \sum_{j=1}^{\infty} b_j (\vec{e}_{bj} + \sum_{k=1}^{\infty} s_{jk} \vec{e}_{bk}) \tag{2.4.3}$$

$$\vec{H} = \sum_{j=1}^{\infty} b_j (\vec{h}_{bj} - \sum_{k=1}^{\infty} s_{jk} \vec{e}_{bk}) \tag{2.4.4}$$

The boundary conditions are: 1. transverse electric and magnetic fields must be continuous across the aperture, and 2. the electric field tangential to the conducting wall must vanish.

After taking cross product of (2.4.1) and (2.4.3) with $\vec{h}_{am}$, and taking cross product of (2.4.2) and (2.4.4) with $\vec{e}_{bn}$, then using orthogonality, normalization and continuity condition for non-degenerate modes, the issue becomes solving the following linear equations [7],

$$\rho \int_b \vec{e}_{bn} \times \vec{h}_{a1} \cdot \vec{u}_z ds + \sum_{j=1}^{N} \frac{b_j}{a_1} \sum_{i=2}^{M} \frac{\int_b \vec{e}_{bn} \times \vec{h}_{a1} \cdot \vec{u}_z ds + \sum_{k=1}^{N} s_{jk} \int_b \vec{e}_{bk} \times \vec{h}_{ai} \cdot \vec{u}_z ds}{\int_b \vec{e}_{ai} \times \vec{h}_{ai} \cdot \vec{u}_z ds} \int_b \vec{e}_{bn} \times \vec{h}_{ai} \cdot \vec{u}_z ds$$

$$+(\frac{b_n}{a_1} - \sum_{j=1}^{N} \frac{b_j}{a_1} s_{jn}) \int_b \vec{e}_{bn} \times \vec{h}_{bn} \cdot \vec{u}_z ds = \int_b \vec{e}_{bn} \times \vec{h}_{a1} \cdot \vec{u}_z ds \tag{2.4.5}$$

$$\rho \int_a \vec{e}_{a1} \times \vec{h}_{a1} \cdot \vec{u}_z ds - \sum_{j=1}^{N} \frac{b_j}{a_1} (\int_b \vec{e}_{bj} \times \vec{h}_{a1} \cdot \vec{u}_z ds + \sum_{k=1}^{N} s_{jk} \int_b \vec{e}_{bk} \times \vec{h}_{a1} \cdot \vec{u}_z ds)$$
$$= -\int_a \vec{e}_{a1} \times \vec{h}_{a1} \cdot \vec{u}_z ds \tag{2.4.6}$$

The infinite series were truncated at M and N in applications, M and N representing quantities which signify the number of modes in waveguides a and b, respectively. Equation (2.4.5) generates N linear equations where $n = 1, 2, ..., N$ and (2.4.6) supplies one equation. For complicated problems, i.e. junctions between rectangular and circular guides, etc., the integrations in (2.4.5) and (2.4.6) should be performed numerically. In the case of this project, the integrations can be completed analytically.

The coefficients of the back-scattered modes in guide a may be found, which are,

$$\frac{a_i}{a_1} = \frac{\sum_{j=1}^{N} \frac{b_j}{a_1} (\int_b \vec{e}_{bj} \times \vec{h}_{ai} \cdot \vec{u}_z ds + \sum_{k=1}^{N} s_{jk} \int_b \vec{e}_{bj} \times \vec{h}_{ai} \cdot \vec{u}_z ds)}{\int_b \vec{e}_{ai} \times \vec{h}_{ai} \cdot \vec{u}_z ds} \tag{2.4.7}$$

where $i \neq 1$.

It can be noted that if power is injected from the left, it is necessary to know the scattering properties of junction 2 prior to solving the problem at junction 1. Similarly, prior to analyzing junction 2, the scattering properties of any discontinuity farther down the guide must be known. It is fundamental that analysis must begin at a simple termination, such as a matched or single-mode or a short circuit which causes

independent reflection of each mode incident upon it, regardless of the amplitude and phase of other modes.

If the length l of a typical waveguide is small, many modes are generated at one junction. If r is the mode incident on junction 1, then ρ_r is its reflection factor and a_i / a_r, with $i \neq r$, denotes the M-1 coefficients of other back-scattered modes. Therefore, there are M scattering coefficients of junction 1, after which the waves decaying to the next junction are given by

$$s_{rj} = \begin{cases} \dfrac{a_i}{a_r} e^{-(\gamma_i + \gamma_r)l} & i \neq r \\ \rho_r e^{-2\gamma_r l} & i = r \end{cases} \tag{2.4.8}$$

Consider each mode r=1, 2,..., M, in turn, to be independently incident on the junction and solve the resulting system of equations each time. In this way, all M^2 scattering coefficients are found.

The junction can be represented by T, Π and transformer networks [13, 14, 15]. To evaluate the equivalent circuit, three ways of determining the input admittance y as a function of a load in guide c are generally required.

2.4.2 Symmetry Considerations

Simplification occurs when discontinuities exhibit symmetry and are either symmetrically or anti-symmetrically excited. The thick irises and finite length bifurcation in Fig. 2.2.1 are symmetrical about a transverse plane, as shown in Fig. 2.2.1(c). If both ports are excited symmetrically, an open circuit appears at the central plane; whereas an anti-symmetrical excitation produces a short circuit [15]. Under these conditions, only pure reflection occurs at the central plane and so $s_{jk} = 0$ when $j \neq k$. s_{jj} is given simply by

$$s_{jj} = \frac{1 - y_{bj}}{1 + y_{bj}} \tag{2.4.9}$$

y_{bj} is the normalized input admittance of the j th mode in b at the discontinuity, distance $l/2$ from the equivalent plane.

Therefore, two parameters are sufficient to specify the equivalent network of such discontinuities, as shown in Fig. 2.4.2. For example, the upper arm impedances of the equivalent T network are both given by $Z_{11} - Z_{12}$ and the common branch by Z_{12}. The computed input impedance with a symmetric excitation yields $Z_{11} + Z_{12}$ and that with an anti-symmetric excitation gives $Z_{11} - Z_{12}$.

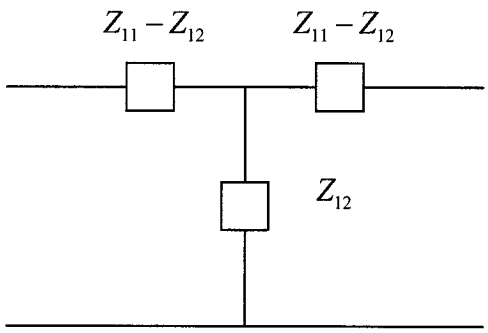

Fig. 2.4.2: The equivalent circuit of the discontinuities in Fig. 2.2.1

2.4.3 Simplified Formula for the Integrations:

(a) Case 1: H-plane bifurcation(Fig.2.2.1(c))

Fig. 2.4.3 shows a rectangular waveguide loaded with a thick, perfectly conducting vane. The y-coordinate dimensions are normalized with respect to the broad dimension a ($= w$). Assuming excitation by an H_{10} mode, only symmetrical modes are generated at the discontinuity in a .

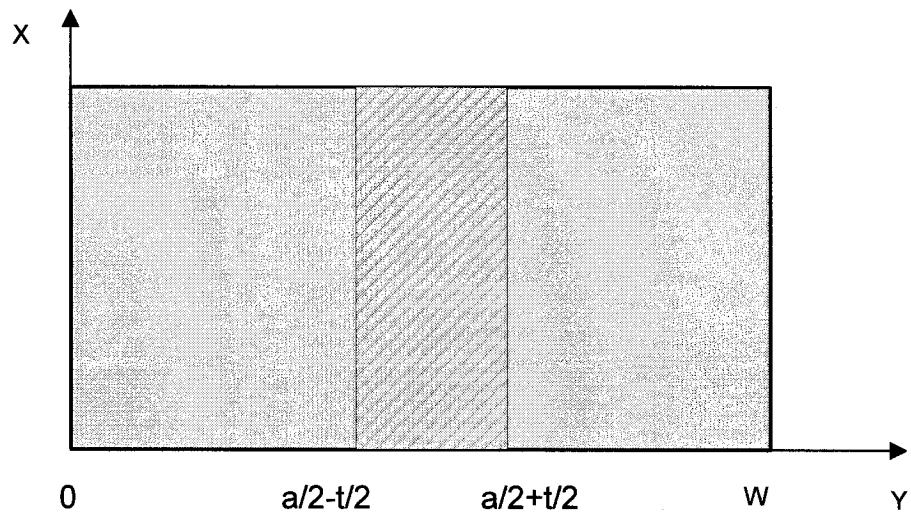

Fig. 2.4.3: Centrally located bifurcation of thickness t in a rectangular waveguide

Expressions for the transverse field and magnetic field in guide a are the following:

$$\vec{e}_{ai} = \vec{u}_x \sin(p\pi y / w) \tag{2.4.10}$$

$$\vec{h}_{ai} = \vec{u}_x y_{ai} \sin(p\pi y / w) \tag{2.4.11}$$

The wave admittance of the i th mode is

$$y_{ai} = \sqrt{\frac{\varepsilon_0}{\mu_0}} \sqrt{1 - (\frac{p\lambda_0}{2w})^2} \tag{2.4.12}$$

Modes are numbered consecutively, i.e. i =1,2, …, M, and so

$$p = 2i - 1 \tag{2.4.13}$$

In the left-hand region of waveguide b the transverse fields are

$$\vec{e}_{bj} = \vec{u}_x \sin(\frac{2q\pi y / w}{1 - t / w}) \tag{2.4.14}$$

$$\vec{h}_{bj} = \vec{u}_y y_{bj} \sin(\frac{2q\pi y / w}{1 - t / w}) \tag{2.4.15}$$

for $0 < y/w < \frac{1}{2}(1 - t/w)$.

By substituting $(1-y/w)$ for y/w when $\frac{1}{2}(1+t/w) < y/w < 1$, the admittance of the j th mode is

$$y_{bj} = \sqrt{\frac{\varepsilon_0}{\mu_0}}\sqrt{1 - (\frac{q\lambda_0/w}{1 - t/w})^2} \tag{2.4.16}$$

Here we have

$$q = j \tag{2.4.17}$$

where j=1,2,..., N. When calculating y_{ai} and y_{bj}, take the positive root when the quantities are real and the negative imaginary root when they are imaginary.

For the symmetric structure in Fig. 2.4.3, referring to equations (2.4.5) and (2.4.6), the integral expressions are available in [7].

Since all fields are uniform along x, the integrations were performed only with respect to y. Having evaluated these integrals, all the analysis required for this case is thus complete. For the structure in Fig. 2.3.1(b), this is a particularly simple problem, what with the s_{jk} terms vanishing due to the infinite length of the bifurcated guide.

The linear equations (2.4.5) and (2.4.6) were solved in the Matlab environment.

Forward- and back-scattered mode coefficients were computed and, from the reflection efficient ρ, the normalized input admittance seen from guide a at the junction was computed using

$$y = \frac{1 - \rho}{1 + \rho} \tag{2.4.18}$$

The Wexler model can be used to treat both thin (w=0) and thick ($w \neq 0$) bifurcation.

Once the forward-scattered mode coefficients b_j / a_1 and the backward-scattered mode coefficients a_i / a_1 are determined, the apportionment of power between scattered modes can be calculated.

The junction fields are expressed by the equations from (2.4.1) to (2.4.4). Substituting (2.4.10), (2.4.11), (2.4.14) and (2.4.15) into them, and dividing by a_1, the following equations are obtained. In waveguide a:

$$E_x = (1+\rho)\sin(\pi y / w) + \sum_{i=2}^{M} \frac{a_i}{a_1} \sin(p\pi y / w) \tag{2.4.19}$$

$$H_y = (1-\rho) y_{a1} \sin(\pi y / w) + \sum_{i=2}^{M} \frac{a_i}{a_1} \sin(p\pi y / w) \tag{2.4.20}$$

and in waveguide b within $0 < y / w < \frac{1}{2}(1 - t / w)$

$$E_x = \sum_{j=1}^{N} \frac{b_j}{a_1} \sin\left(\frac{2q\pi y / w}{1 - t / w}\right) \tag{2.4.21}$$

$$H_y = \sum_{j=1}^{N} \frac{b_j}{a_1} y_{bj} \sin\left(\frac{2q\pi y / w}{1 - t / w}\right) \tag{2.4.22}$$

When $\frac{1}{2}(1+t/w) < y/w < 1$, substitute $(1-y/w)$ for y/w in (2.4.21) and (2.4.22).

The propagation constant of the j th mode in guide b is given by

$$\gamma_j = \frac{\pi}{w} \sqrt{\left(\frac{2q}{1 - t / w}\right)^2 - \left(2\frac{w}{\lambda_0}\right)^2} \tag{2.4.23}$$

The normalized input admittance of the j th mode at a distance $l/2$ from an open circuit at the central plane, is

$$y_{bj} = \tanh(\gamma_j l / 2) \tag{2.4.24}$$

and with a short circuit at the central plane,

$$y_{bj} = \coth(\gamma_j l / 2) \tag{2.4.25}$$

S_{jj} is then computed from (2.4.9).

(b) Case 2: Thick Asymmetric Iris (Fig. 2.2.1(b))

Fig. 2.4.4 shows a general situation of an iris structure in a waveguide. The transverse fields in guide b are expressed as:

$$\bar{e}_{bj} = \bar{u}_x \sin\left(\frac{q\pi y}{w - w_1 - w_2}\right) \tag{2.4.26}$$

$$\bar{h}_{bj} = \bar{u}_y y_{bj} \sin\left(\frac{q\pi y}{w - w_1 - w_2}\right) \tag{2.4.27}$$

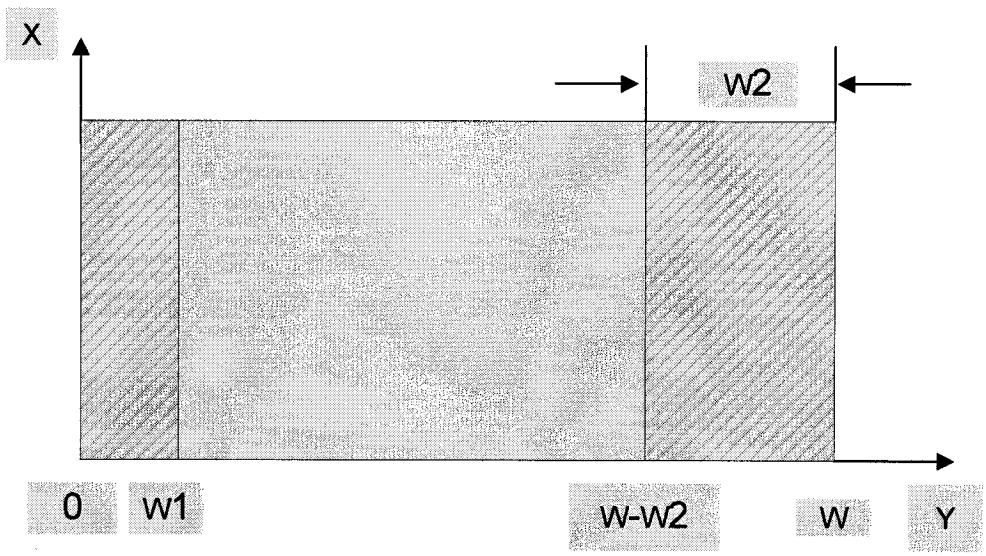

Fig. 2.4.4: cross-section view: asymmetric iris

The admittance is determined with the following:

$$y_{bj} = \sqrt{\frac{\varepsilon_0}{\mu_0}}\sqrt{1 - \left(\frac{q\lambda_0 / 2}{w - w_1 - w_2}\right)^2} \tag{2.4.28}$$

The propagation constant of the j th mode in guide b is given by

$$\gamma_j = \frac{\pi}{w}\sqrt{\left(\frac{q}{1-\frac{w_1+w_2}{w}}\right)^2 - \left(2\frac{w}{\lambda_0}\right)^2} \tag{2.4.29}$$

Referring to equations (2.4.5) and (2.4.6), the integrations are given below.

$$\int_a \vec{e}_{ai} \times \vec{h}_{ai} \cdot \vec{u}_z \, ds = \frac{1}{2} w \, y_{ai} \tag{2.4.30}$$

$$\int_b \vec{e}_{bj} \times h_{bj} \cdot \vec{u}_z ds = \frac{1}{2} y_{bj} [w_1 \frac{\sin(f)}{f} - (w - w_2)\frac{\sin(g)}{g} + w - w_1 - w_2] \tag{2.4.31}$$

$$\int_b \vec{e}_{bj} \times \vec{h}_{ai} \cdot \vec{u}_z ds = -\frac{1}{2} y_{ai} \{(w - w_2)[\frac{\sin(f_1)}{f_1} - \frac{\sin(g_1)}{g_1}] - w_1[\frac{\sin(f_2)}{f_2} - \frac{\sin(g_2)}{g_2}]\} \tag{2.4.32}$$

where

$$f = \frac{2q\pi w_1}{w - w_1 - w_2}$$

$$g = \frac{2q\pi (w - w_2)}{w - w_1 - w_2}$$

$$f_1 = \pi(w - w_2)[\frac{q}{w - w_1 - w_2} + \frac{p}{w}]$$

$$f_2 = \pi w_1[\frac{q}{w - w_1 - w_2} + \frac{p}{w}]$$

$$g_1 = \pi(w - w_2)[\frac{q}{w - w_1 - w_2} - \frac{p}{w}]$$

$$g_2 = \pi w_1[\frac{q}{w - w_1 - w_2} - \frac{p}{w}]$$

For the purposes of this project, parameter w_1 was set to zero for the asymmetric iris calculation.

(c) Case 3: Thick Symmetric Iris

The transverse fields, the admittance and the propagation constant of the j th mode in guide b were obtained by setting $w_2 = w_1$ in (2.4.26), (2.4.27), (2.4.28) and (2.4.29).

The integral terms of equations (2.4.5) and (2.4.6) were simplified significantly. For case 3, in both waveguides, a and b, only symmetric modes exist. Thus, j and k in equations (2.4.5) and (2.4.6) are odd numbers.

2.4.4 The Convergence of the Problem

Since the fields in different regions are expanded in terms of discrete sets of modes with unknown coefficients, the boundary value problem involves the calculation of these amplitude coefficients from an appropriate truncation of the expanding terms.

Some authors studied the convergence of the problem. To make the numerical solution exact, many modes are necessary in each waveguide so as to reach the true value with good accuracy. In practice, for each guide, a few dozen modes (i.e. $M \geq 30, N \geq 30$) may supply a good approximation of the fields. For our boundary value problem, there is the hazard of converging to a relative convergence result [17, 18]. The authors found that, when the ratio of the number of modes in waveguide a to those in waveguide b is close to a/b, the numerical solution may avoid relative convergence [8, 16, 17, 18].

REFERENCES

[1] G. L. Matthaei, L. Young and E. M. T. Jones, Microwave filters, impedance-matching networks, and coupling structures, McGraw-Hill Book Company, New York

[2] N. Marcuvitz, Waveguide Handbook, McGraw-Hill Book Company, London, 1986

[3] Leviatan, Y.; Li, P.G.; Adams, A.T.; Perini, J., "Single-Post Inductive Obstacle in Rectangular Waveguide," IEEE Trans. Microwave Theory and Tech., vol. MTT-31, pp. 806-812, Oct. 1983.

[4] Ping Guan Li; Adams, A.T.; Leviatan, Y.; Perini, J.;"Multiple-Post Inductive Obstacles in Rectangular Waveguide," IEEE Trans. Microwave Theory and Tech., vol. MTT-32, pp. 365-373, April 1984.

[5] Dominic Deslandes, Ke Wu, "Single-substrate integration technique of planar circuits and waveguide filters," IEEE Trans. Microwave Theory and Tech., vol. MTT-51, pp593-596, Feb. 2003.

[6] Giuseppe Conciauro, Marco Guglielmi and Roberto Scrrentino, Advanced Modal Analysis. John Wiley & Sons, Ltd., 1999

[7] A. Wexler, "Solution of waveguide discontinuities by modal analysis," IEEE Trans. Microwave Theory and Tech., vol. MTT-15, pp508-517, Sept. 1967.

[8] Y. C. Shih, "Design of waveguide E-plane filters with all-metal inserts," IEEE Trans. Microwave Theory and Tech., vol. MTT-32, pp695-704, July 1984.

[9] H. Patzelt and F. Arndt, "Double-plane steps in rectangular waveguides and their application for transformers, irises, and filters," IEEE Trans. Microwave Theory and Tech., vol. MTT-30, pp771-776, May 1982.

[10] R. J. Luebbers, B. A. Munk "Analysis of thick rectangular waveguide windows with finite conductivity," IEEE Trans. Microwave Theory and Tech., vol. MTT-21, pp461-468, July 1973.

[11] M. Guglielmi, F. Montauti, L. Pellegrini, and P. Arcioni, "Implementating transmission zeros in inductive-window bandpass filters," IEEE Trans. Microwave Theory and Tech., vol. MTT-43, pp1911-1915, Aug. 1995.

[12] P. M. Morse and H. Feshbach, Methods of Theoretical Physics. New York: McGraw-Hill, 1953, pp928-929.

[13] N. Marcuvitz, Waveguide Handbook. London: Peter Peregrinus Ltd. 1986, Chapter 4.

[14] R. E. Collin, Foundations for Microwave Engineering. IEEE Press. New York, 1992

[15] R. E. Collin, Field Theory of Guided Waves. IEEE Press, New York, 1991

[16] S. W. Lee, W. R. Jones, and J. J. Campbell, "Convergence of Numerical Solution of Iris Type Discontinuity Problems," IEEE Trans. Microwave Theory Tech., vol. MTT-19, pp.528-536, June 1971.

[17] R. Mittra, T. Itoh, T. S. Li, "Analytical and numerical studies of the relative convergence phenomena arsing in the solution of an integral equation by the moment method," IEEE Trans. Microwave Theory Tech., vol. MTT-20, pp.96-104, Feb. 1972.

[18] Y. C Shih, K. G. Gray, "Convergence of numerical solutions of step-type waveguide discontinuity problems by modal analysis," in 1983 IEEE/MTT-S Intl. Microwave Symp. Dig., May 1983, pp.233-235

Chapter 3 Cascaded Direct-Coupled Cavity Substrate Integrated Filters

3.1 Filter Design

3.1.1 Filter Synthesis

There are two basic design approaches for direct-coupled cavity filters. One is based on Cohn's low-pass prototype [25] and the other is based on the quarter-wave transformer prototype circuit by Young [19, 20, 21]. Their prototype circuits are described in chapters 4 and 6 of [1], respectively, and the applications to band-pass filter design are more generally summarized in chapters 8 and 9, respectively.

In a distributed filter consisting of a cascade of n cavities, each cavity formed by a transmission line with length $l = \lambda_{g0}/2$ behaves as a resonator in the configuration. In this thesis, the design method is based on the general synthesis theory of a distributed stepped impedance low-pass prototype [19, 20, 21, 22, 23].

Wave reflections are produced by inserting discontinuities between the unit elements. These discontinuities behave as impedance inverters, i.e. the K inverter. The values of the K inverter are given by Rhode's explicit formula [23]:

$$K_{r,r+1} = \frac{\sqrt{1 + (\sin[\frac{r\pi}{n}] / y)^2}}{\sqrt{Z_r Z_{r+1}}} \qquad \text{for r=0, 1, .., n} \qquad (3.1.1)$$

with

$$y = \sinh[\frac{1}{n}\sinh^{-1}\frac{1}{h}]$$

and

$$Z_r = \begin{cases} 1, \\ \dfrac{2\sin[\dfrac{(2r-1)\pi}{2n}]}{y\alpha} - \dfrac{\alpha}{4y}[\dfrac{y^2+\sin^2[\dfrac{r\pi}{n}]}{\sin[\dfrac{(2r+1)\pi}{2n}]} + \dfrac{y^2+\sin^2[\dfrac{(r-1)\pi}{2n}]}{\sin[\dfrac{(2r-3)\pi}{2n}]}], \end{cases} \tag{3.1.2}$$

Here h denotes the pass-band ripple level and n denotes the number of resonators.

The design procedure employs Levy's modified formula [8, 24], which can be applied to filters with moderate bandwidth ($\geq$ 20%).

The reflection coefficient is determined by

$$(S_{11})_{r-1,r} = \frac{K^2_{r-1,r} - 1}{K^2_{r-1,r} + 1} \tag{3.1.3}$$

According to Levy's modified formula for the prototype of reactance-coupled filters, an optimum equiripple band-pass response occurs around $\theta = \pi$ when the transmitted power is given by the following equation:

$$|S_{12}|^2 = \frac{1}{1 + h^2 T_n^2(\dfrac{\pi \sin\theta}{\theta\alpha})} \tag{3.1.4}$$

where $\theta = \pi\lambda_{g0}/\lambda_g$ and $T_n(x) = \cosh(n\cosh^{-1}x)$ is the nth-degree Chebyshev polynomial of the first kind. This modified expression takes into account the frequency dependence of the discontinuities. Alpha (α) denotes the pass-band bandwidth.

The filter synthesis procedure based on a distributed step-impedance filter prototype is described in [8]. Normally, to design such a filter, the pass-band ripple, the stop-band attenuation, and the two pass-band edge frequencies must be given.

1) The corresponding waveguide wavelengths λ_{g1} and λ_{g2} are calculated at the band-edge frequencies. From λ_{g1} and λ_{g2}, the parameters α and λ_{g0} are determined by the following equation:

$$\frac{\lambda_{g1}}{\lambda_{g0}}\sin\frac{\pi\lambda_{g0}}{\lambda_{g1}} = -\frac{\lambda_{g2}}{\lambda_{g0}}\sin\frac{\pi\lambda_{g0}}{\lambda_{g2}} = \alpha \tag{3.1.5}$$

2) If the pass-band ripple is given as a maximum insertion loss x in dB, the parameter h is determined by

$$h = \sqrt{10^{(0.1x)} - 1} \tag{3.1.6}$$

3) With the help of (3.1.4), a value of n, the number of cavities of the filter, is set by the stop-band attenuation specification.

4) With parameters α, h and n, one can obtain the junction reflection coefficient for each discontinuity using equations (3.1.3), (3.1.1) and (3.1.2).

5) For the required reflection level in Step (4), the bifurcation transverse width (fixed longitudinal length=10 mil) or the iris width (fixed longitudinal length=10 mil) of each junction is determined at the center frequency by the numerical analysis based on the Wexler model [7].

6) The corresponding phase angles for the bifurcation or iris are obtained, from which the resonator lengths are determined by

$$cl_r = \lambda_{g0} \cdot \theta_r / 2\pi = \lambda_{g0} \cdot (\pi + \frac{\varphi_{r-1,r} + \varphi_{r,r+1}}{2}) \Big/ 2\pi \tag{3.1.7}$$

where $\varphi_{r,r+1}$ is the negative phase angle of the reflection coefficient supplied by the impedance inverter $K_{r,r+1}$, l_r is the physical length, and θ_r the electrical length of the r-th resonator.

For a lossless junction, the S matrix is unitary and reciprocal. Therefore, the S matrix is uniquely determined by the magnitude and phase of one of its elements, e. g. the reflection coefficient S_{11}. In section 3.1.2, we will analyze the bifurcation and iris of given dimensions in order to obtain the reflection coefficient; there, inversely, we can determine the dimensions of a bifurcation and of an iris for a given reflection coefficient.

3.1.2 Determining the dimensions of the Coupling Components

Consider the case of an incident H_{10} wave propagating in a single mode rectangular waveguide. The wave propagation is disturbed by a finite length bifurcation at the waveguide center, as shown in Fig. 2.2.1(c) or an iris with finite thickness, as shown in Fig 2.2.1(a) and (b).

In the portion between the two junctions, the wave becomes cutoff while propagating in both the left and right sides. The portion between the two junctions forms the coupling part which connects the two cavities. A fraction of the wave goes through the discontinuities while the rest is reflected back to the input port. Near the waveguide junction in the transmitting waveguide, higher modes (evanescent modes) are produced so as to meet the boundary condition by the discontinuities. The evanescent modes in the cutoff portion supply the couplings of the cavities.

The Wexler mode matching model described in Section 2.4 is used to obtain the scattering matrix of these waveguide discontinuities. This mode matching model is generalized for these types of discontinuities, as shown in Section 2.4.

Simply considering one coupling part in the waveguide as shown in Fig. 2.2.1, each coupling part produces two junctions in the waveguide, which are actually symmetric about a transverse plane. We may use such characteristics to get the equivalent network of such discontinuities [8, 15]. Hence the reflection of the coupling parts is obtained in this way. In order to get the desired reflection due to the coupling part, either its width or length can be changed. In an actual design, one of the two dimensions is usually fixed while the best value for the second is selected.

As stated in Section 2.4, the convergence of the results to the correct values should be reached by giving the required ratio of the mode numbers in the waveguide portions. In our application, we apply the Matlab code on this model to the structures in Figure 2.2.1.

3.1.3 Transition Design

The coupling between the SIW component and other planar component employs transitions. A waveguide to micro-strip transition was used for the project.

For a micro-strip line with width w, substrate thickness h and relative permittivity ε_r, the effective relative permittivity is given in [29]:

The equivalent wavelength is $\lambda_{eff} = \lambda / \sqrt{\varepsilon_{re}}$. When RT/duroid 6002 of 10 mil thickness is used for the current project, a 50 Ohm micro-strip line on the substrate requires a width of $w = 25.7mil$.

In some cases, integrating an SIW filter or other SIW components on a substrate needs a new transition to perform the couplings. Waveguide-CPW is one of the examples [31, 32].

The impedance for a dispersive rectangular waveguide has no real physical meaning. It is only used for impedance matching. If the power-current relation is used to define the impedance of the 10 mil thick SIW waveguide, the value of the SIW impedance is relatively small (13.1 Ohm). A portion of micro-strip of a quarter-wave length is stretched from the SIW. Then a quarter-wave length transformer connects this portion with a 50 Ohm micro-strip line. The length of the quarter-wave line was optimized in the HFSS environment.

A transition of micro-strip taper is proposed in [30], which yields a good broad-band response and excellent reflection performance. For its design the structural parameters l and d are optimized in the HFSS environment.

3.2 Numerical Results

3.2.1 Numerical results from the Wexler model

The mode amplitude coefficients solved in the case of bifurcation are shown in Fig. 3.2.1 and Fig. 3.2.2. The situations for symmetrical and asymmetrical irises are shown in Fig. 3.2.3 and Fig. 3.2.4. We have seen that the plotted fields are precisely matched at the junction of the waveguide bifurcation.

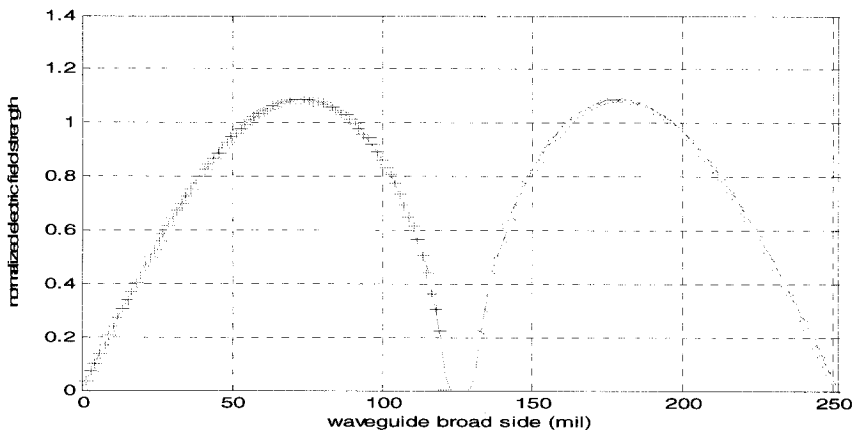

(a) w=252 mil, t=10 mil, f=24 GHz, $\varepsilon_r = 2.94$, M=63, N=60.
dashed line: in guide a; plus line & cross line: in guide b

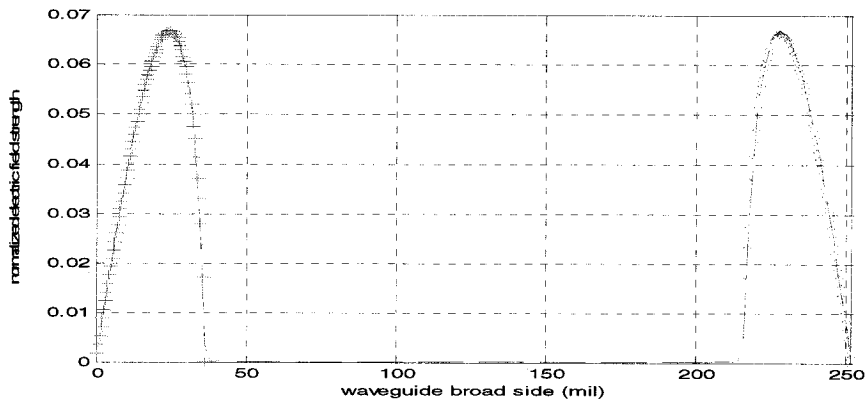

(b) w=252 mil, t =180 mil, f=24 GHz, $\varepsilon_r = 2.94$, M=181, N=60.
dashed line: in guide a; plus line & cross line: in guide b

Fig. 3.2.1: Electric field distributions at junction formed by infinite long bifurcation

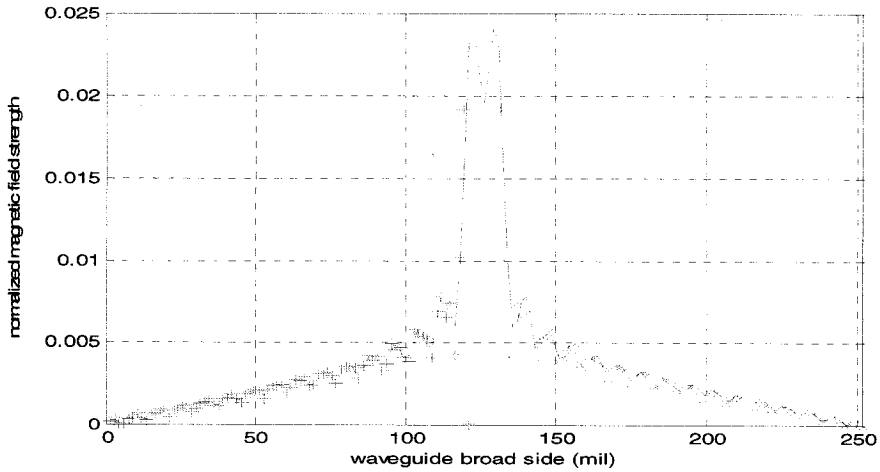

(a) w=252 mil, t=10 mil, f=24 GHz, $\varepsilon_r = 2.94$, M=63, N=60.

dashed line: in guide a; plus line & cross line: in guide b

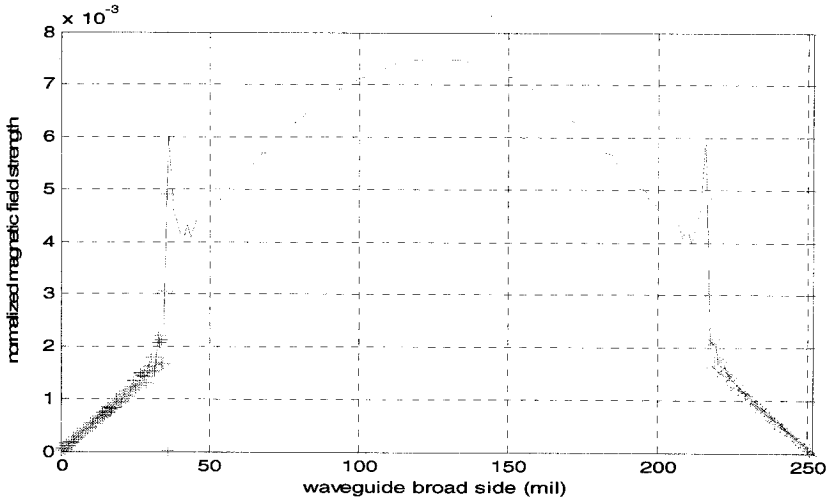

(b) w=252 mil, t =180 mil, f=24 GHz, $\varepsilon_r = 2.94$, M=181, N=60.

dashed line: in guide a; plus line & cross line: in guide b

Fig. 3.2.2: Transverse magnetic field distributions

at junction formed by infinite long bifurcation

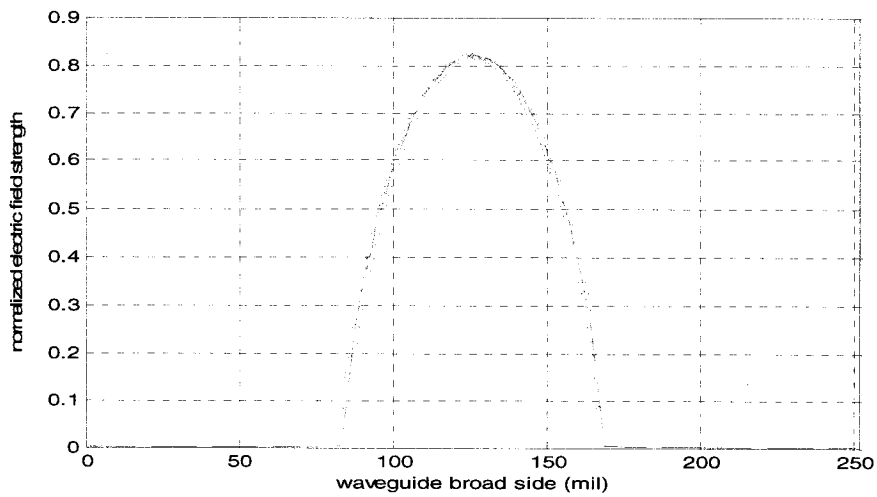

(a) symmetric iris: w=252 mil, w_1 =84 mil, w_2=84 mil;

f=24 GHz, $\varepsilon_r = 2.94$, M=123, N=41. dashed line: in guide a; cross line: in guide b

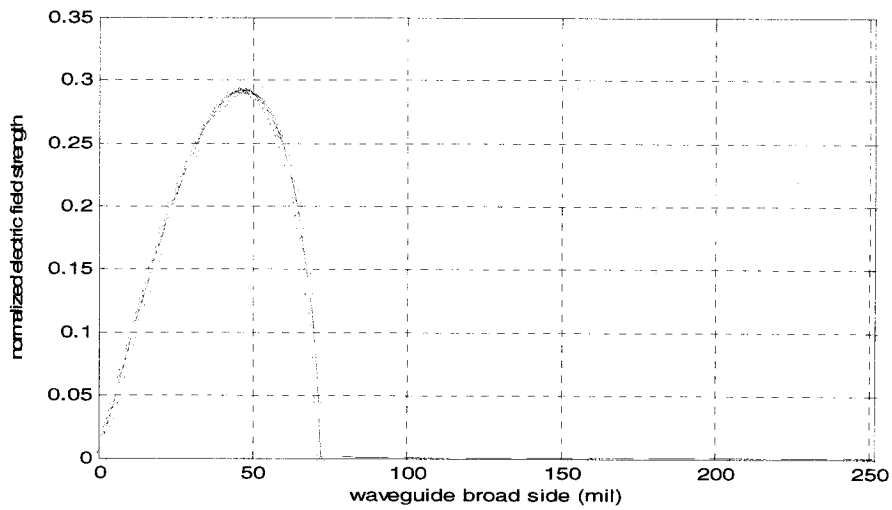

(b) asymmetric iris: w=252 mil, w_1 =0 mil (aperture at left), w_2=180 mil; f=24 GHz,

$\varepsilon_r = 2.94$, M=141, N=40. dashed line: in guide a; cross line: in guide b

Fig. 3.2.3: Electric field distributions at junction

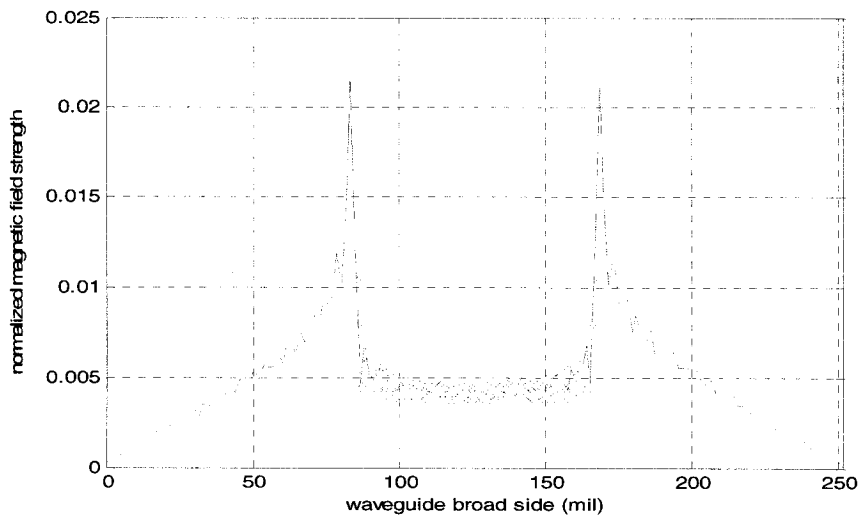

(a) symmetric iris: w=252 mil, w_1=84 mil, w_2=84 mil; f=24 GHz, $\varepsilon_r = 2.94$, M=123, N=41. dashed line: in guide a; cross line: in guide b

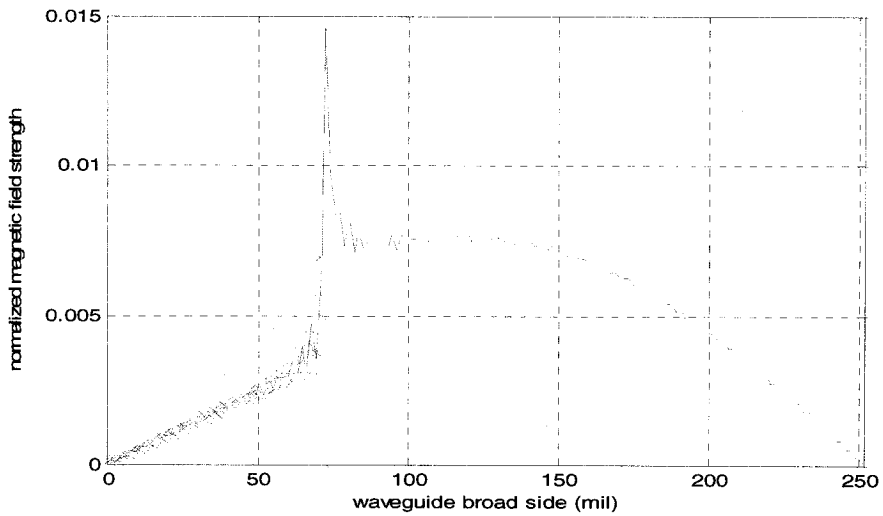

(a) asymmetric iris: w=252 mil, w_1 =0 mil(aperture at left), w_2=180mil; f=24 GHz, $\varepsilon_r = 2.94$, M=141, N=40. dashed line: in guide a; cross line: in guide b

Fig. 3.2.4: Transverse magnetic field distributions at junction

3.2.2 Results for Structural Parameters from the Filter Synthesis Procedure

Case 1: Metal Insert Configuration (l □ t in Fig. 2.2.1(c))

Band-pass filter specifications are given in Table 3.2.1. According to (3.1.4), the value of n is determined and is equal to 4. The rejections at the stop-bands are: $IL|_{f_a} \le -65dB$ and $IL|_{f_b} \le -60dB$. The remaining values of the design parameters are: $\alpha = 0.0333$, $h = 0.1526$. The impedance inverters are:

$$K_{0,1} = 0.1734, K_{1,2} = 0.0277, K_{2,3} = 0.0219, K_{3,4} = 0.0277, K_{4,5} = 0.1734 \quad (3.2.1)$$

The corresponding reflections are:

$$s_{0,1} = -0.9416, s_{1,2} = -0.9985, s_{2,3} = -0.9990, s_{3,4} = -0.9985, s_{4,5} = -0.9416 \quad (3.2.2)$$

Table 3.2.1 Band-pass filter specification

f_0(GHz)	24	BW(MHz)	340	IL	0.1 dB
f_1(GHz)	23.83	f_a(GHz)	23	$IL\|_{f_a}$	$\le -60dB$
f_2(GHz)	24.17	f_b(GHz)	25	$IL\|_{f_b}$	$\le -60dB$

The dimensions of the copper coated longitudinal (axial) slots are:

$$\begin{cases} t = 10mil \\ l_1 = 70mil \end{cases} \begin{cases} t = 10mil \\ l_2 = 198mil \end{cases} \begin{cases} t = 10mil \\ l_3 = 220mil \end{cases} \begin{cases} t = 10mil \\ l_2 = 198mil \end{cases} \begin{cases} t = 10mil \\ l_1 = 70mil \end{cases} \quad (3.2.3)$$

The corresponding phase angles due to the coupling components are:

$$\varphi_{0,1} = -1.0203, \varphi_{1,2} = -1.0343, \varphi_{2,3} = -1.0344, \varphi_{3,4} = -1.0343, \varphi_{4,5} = -1.0203$$

Cavity lengths are given by (3.1.7):

$$cl_1 = 117.45mil, cl_2 = 117.10mil, cl_3 = cl_2, cl_4 = cl_1 \quad (3.2.4)$$

Case 2: Symmetric bifurcation Configuration (l □ t in Fig. 2.2.1(c))

Specifications: the same as in Case 1.

According to (3.1.4), the value of n is determined and equal to 4. The rejections at the stop-bands are: $IL|_{f_a} \le -67dB$ and $IL|_{f_b} \le -62dB$. The remaining values of the design parameters are: $\alpha = 0.0314$, $h = 0.1526$. The impedance inverters are:

$$K_{0,1} = 0.1681, K_{1,2} = 0.0261, K_{2,3} = 0.0206, K_{3,4} = 0.0261, K_{4,5} = 0.1681 \quad (3.2.5)$$

The corresponding reflections are:

$$s_{0,1} = -0.9450, s_{1,2} = -0.9986, s_{2,3} = -0.9991, s_{3,4} = -0.9986, s_{4,5} = -0.9450 \quad (3.2.6)$$

And the dimensions of the copper coated transverse slots are:

$$\begin{cases} t_1 = 54mil \\ l = 10mil \end{cases} \begin{cases} t_2 = 116mil \\ l = 10mil \end{cases} \begin{cases} t_3 = 124mil \\ l = 10mil \end{cases} \begin{cases} t_2 = 116mil \\ l = 10mil \end{cases} \begin{cases} t_1 = 54mil \\ l = 10mil \end{cases} \quad (3.2.7)$$

The corresponding phase angles due to the coupling components are:

$$\varphi_{0,1} = -0.4314, \varphi_{1,2} = -0.0886, \varphi_{2,3} = -0.0689, \varphi_{3,4} = -0.0886, \varphi_{4,5} = -0.4314$$

Cavity lengths are given by (3.1.7):

$$l_1 = 160.13mil, l_2 = 170.20mil, l_3 = l_2 = 170.20mil, l_4 = l_1 = 160.13mil \quad (3.2.8)$$

Case 3: Asymmetric Iris Configuration ($w_1 = 0, w_2 \neq 0$ in Fig. 2.2.1(b))

Table 3.2.2 Band-pass filter specification

f_0(GHz)	24	BW(MHz)	440	IL	0.1 dB
f_1(GHz)	23.78	f_a(GHz)	23	$IL\|_{f_a}$	$\le -55dB$
f_2(GHz)	24.22	f_b(GHz)	25	$IL\|_{f_b}$	$\le -55dB$

According to (3.1.4), the value of n is determined and equal to 4. The rejections at the stop-bands are: $IL|_{f_a} \le -61dB$ and $IL|_{f_b} \le -56dB$. The remaining

values of the design parameters are: $\alpha = 0.0393$, $h = 0.1526$. The impedance inverters are:

$$K_{0,1} = 0.1883, K_{1,2} = 0.0327, K_{2,3} = 0.0259, K_{3,4} = 0.0327, K_{4,5} = 0.1883 \quad (3.2.9)$$

The corresponding reflections are:

$$s_{0,1} = -0.9315, s_{1,2} = -0.9979, s_{2,3} = -0.9987, s_{3,4} = -0.9979, s_{4,5} = -0.9315 \quad (3.2.10)$$

And the dimensions of the irises are:

$$\begin{cases} l = 10mil \\ w_1 = 0mil \\ w_{2,1} = 137mil \end{cases} \begin{cases} l = 10mil \\ w_1 = 0mil \\ w_{2,2} = 170mil \end{cases} \begin{cases} l = 10mil \\ w_1 = 0mil \\ w_{2,3} = 175mil \end{cases} \begin{cases} l = 10mil \\ w_1 = 0mil \\ w_{2,2} = 170mil \end{cases} \begin{cases} l = 10mil \\ w_1 = 0mil \\ w_{2,1} = 137mil \end{cases} \quad (3.2.11)$$

The corresponding phase angles due to the coupling components are:

$$\varphi_{0,1} = -0.4373, \varphi_{1,2} = -0.0995, \varphi_{2,3} = -0.0759, \varphi_{3,4} = -0.0995, \varphi_{4,5} = -0.4373$$

Cavity lengths are given by (3.1.7):

$$cl_1 = 159.66mil, cl_2 = 169.71mil, cl_3 = cl_2, cl_4 = cl_1 \quad (3.2.12)$$

3.2.3 Optimization of the Structural Parameters

The structural parameters were optimized in a software tool environment called *u-wave wizard*. The structural parameters in (3.2.3) and (3.2.4) were optimized and the final values are listed below.

Table 3.2.3 Optimization results for case 1.

l_1	cl_1	l_2	cl_2	l_3	cl_3	l_4	cl_4	l_5
25.49	128.15	126.85	127.98	149.83	127.98	126.85	128.15	25.49

Note: $t = 10mil$, unit in mil

Similarly, after optimizing, the parameters in (3.2.7) and (3.2.8) are given in Table 3.2.4.

Table 3.2.4 Optimization results for case 2.

t_1	cl_1	t_2	cl_2	t_3	cl_3	t_4	cl_4	t_5
26.81	149.21	90.84	166.15	102.69	166.15	90.84	149.21	26.81

Note: $l = 10mil$, unit in mil

Those in (3.2.11) and (3.2.12) are updated by the values in Table 3.2.5.

Table 3.2.5 Optimization results for case 3.

$w_{2,1}$	cl_1	$w_{2,2}$	cl_2	$w_{2,3}$	cl_3	$w_{2,4}$	cl_4	$w_{2,5}$
125.01	151.61	164.31	167.97	170.84	167.97	164.31	151.61	125.01

Note: $l = 10mil$, $w_1 = 0$

3.3 Simulation, Fabrication and Measurement

3.3.1 Simulation with full-wave analysis

The optimized filters were simulated in the HFSS environment. The dielectric loss $\tan\delta = 0.0012$ ($\varepsilon_r = 2.94$) and finite conductivity $\sigma = 5.8\times10^7$ (s/m) were used for the simulation.

Case 1: The simulation results of the metal insert filter are shown Fig. 3.3.1.

Case 2: The simulation results of the wide bifurcation filter are shown Fig. 3.3.2.

Case 3: The simulation results of the asymmetric iris filter are shown Fig. 3.3.3.

The frequency response of a transition with a quarter-wave transformer is shown in Fig. 3.3.4. The width w_1 was determined by the equivalent impedance value defined by the power-current relationship of the SIW guide in the HFSS environment. w_3 was obtained for the requirement of a 50 Ohm micro-strip line on the chosen

substrate thickness and with the dielectric permittivity. w_2 was obtained by the requirement of a quarter-wave transformer between the 50 Ohm line and the wider lower impedance line. The insertion loss of a single transition is about 0.16 dB at the central frequency of 24 GHz, and almost keeps the same value at the narrow pass-band edge ($f_1 = 23.8GHz$, $f_2 = 24.2GHz$).

The simulation results of a new transition with a micro-strip taper [30] are shown in Fig. 3.3.5. The taper length l and taper width on the SIW side d were obtained by optimizing the reflection and insertion loss of the structure in the HFSS environment, which are $l = 103mil$ and $d = 76mil$ for the given thickness of $h = 10mil$ and $\varepsilon_r = 2.94$ RT/duroid 6002 laminate microwave material. The transition with a taper offers a wider frequency response and much better reflection performance compared to that in Fig. 3.3.4. In Fig. 3.3.3, the transitions were included in the filter simulation while the results in Fig. 3.3.1 and Fig. 3.3.2 were just for the filtering portion.

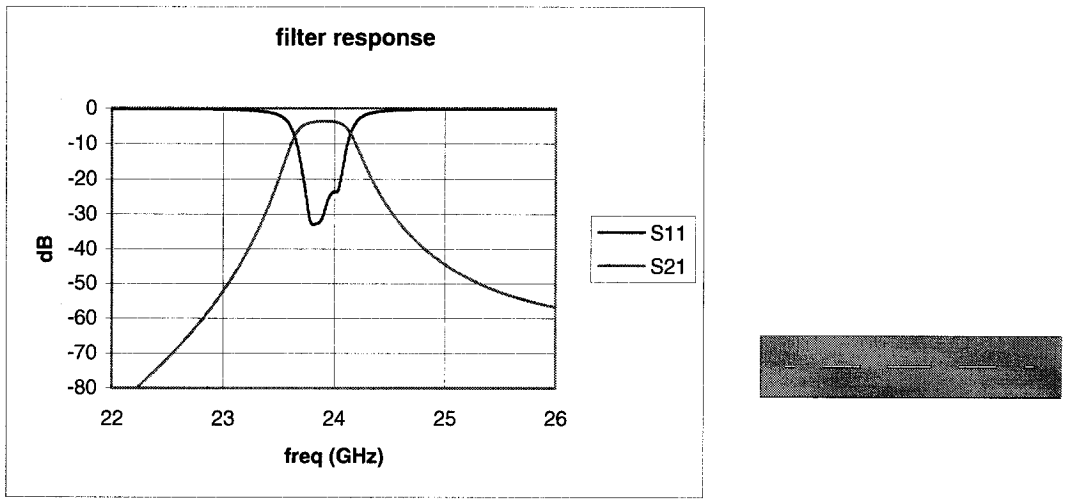

(a) Insertion loss and return loss (b) The simulated structure

$\varepsilon_r = \varepsilon_r'(1 - j\tan\delta_l) = 2.94(1 - j0.0012)$, $h = 10mil$, $\sigma = 5.8\times10^7 S/M$

Fig. 3.3.1: Case 1: Filter response in HFSS

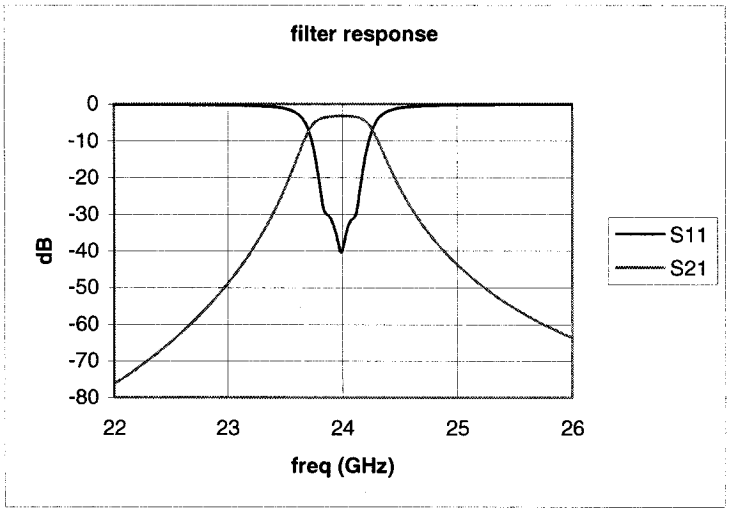

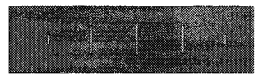

(a) Insertion loss and return loss (b) The simulated structure

$\varepsilon_r = \varepsilon_r'(1 - j\tan\delta_l) = 2.94(1 - j0.0012)$, $h = 10mil$, $\sigma = 5.8\times10^7 S/M$

Fig. 3.3.2: Case 2: filter response in HFSS

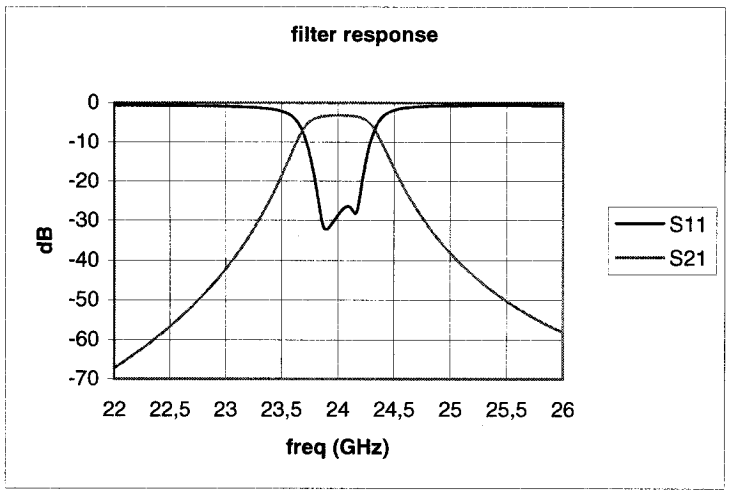

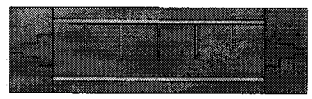

(a) Insertion loss and return loss (b) The simulated structure

$\varepsilon_r = \varepsilon_r'(1 - j\tan\delta_l) = 2.94(1 - j0.0012)$, $h = 10mil$, $\sigma = 5.8\times10^7 S/M$

Fig. 3.3.3: Case 3: filter response with transition
of quarter-wave transformer in HFSS

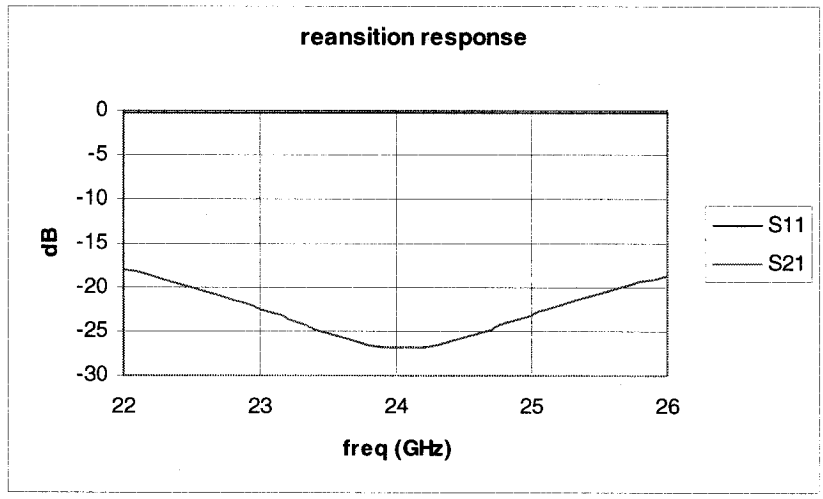

a=252 mil, b= 10 mil; l=69.8 mil, $w_1 = 143.6mil$, $w_2 = 64.6mil$, $w_3 = 25.7mil$;

$\varepsilon_r = \varepsilon_r'(1 - j\tan\delta_l) = 2.94(1 - j0.0012)$, $\sigma = 5.8\times10^7 S/M$

Fig. 3.3.4: Simulation of the transition with quarter-wave transformer in HFSS

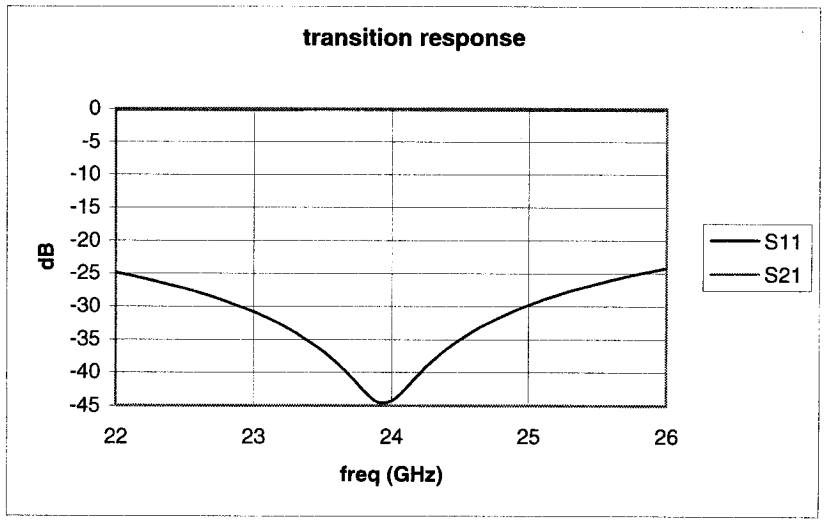

a=252 mil, b=10 mil; h=10 mil, w=25.7 mil; l=103 mil, d=76 mil;

$\varepsilon_r = \varepsilon_r'(1 - j\tan\delta_l) = 2.94(1 - j0.0012)$, $\sigma = 5.8\times10^7 S/M$

Fig. 3.3.5: Simulation of the transition with micro-strip taper in HFSS

3.3.2 Fabrication

The PCB process in the PolyGrames Research Center is implemented by either laser cut or drilling. The minimum slot or groove width which can be obtained by laser cutting is 10 mil. Moreover, this value is also confined by the substrate thickness, i.e. the minimum slot width cannot be smaller than the substrate thickness. In other words, if a thicker substrate, such as 20 mil or 30 mil, is used, the slot widths must increase to the corresponding 20 mil and 30 mil, the reason being that it is hard to neatly align the cutting edge of the top and bottom copper along the same vertical line.

In our laboratory, there were three reasons which made us choose a 10 mil thick RT/Duroid 6002.

1. The u-wave optimization software was used over a short period of fifty days. The original design scenario included the verification of the worst design point, which is h=10 mil for the available laminate material;
2. The process to coat copper onto alumina ceramic was found to be difficult; although alumina has much lower dielectric loss, we could not use it;
3. The laser cutting machine had difficulty keeping the top and bottom cutting edge on the Rogers substrate in an exact vertical plane when the thickness of the substrate was more than 10 mil.

A high Q cavity reduces loss. As we will state later, in a planar flat structure as thin as 10 mil and 20 mil, conductive loss on the conductor walls is the predominant mechanism compared with dielectric loss if the tangent loss of the dielectric is very small. For the RT/duroid 6002, the attenuation constants for both conductive and dielectric losses are in Table 1.2.1. They are in the same dissipation level. Increasing the thickness of the substrate may increase Q and decrease the conductor loss of the filter. Thus, a via hole must be used to replace the slot and groove if a substrate thicker than 10 mil is used, as our colleague Dominic Deslandes has shown [5, 31].

In the filter design of this project, the filters are realized in 10 mil RT/Duroid 6002 substrate. Various physical parameters of RT/duroid 6002 high frequency laminates can be found in the datasheet of Rogers Corporation.

3.3.3 Measurements of the filters

The filters in Fig. 3.3.1, 3.3.2 and 3.3.3 were measured after calibrating the HP 8510 Vector Network Analyzer with OPEN-SHORT-LOAD calibration standards. The test results for insertion loss include the insertion loss due to the test fixture, and the results of phases are not true. The results for filters with quarter-wave transformer transitions are shown in Fig. 3.3.6, Fig. 3.3.7 and Fig. 3.3.8, corresponding to Case 1, Case 2 and Case 3 of Section 3.3.1, respectively.

The central frequency up-shift is due to the permittivity of the RT/duroid 6002, which is smaller than the simulating value 2.94. We will account for this further.

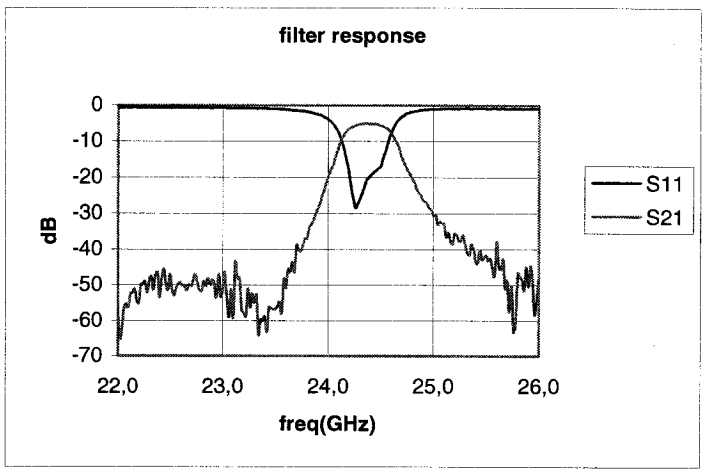

(a)Filter response of the metal insert filter

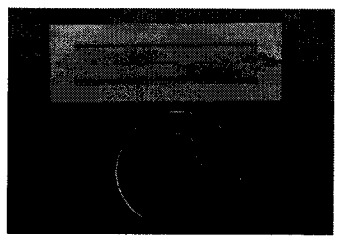

(b)The metal insert filter

Fig. 3.3.6: Filter response of the metal insert filter

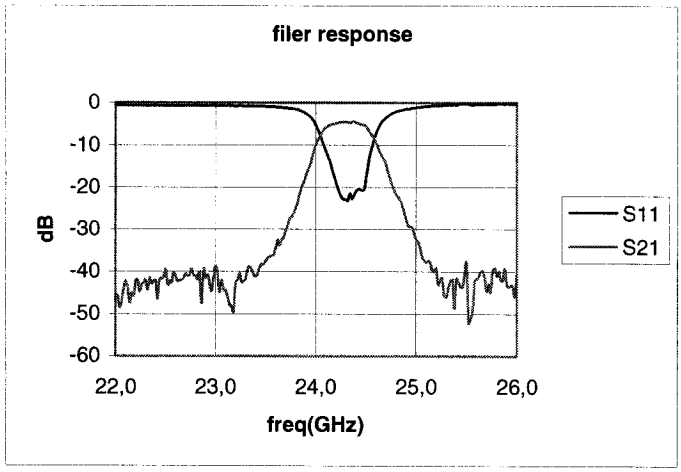

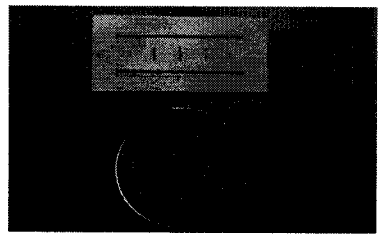

(a) Filter response of the wide bifurcation filter (b)The wide bifurcation filter
Fig. 3.3.7: Filter response of the wide bifurcation filter

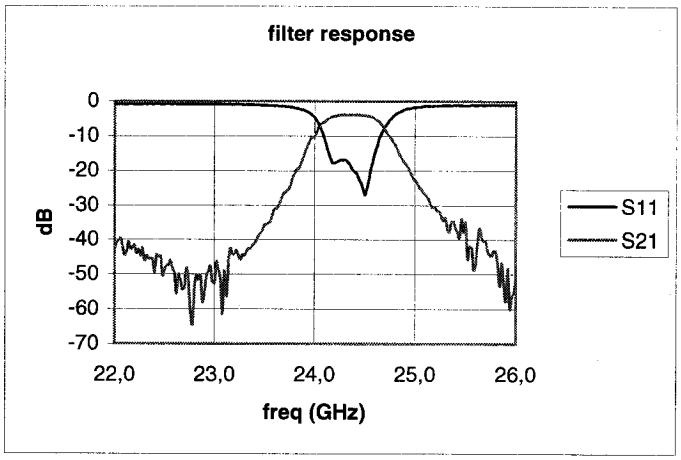

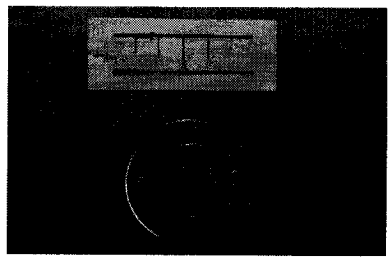

(a) Filter response of the asymmetric iris filter (b) The asymmetric iris filter
Fig. 3.3.8: Filter response of the asymmetric iris filter

The central frequency shifting to 24.36 GHz, 24.32 GHz, 24.38 GHz respectively, is due to the relative permittivity error. The actual relative permittivity of the Rogers RT/duroid 6002 laminated substrate used is about 2.86. The comparisons between the results of simulation using such a value and the test results of the filters in Fig. 3.3.7 and 3.3.8 is shown in Fig. 3.3.9(a) and (b), respectively.

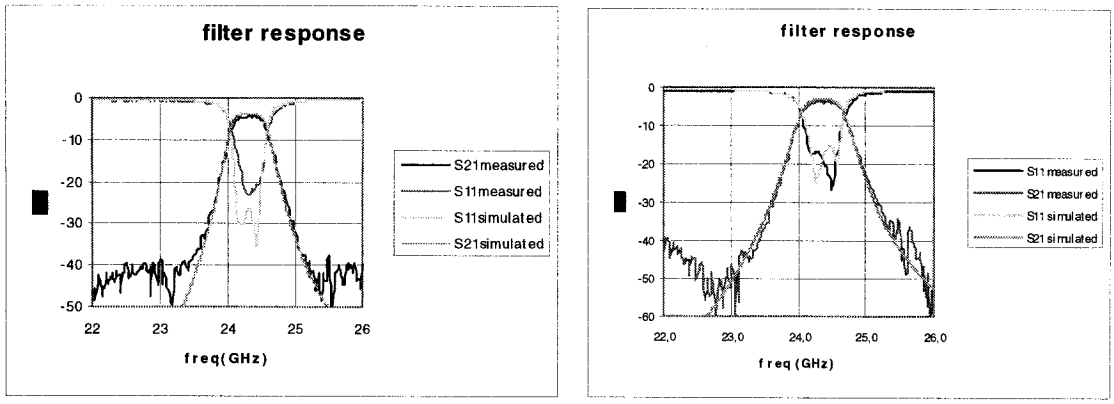

(a) The wide bifurcation filter (b) The asymmetric iris filter

Fig. 3.3.9: Comparison between the test and simulated results

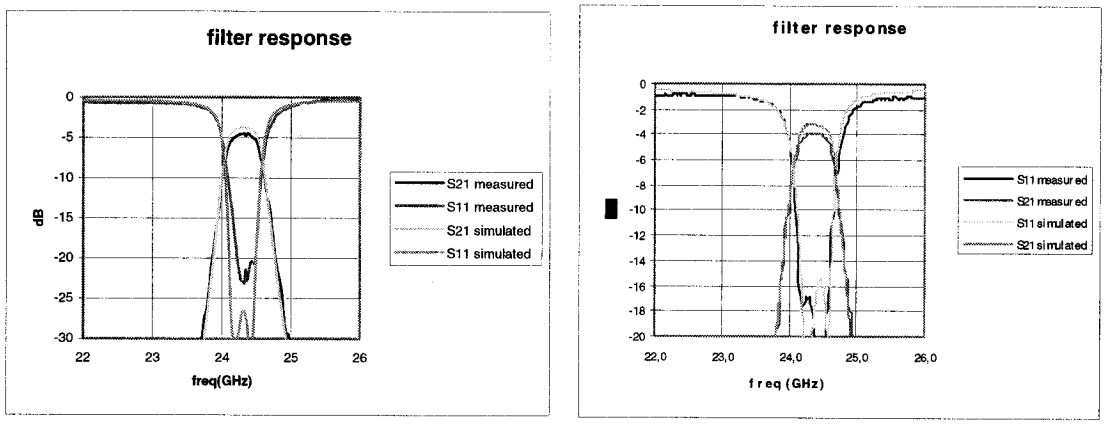

(a) The wide bifurcation filter (b) The asymmetric iris filter

Fig. 3.3.10: Pass-band insertion loss

In the pass-band and on the rejection skirts, the test results agree with the simulated results. In the stop-band, the tested transmission rejections are smaller than the simulated ones.

Since OPEN-SHORT-LOAD calibration standards were used to define the reference planes of the tests, results shown in Fig. 3.3.7, 3.3.8 and 3.3.9 include the

additional insertion loss of the test fixture. So do the results in Fig. 3.3.9(a) and (b). According to measurements, the estimated insertion loss of the test fixture is about 0.5 ± 0.1dB at 24 GHz. Therefore, at the central frequencies, the insertion losses are 4.9 ± 0.1 dB , 4.0 ± 0.1 dB, 3.4 ± 0.1 dB .

3.3.4 Tolerance Analysis

Tolerance analysis was implemented for the asymmetric iris filter in Fig. 3.3.8. The broad wall width of the SIW guide, the thickness of the inductive iris in the longitudinal direction and the width of the iris in the transverse direction were deviated within an error of $\pm\Delta$. The resonant cavity lengths were deviated as the consequence of the changing iris thicknesses. Uniformly distributed random numbers were produced for 20 sets of the filter dimensions.

In order to ensure the minimum filtering characteristics of the structures, a minimum specification for the return loss was set at -15 dB between 23.78 GHz and 24.22 GHz. The insertion losses corresponding to this return loss specification represent a strict confinement to the design requirement. When Δ=0.25, 0.5 mil, the simulated filter responses are shown in Fig. 3.3.11(a) and (b) For a small number of iterated calculations, the tolerance to ensure the performance of the filter is about 0.4 mil.

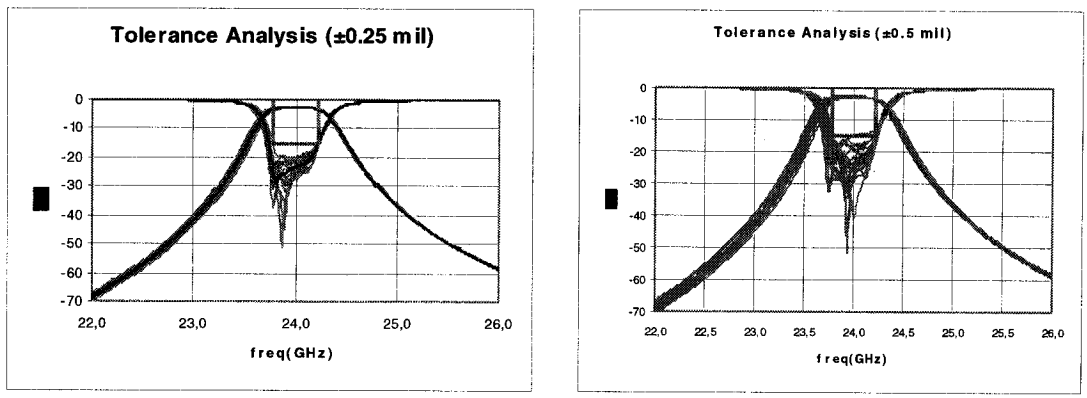

(a) when Δ=0.25 mil (b) when Δ=0.5 mil

Fig. 3.3.11: Tolerance Analysis of the asymmetrical iris filter

3.4 Pulse-power Capacity

Microwave filters are limited in their power-handling capacity by high fields generated inside the filter. Operating at high power, filters need to prevent electric field strengths approaching the breakdown point.

In order to state the physics of the analysis by Cohn, we suppose g_1, g_2 , g_3 , ..., g_n are element values of the low-pass prototype synthesized with Cohn's method [26]. E_T is the electric strength of the matched output waveguide, and E_1 , E_2 , E_3 , ... , E_n are the maximum electric field strength in the cavities. The cavity electric field strengths at the center of the pass-band for our planar SIW filter are given by the following formula [26]:

$$E_k = E_T \frac{\lambda_0}{\lambda_{g0}} \sqrt{\frac{2 g_k \omega_1'}{\pi w}} \tag{3.4.1}$$

where λ_0 is the wavelength in the dielectric, and λ_{g0} the guided wavelength of H_{10} wave in the input and output SIW waveguide, $w = (f_2 - f_1)/f_0$ the fractional band-width of the pass-band filter, and ω_1' is the equal-ripple band edge of the low-pass prototype. k is the cavity number.

The pulse-power capacity of a direct-coupled-resonator filter, at the center frequency, is given by [1, 26]:

$$(P_{qk})_0 = \frac{P_{qk}' \pi w}{2 g_k \omega_1'} \left(\frac{\lambda_{g0}}{\lambda_0}\right)^2 \tag{3.4.2}$$

where P_{qk}' is the pulse-power capacity of a matched waveguide having the same cross section as the cavity; g_k and ω_1' are the element value and equal-ripple band edge for low-pass prototype of Cohn, respectively.

If P_{qk} is moved to the left side, the relative power capacity can be obtained. This is a proper way to describe the power-handling capacity. Surely, the breakdown voltage of the dielectric material supplies the maximum value of E_k .

Setting $g_k = 1$, $\omega_1 = 1$, $w = 1.2\%$, λ_{g0}=8.87 mm and λ_0 = 7.29 mm into (3.4.2), the relative pulse-power capacity $\frac{(P_{qk})_0}{P_{qk}} = 2.8\%$.

The power flow of the H_{10} mode in an SIW waveguide is given by [14]:

$$P_{qk} = P_{10} = \frac{|A_{10}|^2 ab}{4}\left(\frac{\beta_{10}}{k_{c,10}}\right)^2 Z_{h,10} \tag{3.4.3}$$

For a rectangular waveguide in an x-y-z coordinate system, the field components expressed in terms of the amplitude coefficient A_{10} are:

$$H_z = A_{10}\cos\frac{\pi x}{a} e^{\mp j\beta_{10} z} \tag{3.4.4a}$$

$$H_x = \pm j\frac{\beta_{10}}{k_{c,10}^2} A_{10}\frac{\pi}{a}\sin\frac{\pi x}{a} e^{\mp j\beta_{10} z} \tag{3.4.4b}$$

$$E_y = -Z_{h,10} A_{10} j\frac{\beta_{10}}{k_{c,10}^2}\frac{\pi}{a}\sin\frac{\pi x}{a} e^{\mp j\beta_{10} z} \tag{3.4.4c}$$

$$E_x = E_z = H_y = 0 \tag{3.4.4d}$$

where $\beta_{10} = (k^2 - k_{c,10}^2)^{1/2} = \pi[(\frac{2}{\lambda})^2 - (\frac{1}{a})^2]^{1/2}$ is the phase constant of

$$Z_{h,10} = \frac{k}{\beta_{10}} Z_0 = \frac{Z_0}{\sqrt{1 - (\frac{\lambda}{2a})^2}}$$

In our application, since $n = 1$ and $m = 0$ in H_{10} mode which leads to $H_y = 0$ and $E_x = 0$, there is only one electric field component E_y whose amplitude in the middle of

the broad waveguide wall is $Z_{h,10}' A_{10} j \frac{\beta_{10}'}{k_{c,10}^2} \frac{\pi}{a}$. Setting this amplitude as the breakdown voltage of the dielectric (RT/duroid 6002), the maximum amplitude $A_{10}|_{max}$ of the longitudinal magnetic vector H_z can be obtained. Taking the value of $A_{10}|_{max}$ into (3.4.3), the maximum power flow of the SIW waveguide is obtained. Using (3.4.2), one may get the pulse-power capacity of the SIW filter.

Since measurement results for the dielectric breakdown voltage (DBV) of RT/Duroid 6002 is not currently available, the value was estimated in the following way.

The contents of RT/duroid 6002 are PTFE and ceramic. Because of its low permittivity characteristics, the main content is PTFE and thus its DBV value is close to that of PTFE. Table 3.4.1 lists the characteristics of PTFE and alumina ceramic.

Setting an estimated value of $30KV/cm$ for DBV, which is almost the same as that of air, into (3.4.4) and (3.4.3), the power capacity of the SIW waveguide is obtained, which is $P_{qk}' = 13.68KW$ for a waveguide cross-section of $a = 252mil$, $b = 10mil$. The power capacity of the SIW filter is limited by the minimum P_{qk}' value ($k = 1,2,3,4$).

Table 3.4.1 Characteristics of PTFE and alumina ceramic

Material	PTFE	Alumina
Relative dielectric constant ε_r	2.1 ~ 2.5	8 ~ 10
Loss tangent: $10^4 \times \tan\delta(@10GHz)$	3 ~ 15	1 ~ 15
Dielectric strength in KV/cm	~ 20	~ 90

Suppose that each cavity has the same power capacity. Simply setting $g_k = 1$ and $\omega_1' = 1$, due to the bandwidth of the narrow-band SIW filter of $w = 1.2\%$, the pulse-power capacity at center frequency $f_0 = 24GHz$ is $(P_{qk})_0 = 382W$. Working in a safety state, the practical power capacity of a waveguide is usually allowed to be one

third and even one fifth of the ultimate value. If one third of 382 W is considered, the safety operating power of the SIW filter is 127 W.

The power flow using different substrate material is an interesting perspective for the SIW guide. Table 3.4.2 lists the values of power flows in different SIW guides.

Table 3.4.2 Power flow of SIW guides of 10 mil thick & filter pulse power-capacity

Material	RT/duroid 6002	RT/duroid 6006	Aluminum nitride	Alumina ceramic	Sapphire
ε_r	2.94	6.15	8.9	9.9	11.5
$a \times b(mil \times mil)$	252x10	174x10	145x10	137x10	127x10
DBV (KV/cm)	30	62	100	150	180
Power flow (KW)	13.68	58.30	152.21	340.70	489.96
Pulse power capacity (KW)	0.382	1.628	4.242	9.526	13.71

Note: band-width $w = 1.2\%$

It is obvious that the pulse-power capacity is proportional to the fractional frequency width. If the band-width gets bigger, the power capacity increases.

Generally, in waveguide filter design, the cavity field strength may be made equal in direct-coupled cavity filters by choosing proper values of g_k , cavity height b_k and changing the number in half wavelength of the cavity. In this way, the power capacity of the waveguide filter may be maximized. In our planar configuration, b_k is a constant and cannot be changed. At the frequencies away from the center frequency in the pass-band, the power capacity decreases. The details of the physics behind that are neglected here.

Obviously, the pulse-power capacity is proportional to the substrate thickness for the SIW filters.

Keeping the same design specifications but using different substrate material, the power-capacities of the direct-coupled cavity filter integrated on a 10 mil substrate are listed in Table 3.4.2, where all the data were from a band-width of $w=1.2\%$ and by setting $g_k=1$, $\omega_1^{`}=1$ for the low-pass prototype.

Electric breakdown is one of the mechanisms for component reliability and failure. For a continuous working electronic component, heat breakdown is usually the main cause. The raise of temperature may result in a significant change of the electric resistivity and breakdown voltage of dielectric parameters, etc.

There are three internal factors producing heat in the SIW filter continuous operation and limiting the power capacity of the filter in steadily operation. AlN ceramic is a good candidate for microwave high power substrate due to its high thermal conductivity, low loss tangent and thermal expansion coefficient.

For the dielectric substrate, there are two mechanisms which lead to dissipation. One is the polarization loss in the dielectric. This is due to the lag of the electric field phase behind that of the $\bar{D}$ vector. The second mechanism is due to the conductive behavior of the dielectric which produces leakage current. The effective conductivity of the dielectric is $\sigma_{eff}=\omega\varepsilon^{``}=\omega\varepsilon_0\varepsilon_r\tan\delta_l$. When a RF electric field is applied to the component, the heat quantity produced due to the leakage current in the dielectric is proportional to the working frequency and the loss tangent.

3.5 Conclusion

Three direct-coupled cavity filters of four cavities are realized with the SIW technique on Rogers RT/duroid 6002 laminate microwave material. Based on the mode matching technique, the equivalent circuit as well as the reflection coefficients of the inductive discontinuities working as the coupling components are obtained numerically. The reflection coefficients are function of the geometrical dimensions of the coupling

parts. Inversely, the structural dimensions of the part are determined for the required reflection coefficient of each inter-cavity coupling. A filter synthesis procedure using Levy's modified formula based on a distributed stepped impedance low-pass prototype are used for the design of the three filters. Measurements have demonstrated that the results agree well with the design theories. The insertion loss of the asymmetrical iris filter reaches 3.4 dB. The high insertion loss of the filters is relatively high because of the high tangent loss material used. This should be improved by using high purity ceramic material whose tangent loss is a tenth of that of RT/Duroid 6002 and was temporarily unavailable at our lab. Increasing the thickness of the substrate may reduce the loss. However, a thickness greater than 20 mil may deteriorate the performance of the transition. A reason might be the radiation of the relatively wide microstrip structure of the 50 Ohm transmission line. Since the optimization software u-wave Wizard was only used for fifty days, the design for a 20 mil thick substrate wasn't completed. In that case, the slot width of the coupling parts needed to be increased to 20 mil. The curves in Chapter 1 give guidance to the reader for choosing the dielectric parameters.

REFERENCES

[1] G. L. Matthaei, L. Young and E. M. T. Jones, Microwave filters, impedance-matching networks, and coupling structures, McGraw-Hill Book Company, New York

[2] N. Marcuvitz, Waveguide Handbook, McGraw-Hill Book Company, London, 1986

[3] Leviatan, Y.; Li, P.G.; Adams, A.T.; Perini, J., "Single-Post Inductive Obstacle in Rectangular Waveguide," IEEE Trans. Microwave Theory and Tech., vol. MTT-31, pp. 806-812, Oct. 1983.

[4] Ping Guan Li; Adams, A.T.; Leviatan, Y.; Perini, J.;"Multiple-Post Inductive Obstacles in Rectangular Waveguide," IEEE Trans. Microwave Theory and Tech., vol. MTT-32, pp. 365-373, April 1984.

[5] Dominic Deslandes, Ke Wu, "Single-substrate integration technique of planar circuits and waveguide filters," IEEE Trans. Microwave Theory and Tech., vol. MTT-51, pp593-596, Feb. 2003.

[6] Giuseppe Conciauro, Marco Guglielmi and Roberto Scrrentino, Advanced Modal Analysis. John Wiley & Sons, Ltd., 1999

[7] A. Wexler, "Solution of waveguide discontinuities by modal analysis," IEEE Trans. Microwave Theory and Tech., vol. MTT-15, pp508-517, Sept. 1967.

[8] Y. C. Shih, "Design of waveguide E-plane filters with all-metal inserts," IEEE Trans. Microwave Theory and Tech., vol. MTT-32, pp695-704, July 1984.

[9] H. Patzelt and F. Arndt, "Double-plane steps in rectangular waveguides and their application for transformers, irises, and filters," IEEE Trans. Microwave Theory and Tech., vol. MTT-30, pp771-776, May 1982.

[10] R. J. Luebbers, B. A. Munk "Analysis of thick rectangular waveguide windows with finite conductivity," IEEE Trans. Microwave Theory and Tech., vol. MTT-21, pp461-468, July 1973.

[11] M. Guglielmi, F. Montauti, L. Pellegrini, and P. Arcioni, "Implementating

transmission zeros in inductive-window bandpass filters," IEEE Trans. Microwave Theory and Tech., vol. MTT-43, pp1911-1915, Aug. 1995.

[12] P. M. Morse and H. Feshbach, Methods of Theoretical Physics. New York: McGraw-Hill, 1953, pp928-929.

[13] N. Marcuvitz, Waveguide Handbook. London: Peter Peregrinus Ltd. 1986, Chapter 4.

[14] R. E. Collin, Foundations for Microwave Engineering. IEEE Press. New York, 1992

[15] R. E. Collin, Field Theory of Guided Waves. IEEE Press, New York, 1991

[16] S. W. Lee, W. R. Jones, and J. J. Campbell, "Convergence of Numerical Solution of Iris Type Discontinuity Problems," IEEE Trans. Microwave Theory Tech., vol. MTT-19, pp.528-536, June 1971.

[17] R. Mittra, T. Itoh, T. S. Li, "Analytical and numerical studies of the relative convergence phenomena arsing in the solution of an integral equation by the moment method," IEEE Trans. Microwave Theory Tech., vol. MTT-20, pp.96-104, Feb. 1972.

[18] Y. C Shih, K. G. Gray, "Convergence of numerical solutions of step-type waveguide discontinuity problems by modal analysis," in 1983 IEEE/MTT-S Intl. Microwave Symp. Dig., May 1983, pp.233-235

[19] L. Young, "Quarter-wave transformer prototype circuit," IRE Trans. on Microwave Theory Tech., vol. MTT-8, pp. 483-489, Sept. 1960.

[20] L. Young, "Stepped-impedance transformers and filter prototypes," IRE Trans. on Microwave Theory Tech., vol. MTT-10, pp. 339-359, Sept. 1962.

[21] L. Young, "Direct-coupled cavity filters for wide and narrow bandwidths," IEEE Trans. Microwave Theory Tech., vol. MTT-10, pp. 162-178, May, 1963

[22] R. Levy, "Tables of element values for the distributed low-pass prototype filter," IEEE Trans. Microwave Theory Tech., vol. MTT-13, pp. 514-536, Sept. 1965.

[23] J. D. Rhodes, "Design formulas for stepped impedance distributed and digital wave maximally flat and Chebyshev low-pass prototype filters," IEEE Trans. Circuits Syst., vol CAS-22, pp. 866-874, Nov. 1975

[24] R. Levy, "Theory of direct-coupled-cavity filters," IEEE Trans. Microwave Theory Tech., vol. MTT-15, pp. 340-348, June. 1967.

[25] S. B. Cohn, "Direct-coupled-resonator Filters," IRE Trans., Proc. IRE, VOL. 45, pp. 187-196, Feb. 1957.

[26] S. B. Cohn, "Design consideration for high power microwave filters," IRE Trans., PGMTT-7, pp. 149-153, Jan. 1959.

[27] S. B. Cohn, "Dissipation loss in multiple-coupled-resonator filters," Proc. IRE 47, pp.1342-1348 (August 1959).

[28] L. Young, "Group delay and transmission loss in transmission-line filters," IEEE Trans. PTGMTT-11, pp. 215-217 (May 1963).

[29] F. D. Paolo, Network and devices using planar transmission lines, CRC Press, 2000

[30] D. Deslandes, Ke Wu, "Integrated microstrip and rectangular waveguide in planar form," IEEE, Microwave and Wireless Components Letters, Vol. 11, Issue 2, pp.68-70, Feb. 2001

[31] D. Deslandes, "Analysis and design of circuit probe transition from grounded coplanar to substrate integrated rectangular waveguide" IEEE Trans. Microwave Theory Tech., vol. MTT-53, pp. 2487-2494, Aug. 2005.

[32] R. N. Simons, Coplanar waveguide Circuits, Components and Systems. New York: Wiley, 2001

[33] Product Note 8510-8A, "Applying the HP 8510 TRL calibration for non-coaxial measurement," Agilent.

Chapter 4 CROSS COUPLINGS, DUAL-MODE RESONANCE IN WAVEGUIDES

In this part of the thesis, the filters designed with the full-wave simulation method are presented. The filters developed in this chapter are based on the dual mode resonance mechanism for rectangular waveguides proposed in [19]. The discontinuities formed by the aperture between the waveguide input/output port and the cavity and the aperture between the cavities might be numerically analyzed on the basis of multiple mode network representation. Therefore, the coupling coefficients between modes can be calculated. They are a function of geometric parameters. The required dimensional parameters of the proposed filtering structure in [19] may be obtained through conventional approaches as described in the example of Section 4.1. However, the performance of the dual mode rectangular cavities does show lower insertion loss compared to that of the filter built in a single mode resonator. This feature gives the predominance to apply the structure to filter design. In this chapter, we simply and directly use the full-wave simulation tool Ansoft HFSS to reach that goal.

The coupling relationship between the modes in the structure can be well explained with general synthesis theory, even though the used coupling coefficients and the corresponding structural parameters such as cavity length and width, aperture length and width etc., were not obtained from the conventional design method, as demonstrated in Section 4.1. In Section 4.1 and 4.2 of this chapter, the coupling relationship in filters will be described and additional examples will be given. The feasibility of employing a few rectangular dual mode combinations shall be demonstrated after introducing the design principle in Section 4.3.1. Then, the designed filters employing a rectangular H_{203} & H_{104} dual mode combination will be demonstrated in Section 4.4.

4.1 General Synthesis Theory

An account of the equivalent circuit theory for generally coupled cavities was given by Reiter [2]. General synthesis theory was developed by Atia and Williams [3, 5, 6, 7, 8] in the 1970s. If the frequency band of interest is narrow, each cavity can be treated as a single resonant circuit with multiple couplings to other cavities, thus reducing the equivalent circuit to that shown in Fig. 4.1.1.

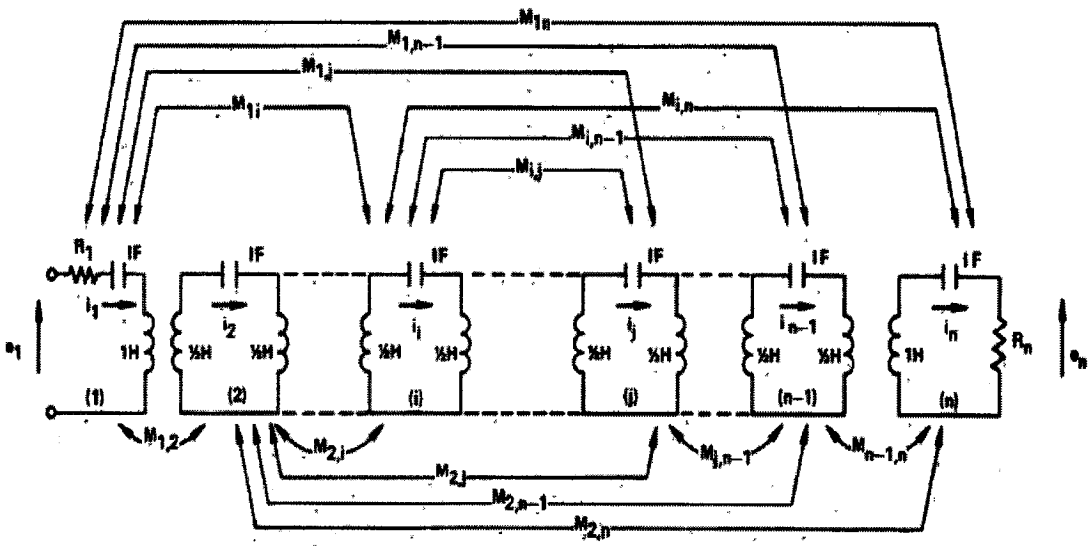

Fig. 4.1.1: General equivalent circuit of n arbitrary coupled cavities.

e_1 and e_n are the input and output voltages, and i_1, ..., i_n are the currents of each cavity, respectively. Mutual couplings between cavities are indicated in the figure as M_{ij}. With reference to the equivalent circuit, the loop equations for narrow bandwidths can be written as:

$$\begin{pmatrix} e_1 \\ 0 \\ 0 \\ . \\ . \\ . \\ 0 \end{pmatrix} = \begin{pmatrix} S+R_1 & jM_{12} & jM_{13} & & . & . & . & jM_{1n} \\ jM_{12} & S & jM_{23} & & . & . & . & jM_{2n} \\ jM_{13} & jM_{23} & S & & . & . & . & jM_{3n} \\ . & . & . & . & . & . & . & . \\ . & . & . & . & . & . & . & . \\ . & . & . & . & . & S & & jM_{n-1,n} \\ jM_{1n} & . & . & . & . & jM_{n-1,n} & & S+R_n \end{pmatrix} \begin{pmatrix} i_1 \\ i_2 \\ i_3 \\ . \\ . \\ i_{n-1} \\ i_n \end{pmatrix} \tag{4.1.1}$$

where

$$S = j(\omega - \frac{1}{\omega})$$

$$jM_{ij} \approx j\omega M_{ij} = j\omega_0 M_{ij}$$

$$\omega_0 = 1 \qquad rad/s$$

Furthermore, the impedance matrix Z can be expressed in the form:

$$Z = (SI + M_R) \tag{4.1.2}$$

Where

I = *the identity matrix*

$M_R = R + jM$

and the matrix R has all zero entries except for the (1, 1), (n, n) elements, which are R_1 and R_2, respectively. M is called the coupling matrix and has general entries of M_{ij} for $i \neq j$, and 0 for $i = j$.

The general coupling theory shows how the matrix M_R can be evaluated in terms of a given low-pass transfer function $t(s)$ $(s = j\omega)$. Then, by following Darlington's procedure [1], the short-circuit input and transfer admittances can be obtained. The poles of the short-circuit admittances are the eigenvalues of the coupling matrix M.

The synthesis of band-pass filters in waveguide cavities is most conveniently accomplished by assuming a symmetric network, i.e. $R_1 = R_n = R$ and that M is symmetrical about the anti-diagonal (as well as about the main diagonal).

Generally, there are three basic types of filtering functions:

1. Butterworth response
2. Chebyshev response
3. Elliptic response

In theory, the transmission zeros (TZ) of a Chebyshev filter are determined at the infinite frequencies. The attenuation in the stop-band of the filter drops monotonically from the pass-band edge to the TZs at infinite frequencies. The conventional direct-coupled cavity filters designed in Chapter 3 are of this type.

The elliptic type response function yields the best frequency selectivity because it provides transmission zeros near the pass-band of the filters, making the insertion loss in the stop-band increase rapidly.

For narrow-bandpass waveguide filters having ripples in both the pass band and stop band (elliptic response), the general low-pass power transfer function that can be synthesized in coupled cavities is given in [6]. A generic coupling scheme in a folded waveguide structure through small slots and cross slots was proposed also.

Taking a four-cavity elliptic waveguide filter as an example, a general synthesis procedure is described below [4].

1. Filtering function producing

A fourth-order antimetric elliptic filtering function for the low-pass prototype is defined as

$$R_{4a}(\omega_1) = \frac{\omega_1^2(\omega_1^2 - \omega_z^2)}{(\omega_1^2 - \omega_p^2)} \tag{4.1.3}$$

where ω_z, ω_p are zeros and poles of the function, respectively, while ω_1 is the angular frequency.

After the filtering function is given and the low-pass-to bandpass transformation $\omega_1 = \frac{1}{\Delta\omega}(\frac{\omega}{\omega_0} - \frac{\omega_0}{\omega}) = \frac{W}{\Delta\omega}$ is applied, the power-transmission function may be written as:

$$|t|^2 = \frac{1}{1+\varepsilon^2 R_{4a}^2(\omega)} = \frac{1}{1+\varepsilon^2(\frac{W}{\Delta\omega})^4\{\frac{W^2-\Delta\omega^2\omega_z^2}{W^2-\Delta\omega^2\omega_p^2}\}^2} \qquad (4.1.4)$$

The above is for a band-pass filter with four transmission poles and two finite transmission zeros on either side of the pass-band. The poles can be established by four-coupled cavities and the zeros by coupling energy directly from the first to the last cavity.

2. Physical Structure to Implement the Filtering Function

A waveguide structure which satisfies these conditions is shown in Fig. 4.1.3. This employs four directly H_{111} mode coupled circular cavities with additional coupling being provided between the first and fourth cavities. The equivalent circuit of this structure which is readily analyzed by using the impedance matrix is shown in Fig. 4.1.2.

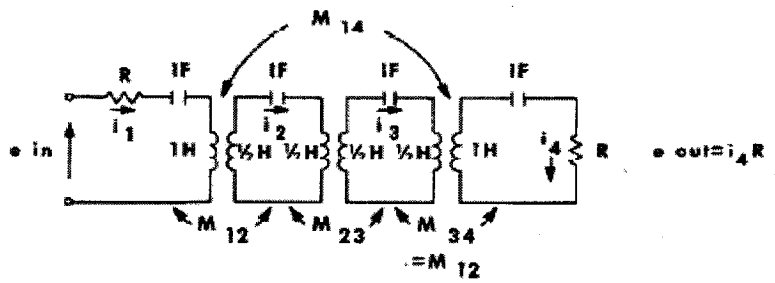

Fig. 4.1.2: Four-cavity waveguide equivalent circuit

The voltage-current equation for this circuit becomes:

$$\begin{pmatrix} e_1 \\ 0 \\ 0 \\ 0 \end{pmatrix} = \begin{pmatrix} R+jW & jM_{12} & 0 & jM_{14} \\ jM_{12} & jW & jM_{23} & 0 \\ 0 & jM_{23} & jW & jM_{12} \\ jM_{14} & 0 & jM_{12} & R+jW \end{pmatrix} \begin{pmatrix} i_1 \\ i_2 \\ i_3 \\ i_4 \end{pmatrix} \tag{4.1.5a}$$

where i_1, i_2, i_3, i_4 are the loop currents, $W = (\omega - 1/\omega)$ and ωM is approximately equal to $\omega_0 M$ $(= M)$ for a narrow-bandpass filter, or

$$(E) = (Z)(I) \tag{4.1.5b}$$

The output current i_4 and hence the output voltage e_4 can be evaluated from

$$i_4 = e_1 \frac{D(cofZ_{14})}{D(\Delta)}$$

and

$$\frac{e_4}{e_1} = \frac{RD(cofZ_{14})}{D(\Delta)} \tag{4.1.6a}$$

where

$D \equiv$ determinant

cof $\equiv$ cofactor

$\Delta \equiv$ elements of Z

Evaluating (4.1.6a) gives

$$RD(cofZ_{14}) = jR\{-M_{12}^2 M_{23} - W^2 M_{14} + M_{23}^2 M_{14}\}$$

and

$$\begin{aligned} D(\Delta) = {} & W^4 + W^2\{-R^2 - M_{23}^2 - M_{14}^2 - 2M_{12}^2\} \\ & + \{M_{23}^2 R^2 - 2M_{12}^2 M_{14} M_{23} + M_{12}^2\} \\ & + jW\{W^2(-2R) + 2M_{12}^2 R + 2RM_{23}^2\} \end{aligned} \tag{4.1.6b}$$

Since the circuit is equally terminated, the overall transmission ratio can be written as

$$|t| = 2\left|\frac{e_4}{e_1}\right| \tag{4.1.7}$$

or

$$|t|^2 = \frac{4R^2\{-M_{12}^2 M_{23} - W^2 M_{14} M_{23}^2 + M_{23}^2 M_{14}\}^2}{D} \tag{4.1.8}$$

where

$$\begin{aligned} D &= W^8 + W^6\{2C + R^2\} \\ &\quad + W^4[2D + C^2 - 8R^2(M_{12}^2 + M_{23}^2)] \\ &\quad + W^2[2CD + 4R^2(M_{12}^2 + M_{23}^2)^2] + D^2 \end{aligned}$$

and

$$\begin{aligned} C &= -R^2 - M_{23}^2 - M_{14}^2 - 2M_{12}^2 \\ D &= M_{23}^2 + \{M_{12}^2 - M_{23}M_{14}\}^2 \end{aligned}$$

3. The Realization of the Coupling Matrix

By equating (4.1.8) to (4.1.4), the unknowns R, M_{12}, M_{23}, M_{14} can be expressed in terms of the zeros (ω_z), the poles (ω_p) and the ripple constant (ε). These equations are the following:

$$\begin{aligned} R^2 &= -\frac{\Delta\omega^2}{2}\{\omega_z^2 - \frac{2\omega_p}{\sqrt{2\varepsilon}}\} \\ &\quad \pm \frac{1}{2}\sqrt{\Delta\omega^4\{\omega_z^2 - \frac{2\omega_p}{\sqrt{2\varepsilon}}\}^2 - 4\Delta\omega^4\{\frac{\omega_p}{2\sqrt{2\varepsilon}} - \frac{\omega_p^2}{2\varepsilon} - \frac{1}{4\varepsilon^2}\}} \end{aligned} \tag{4.1.9}$$

$$M_{14} = -\frac{\Delta\omega^2}{2\varepsilon R} \tag{4.1.10}$$

$$M_{23} = \Delta\omega^2 \frac{\omega_p}{\sqrt{2\varepsilon}} \frac{1}{R} \tag{4.1.11}$$

$$M_{12}^2 = RM_{23} + M_{14}M_{23} \tag{4.1.12}$$

The four-coupled cavity structure was designed in the following manner. First, the parameter R which represents the reciprocal of the loaded cavity $Q(Q_e)$ of the first and last cavity is achieved by designing a long thin coupling slot. Second, coupling slots between the second and third cavities and the first and fourth cavities can be made to reproduce the parameters M_{23} and M_{14} . Third, the parameter M_{12} can be produced by coupling screws oriented at 45° to the normal field polarizations. It should be noted that for a positive and real R, M_{14} must be negative. This is achieved by placing the two coupling screws at spatial orientations 90° apart to obtain a field reversal of 180°. Finally, the effect of all these couplings is to increase the cavities' electrical lengths; this must be compensated for in the cavity design.

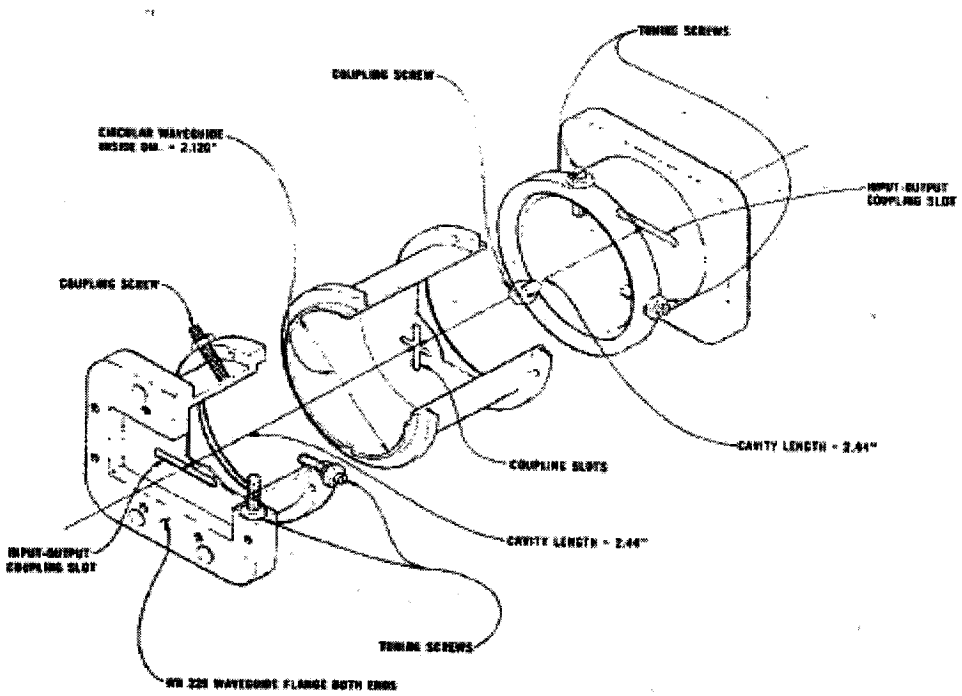

Fig. 4.1.3: The realization of the filter

4. The Physical Dimensions of the Cavities and the Coupling Parts

The magnetic polarizability of the long coupling slot after it is modified for slot thickness (t_s) [10, 11] is:

$$M_{1,2}(new) = \frac{M_{1,2}(old)}{1-(\frac{\lambda_l}{\lambda_0})^2} 10^{-\alpha} \tag{4.1.13}$$

where λ_l is the resonant slot length and λ_0 is the free-space wavelength.

The input-output transformers of the filter are designed to give the required loaded $Q_e(=1/R)$ of the first and last circular waveguide cavities. Matching of the filter to and from the rectangular waveguide was chosen to simplify subsequent waveguide measurements.

The loaded Q_e and magnetic polarizability M are related by

$$M^2 = \frac{abl_c\lambda_g(3R_0^2)}{4\pi Q_e\lambda_0^2} \tag{4.1.14}$$

where

l_c length of the circular cavity

a,b inside dimensions of the rectangular waveguide

λ_g rectangular waveguide wavelength

λ_0 free-space wavelength

R_0 circular cavity inside radius

A combination of (4.1.14), (4.1.13), and Cohn's curves for M gives the required coupling-slot dimensions for a given R.

The coupling coefficient (k) between circular waveguide cavities is related to the magnetic polarizability (M) by

$$k = \frac{M \lambda_0^2}{l_c^3 (3 R_0^2)} \tag{4.1.15}$$

Since the coupling coefficient can be directly related to the mutual couplings of the equivalent circuit in Fig. 4.1.2., the appropriate coupling-slot lengths can be determined with equation (4.1.14).

Since the cavity oscillation is the fundamental circular H_{111} mode, the electrical length of cavities is given by $\lambda_{gc}/2(=l_c)$. The physical length of each cavity must be adjusted because of the resonant frequency changing due to each coupling.

The reactance (x/Z_0) of the input coupling slot is given by

$$(\frac{x}{Z_0}) = \frac{4\pi (M)}{3 R_0^2 \lambda_{gc}} \tag{4.1.16}$$

and therefore the length correction due to R is approximately

$$\frac{l_c}{2\pi} \tan^{-1}(\frac{2x}{Z_0}) \tag{4.1.17}$$

The correction due to the internal iris and screw couplings can be calculated by equating the fractional change in resonant frequency of each cavity to the coupling k.

The filter response is shown in Fig. 4.1.4. The structure is actually a two cavity dual mode filter in a circular waveguide.

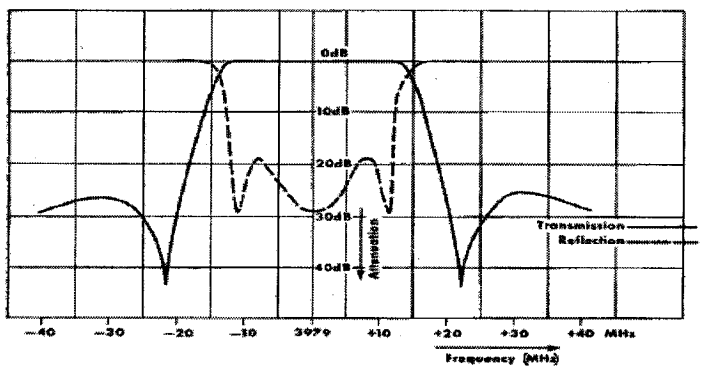

Fig. 4.1.4: Filter response

4.2 More Examples of Coupling Scenarios --- Realization of Finite Transmission Zero

Simple cascaded waveguide filters, of either Chebyshev or Butterworth design, have no finite transmission zeros. This cannot make the frequency selectivity on the skirt of the filter be able to achieve better band rejection. General synthesis theory supplies a method which considers all possible mutual couplings between cavities. Extra couplings between non-adjacent cavities have been widely used to improve filter performance. However, the synthesized coupling matrix is not always able to be physically realized in practice.

In this section, a few physical realizations which are adopted to improve filter properties are listed. Some were based on the general synthesis theory and some were designed by using other methods. The following examples were chosen for depicting the principles we need.

4.2.1 Direct-Coupled Cavity Filter

Three-resonator filters with extra coupling K_{13} between resonator 1 and 3 have been reported [13]. Double posts were used to implement the couplings K_{01} and $K_{34}(=K_{01})$ between input (output) waveguide and cavity 1 (cavity 3). Sidewall couplings K_{12} and K_{23} employing circular apertures, which is the same as that in a directional coupler, were used between cavities 1 and 2, and between cavities 2 and 3. The bridging coupling K_{13} used an inductive circular iris in a thin metallic plate. This configuration provides band rejection behavior on one filter skirt.

In order to produce band reject behavior on both filter skirts, a general four-resonator filter was employed in the coaxial cavity by the same researcher [14]. The bridging coupling K_{14} holds the opposite sign of the normal couplings (K_{12}, K_{23}).

Providing phase reversal in the cross-coupling results in TZs in the stop-band of the filters.

Filter prototypes implementing TZs at finite frequencies, in view of equalizing the time delay, were introduced by Rhodes [15]. Rhodes provided the exact prototype of a filter formed by two parallel direct-coupled waveguide filters, where adjacent cavities were cross-coupled via their common narrow wall in order to generate TZs. In specific cases, there is a possibility to change the circular coupling holes into other shapes.

A structure similar to that in [13] is shown in [16] where the side wall circular apertures were replaced by square apertures with equal height to the cavity. The element values were explicitly given in terms of the classical Cohn's in-line prototype, with minor modifications. The apertures with the same height as the waveguide coupling the cavities allow for it to be directly applied to planar SIW filter realization.

With the same mechanism as that used to produce TZs, a folded E-plane metal insert filter was realized [17]. In the configuration, one more cross-coupling is used for source-load coupling. The responses of the conventional Chebyshev filter, cross-coupling filter and cross-coupling filter with load-source coupling are demonstrated. The obvious improvement of frequency selectivity on both the filter skirts can be seen in the two four-cavity filters with cross-coupling.

4.2.2 Dual-mode Waveguide Cavity Filter

Reversing the phases between the coupled non-adjacent cavities so as to produce negative coupling K_{14} can be amazingly realized in dual mode waveguide structures. The filter by Williams, with four poles and two TZs, was realized with circular waveguide $H_{111}-$moded circular cavities [4]. As shown in Fig. 4.1.3, two circular waveguide cavities were separated by a thin plate with a cross slot and the input and output cavities were coupled to the rectangular waveguide through horizontal coupling slots. The cross slot between the two cavities, together with the coupling screws, make it possible to

excite two degenerate H_{111} modes in the cavities. As an example of the general synthesis theory, the design method has been described in Section 4.1.

In the filter structure, a coupling screw is inserted at an orientation of 45° to the normal field polarization. The incident wave in the first cavity is split into modes 1 and 2 of $H_{111}^{\square}$, which produces M_{12}. In the second cavity, a coupling screw splits the field into two degenerate modes, 3 and 4. The spatial orientation of 90° apart gives a field reversal of 180°, producing $M_{14} < 0$.

Fig. 4.2.1 demonstrates the polarizations and mode couplings of a generic longitudinal dual mode filter in a circular waveguide.

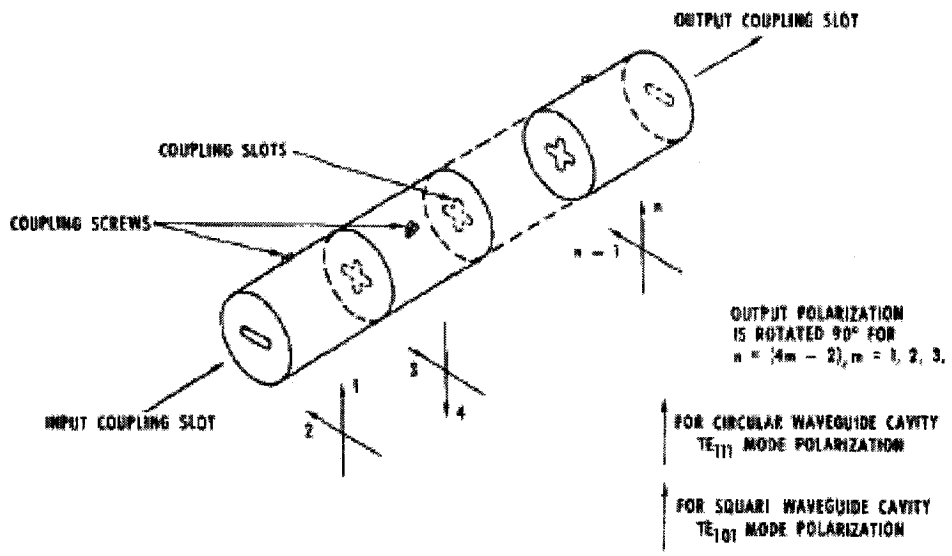

Fig. 4.2.1: Longitudinal dual mode filter in circular waveguide

It is demonstrated in literature that the general form of band-pass transfer functions of symmetrical networks can be realized in either single- or dual-mode coupled-waveguide cavities. The filter realization in a rectangular cavity dual-mode waveguide

was reported [7], where a sixth-order elliptic response with four TZs from a rectangular-cavity dual-mode waveguide was obtained. Two TZs are on the lower side of the pass-band while the other two are on the upper side of the bass-band. However, we should be aware that the fabrication of the rectangular dual mode cavity filter is more difficult due to the small slot on cavity side walls.

4.3 Rectangular Waveguide Dual-Mode Filter

As we have seen from the examples in Section 4.2, employing two degenerate modes in one resonator can greatly reduce the weight and volume of the conventional waveguide filters. From the perspective of the SIW technique, it is almost impossible to make a circular waveguide cavity in a dielectric substrate. Moreover, the coupling component and tuning screw necessary for the dual mode excitation, in many cases, can only be realized in three dimensional spaces, which is impossible to integrate in a thin planar substrate. Hence, our choice is naturally converted to using the rectangular cavity for the dual mode filter design.

Being confined to the coupling scenario on a SIW cavity, two types of topologies may meet the requirement of a rectangular cavity dual mode filter. If a coupling aperture is put on the broad wall of the rectangular cavity, multiple layer substrates must be employed. This increases the difficulty of the fabrication process. If a coupling aperture is only placed on the end and side walls of the rectangular waveguide, the component can be fabricated on one layer of substrate. We use the later one in this project.

Conventional single mode resonator filters and many other designs [14, 15, 16, 17, 18, 19], basically present single-mode filter structures in which each resonator provides one transmission pole, and where the higher order mode interactions are used to implement transmission zeros to improve the filter selectivity. Reference [19] proposed a new family of all-inductive dual-mode scenarios, where the novelty introduced is that

each cavity of the structures produces two transmission poles and at least one transmission zero and the all-inductive coupling of the inter-cavity allows for the implementation of simple planar dual-mode filters on the substrate.

4.3.1 Basic Characteristics of rectangular dual mode cavity

Let us suppose an ideal rectangular waveguide cavity of dimensions a, b and l. Suppose the eigenvalue relative to dimension b is equal to zero, the condition so that both modes resonate at the same frequency is:

$$\left(\frac{m\pi}{a}\right)^2+\left(\frac{n\pi}{l}\right)^2=\left(\frac{p\pi}{a}\right)^2+\left(\frac{q\pi}{l}\right)^2 \tag{4.3.1}$$

Where the subscripts m, n refer to the first mode and p, q refer to the second. Equation (4.3.1) leads to the following expression for the initial choice of the ratio a/l in relation to the chosen mode pair:

$$\frac{a}{l}=\sqrt{\frac{m^2-p^2}{q^2-n^2}} \tag{4.3.2}$$

The resonance wavenumber is given by

$$k_0=\sqrt{\left(\frac{m\pi}{a}\right)^2+\left(\frac{n\pi}{l}\right)^2} \tag{4.3.3}$$

The constraint condition that must be imposed in order to obtain a dual-mode operation is that the modal indexes m and p (and n and q) must be different. By imposing this condition, one ensures that on each side of the resonator the fields of the chosen resonant modes are orthogonal, thereby allowing for dual-mode operation.

With the help of a full-wave simulator, the design of filters in this family could be very easy. The only inconvenience is that it is hard to give a strict relationship between frequency response and the filter specification. However, although microwave filters are

theoretically designed with the lumped-components theories, they are realized in an approximate distribution circuit. All microwave filters are difficult to replicate with exact conformity. Usually, this difficulty is overcome by iteration in the second routine to correct and complete the design procedures. Correction may be done by iteration so as to fulfill a precise design's specifications. In the stage of optimization, software such as u-wave Wizard or CST may implement this task efficiently by producing the optimal structural parameter set. Furthermore, the numerical efficiency of the electromagnetic analysis in full-wave simulation is pretty high.

The investigation of a single cavity with different mode-pair combination is a must, and this compensates for the weakness and gives brief information on cavity selection for given specifications.

4.3.2 Full-Wave EM Simulating Investigation on single cavities

When the rectangular waveguide is filled with dielectric, the wave number in the dielectric is given by:

$$k_0 = \frac{2\pi\sqrt{\varepsilon_r}}{\lambda_0} = \frac{2\pi f_0\sqrt{\varepsilon_r}}{c} \tag{4.3.4}$$

Equating (4.3.3) and (4.3.4), the length and width of the resonator cavity can be evaluated.

Table 4.3.1 lists the structural parameters of a few cavities on different substrates and at different resonant frequencies. When two cavities are connected, the presence of the coupling apertures between them makes their effective length longer, resulting in the resonant frequency shift to the lower frequency. This can be adjusted by reducing the cavity length and width.

Table 4.3.1 Structural parameters l and a of closed single SIW cavities

$f_0(GHz)$	m	n	p	q	material	ε_r	l (mil)	a (mil)
25	1	2	2	1	Duroid 5880	2.2	356	356
32	1	2	2	1	ceramic	9.9	131	131
25	3	1	1	2	Duroid 5880	2.2	333	544
25	3	1	1	2	ceramic	9.9	157	256
24	3	1	1	2	Duroid 5880	2.2	347	567
25	2	3	1	4	ceramic	9.9	321	210
31	2	3	1	4	ceramic	9.9	259	170
32	2	3	1	4	ceramic	9.9	251	164
24	2	3	1	4	Duroid 6002	2.94	614	402
77	2	3	1	4	Duroid 6002	2.94	191	125

The dual mode response of a H_{102} & H_{201} cavity resonating at 11 GHz is given in Fig. 4.3.1. The resonant size (air filled) is about 30 mm given in [19]. The result was obtained using a coupling aperture 10-mm wide and 2-mm thick with zero offset and a standard WR75 waveguide as input and output port. The basic dual behavior is clearly evident. The cavity presents one transmission zero on the right hand side of the pass-band. The zero is due to the fact that the input output apertures couple to both the H_{102} and H_{201} modes. Since the H_{102} resonance changes sign with respect to the field going from the input to the output, a destructive interference is produced, resulting in a transmission zero. The position of the transmission zero can be easily moved to the left-hand side of the pass-band by changing the ratio of cavity length to cavity width. Besides the computation in [19], this is also confirmed by the simulation of a 25 GHz SIW cavity on RT/duroid 5880, shown in Fig. 4.3.2.

The frequency response of a H_{102} & H_{301} single cavity is shown in Fig. 4.3.3.

The frequency response of a H_{203} & H_{104} single cavity is shown in Fig. 4.3.4.

If the aperture offset has different values, a single cavity may produce two TZs, which is shown in Fig. 4.3.5.

Compared to the performance of the H_{102} & H_{201} combination, the transmission zero produced in H_{203} & H_{104} is slightly further away from the pass-band, as shown in Fig 4.3.4.

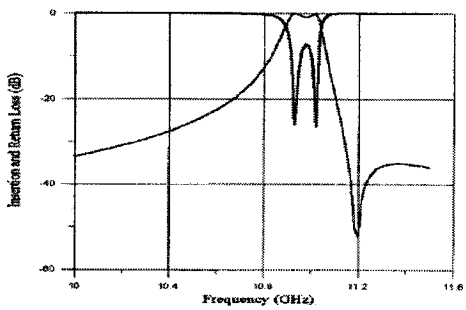

Fig. 4.3.1: The response of a single cavity

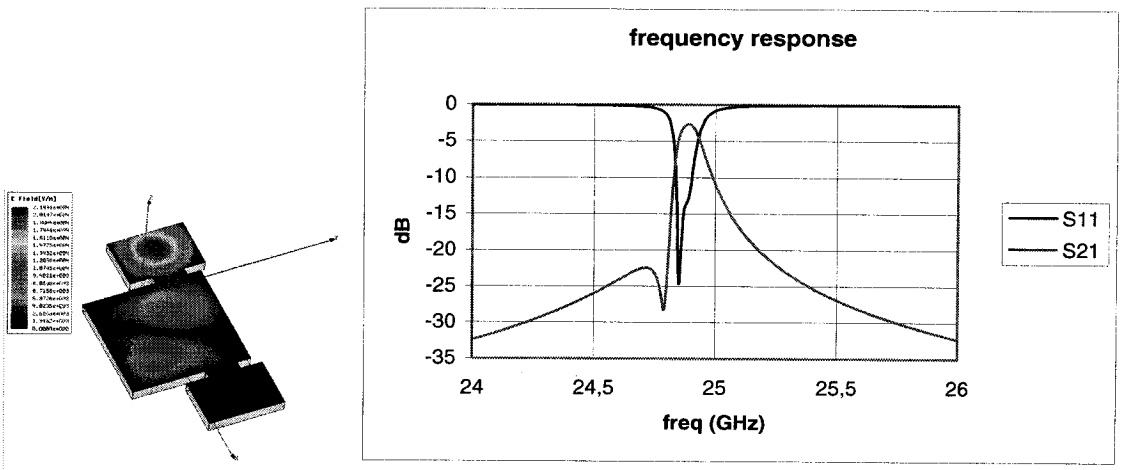

(a) H_{102} & H_{201} single cavity & wave injection (b) Frequency Response

Fig. 4.3.2: H_{102} & H_{201} single cavity response: $\varepsilon_r = 2.2$; cavity: l=346.85 mil, a=356.3 mil; Aperture: 25.2 mil x 94.5 mil; offset: 90.6 mil; input/output port: 228.3 mil; thickness: 31 mil.

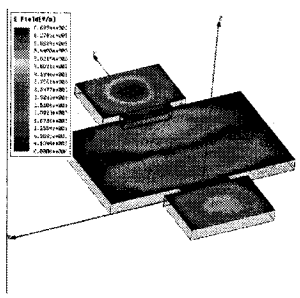

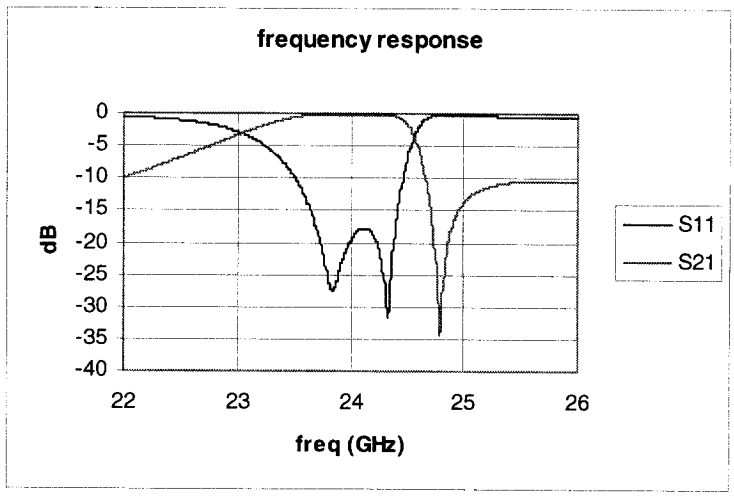

(a) H_{102} & H_{301} single cavity (b) Frequency response

Fig. 4.3.3: H_{102} & H_{301} single cavity: $\varepsilon_r = 2.2$; cavity: l=315 mil, a=551 mil; Aperture: 17.7 mil x 145.3 mil; offset: 0 mil; input/output port : 249.2 mil; thickness : 31 mil

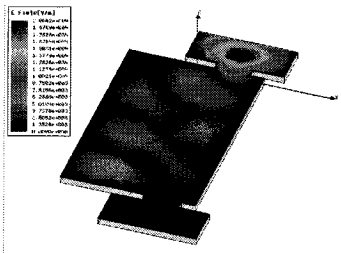

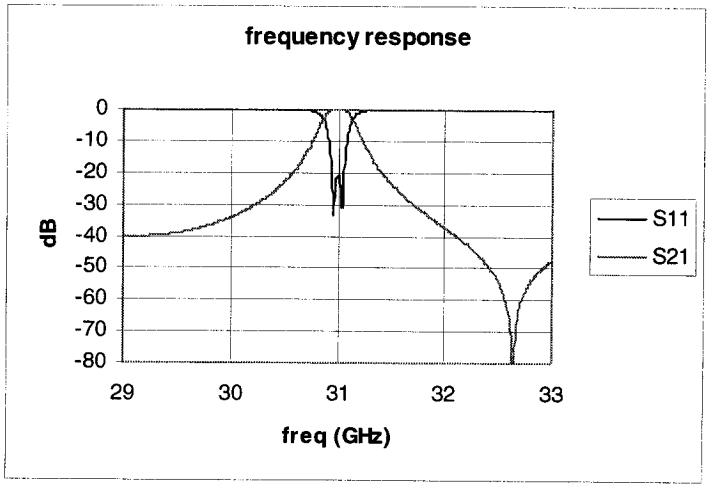

(a) H_{203} & H_{104} single cavity & wave injection (b) frequency response

Fig. 4.3.4: Single cavity: $\varepsilon_r = 9.9$; cavity: l=253.2 mil, a=168.1 mil; Aperture: 9mil x 45 mil; offset: 20.5 mil; input/output port; 122 mil; h = 31 mil

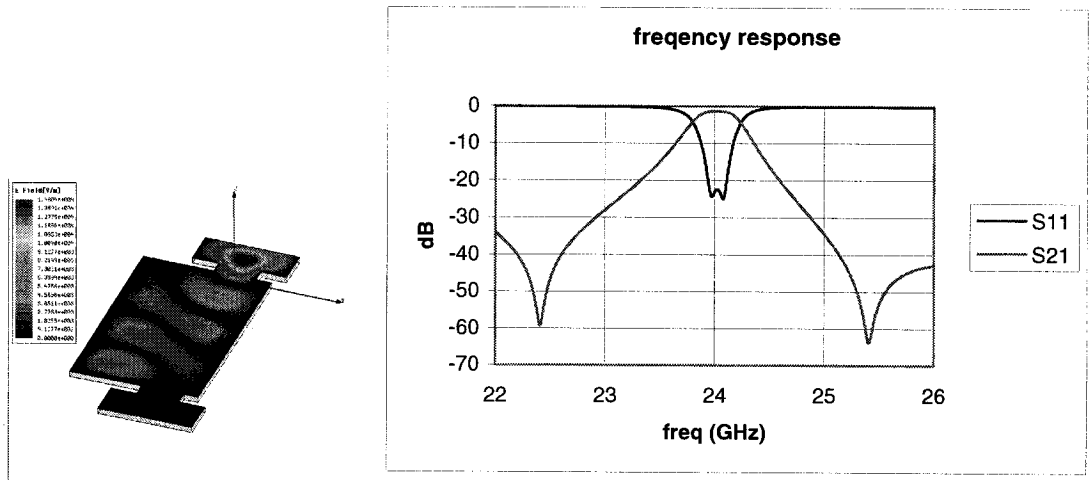

(a) H_{203} & H_{104} single cavity & wave injection (b) frequency response

Fig. 4.3.5: Single cavity on TMM3 15 mil thick: $\varepsilon_r = 3.27$; cavity: l=565.09 mil, a=365.3 mil; Aperture: 37.11mil x 120.16 mil; offset 1: 77.25 mil, offset 2: 71.99 mil ; input/output port : 268.13 mil; h = 15 mil

4.3.3 Full-Wave EM Simulation Investigation of Combinations of Two Cavities

Based on the mechanism that the field phase interference at the input and output aperture of the single dual mode cavity, one can make use of one dual mode cavity to supply one transmission zero. When two dual mode cavities are combined, it is expected to produce two transmission zeros. As stated in Section 4.3.2, the position of the transmission zero can be changed either by adjusting the cavity size or the position of the aperture. The TZs may be put on one side of the pass-band, as shown in Fig. 4.3.6. One TZ on the left side and the other on the right side of the pass-band is realized by either two H_{102} & H_{201} cavities or two H_{203} & H_{104} cavities, as shown in Fig. 4.3.7 and Fig. 4.3.8.

When two cavities are connected through an aperture, the values of the coupling coefficients for a direct-coupled cavity filter can be referenced to decide the aperture lengths. Since the inter-cavity coupling coefficients in the middle are usually smaller

compared with that between cavity and input/output waveguide, the aperture length in the middle is longer so as to produce smaller coupling. In contrast, the input/output coupling aperture length is small so as to supply bigger coupling coefficients.

Because of difficulties in realizing this process in our lab, bigger sizes are expected for higher frequency and millimeter wave components so that the fabrication is easier. We chose a cavity with the combination of H_{203} and H_{104} in the following designs.

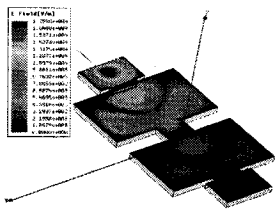

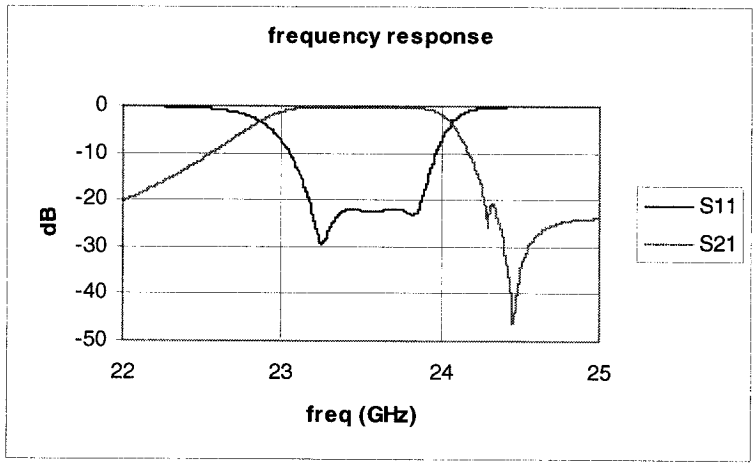

(a)The structure of two H_{301} & H_{102} cavity (b) Frequency response of the non-optimized structure

Fig. 4.3.6: The combination of two H_{301} & H_{102} cavities: $\varepsilon_r = 2.2$; cav_1: 8.12 mm x 14.3 mm; cav_2: 8.08 mm x 14.2 mm; apert_1: 0.45 mm x 3.62 mm; apert_2: 2.3 mm x 3.69 mm; apert_3: 0.45 mm x 3.76 mm; offset: o; port: 6.33 mm, h=31 mil

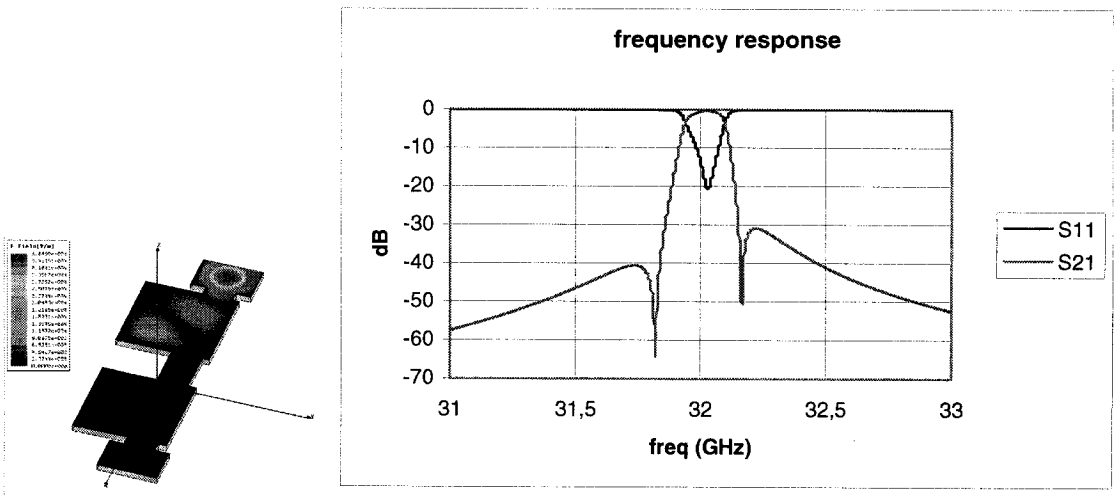

(a) The structure of two H_{102} & H_{201} (b) Frequency response of the non-optimized structure

Fig. 4.3.7: The combination of two H_{102} & H_{201} cavities: $\varepsilon_r = 9.9$; cav_1: 125.6 mil x 129.4 mil; cav_2: 123.8 mil x 130.5 mil; apert_1 & apert_3: 13.2 mil x 41.8 mil, offset_1 =21.4 mil; apert_2: 58.9 mil x 28.8 mil, offset_2 = 21.4 mil; port: 83.6 mm, h=10 mil

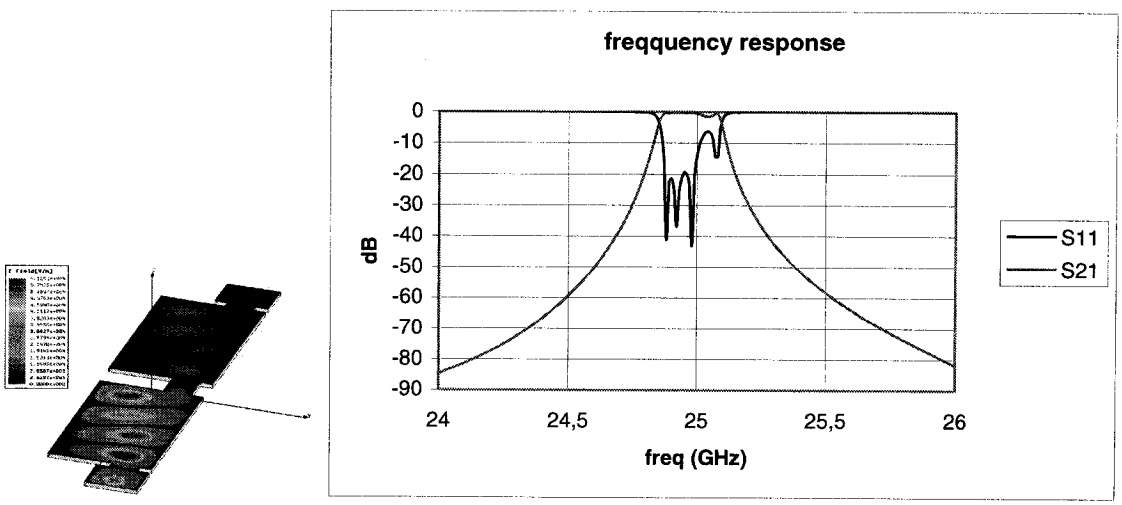

(a)The structure of two H_{203} & H_{104} cavities (b) Frequency response of the non-optimized structure

Fig. 4.3.8: The combination of two H_{203} & H_{104} cavities: $\varepsilon_r = 9.9$; cav_1 = cav_2 = 313 mil x 209 mil; apert_1 = apert_3: 14.7 mil x 56 mil, apert_2 = 54.6 mil x 56 mil; offset_1 = offset_2 = offset_3 = 40 mil; port: 107 mm, h=10 mil

4.3.4 Tuning Properties of the H_{203} & H_{104} cavity

Detailed investigation of the H_{203} & H_{104} cavity was carried out in a full-wave electromagnetic simulation (Ansoft HFSS) environment. An aluminum ceramic substrate of permittivity 9.9 and of thickness h=10 mil was employed. The filtering structure consists of three parts: 1. resonant cavity; 2. coupling apertures; and 3. waveguide input/output port. Transitions were added to the filtering structure, as shown in Fig. 4.3.9. The numerical results in Fig. 4.3.10, 4.3.11, 4.3.12 and 4.3.13 were obtained from this SIW single cavity filtering structure. In step (d) of the described tuning properties below, when the waveguide input/output port width changes, the structural parameters of the transitions change accordingly. The origin point of the axis is set at the center of the broad wall of the cavity end, as shown in Fig. 4.3.9. Offset refers to the distance of the aperture center to this axis origin in the y direction.

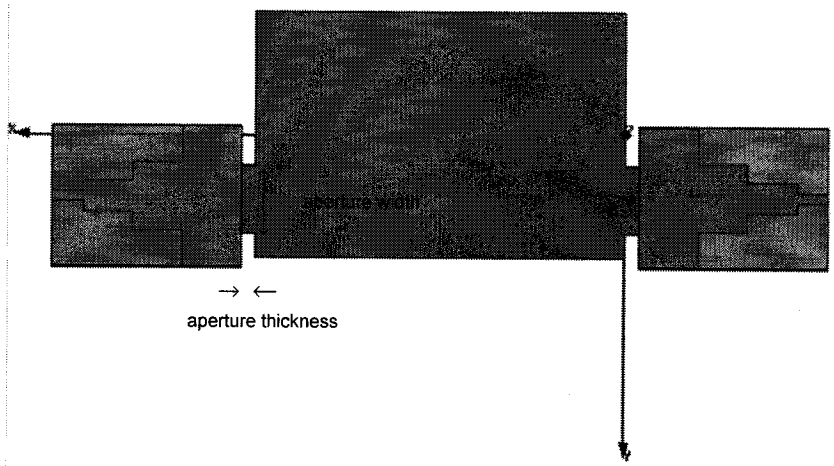

Top view of the single cavity filtering structure

Fig. 4.3.9: Structure of simulated cavity with transitions.

(a) Cavity Size: The resonant center frequency varies with the cavity sizes. When the length and width of the cavity is properly adjusted, the dual mode resonance can be maintained. This is confirmed by the results of simulating on three H_{203} & H_{104} cavities of different sizes. The results are shown in Fig. 4.3.10. The ratio of cavity length to width is $l/a \approx 1.53$; that is the key to maintain dual mode response. It can be seen that the resonance center frequency shifts to a higher frequency (case (c) in Fig. 4.3.10) when the cavity sizes are reduced, and to a lower frequency (case (a) in Fig. 4.3.10) when the cavity sizes are enlarged in size according to the ratio.

(b) Aperture Thickness: In the aperture, the wave is evanescent (cutoff) which means the wave field decays in the aperture after being injected from the input port. The thicker the aperture, the more the wave decays. Hence, the coupling becomes weak when the aperture thickness is increased. When both the aperture width (w=57 mil) and offset (offset= 41.75 mil) is fixed, the single cavity frequency response of aperture thicknesses t = 11, 12, 13 mil are shown in Fig. 4.3.11. It is seen that the two resonant poles can be set apart more when the coupling becomes weak with increasing aperture thickness. This may supply a mechanism to adjust the bandwidth of the resonant cavity.

(c) Aperture Width: The frequency response of a single H_{203} & H_{104} cavity is sensitive to the influence of the aperture width. Keeping both the aperture thickness (t=12 mil) and aperture offset (= 41.75 mil) fixed, the responses for aperture widths of 56, 57, and 58 mil are shown in Fig. 4.3.12. The two poles separate more when the aperture width increases, thus producing an effective mechanism to control the band-width. In other words, the resonant quality factor

Q increases with the decrease of the aperture width. The phenomena that the resonant poles' separation increases with increased aperture width supply an effective way to control the quality factor Q and the band-width of such single H_{203} & H_{104} cavities. A slight frequency down shift is observed with increasing aperture width. By comparison with the closed ideal cavity, this is due to the presence of the aperture results in the increase of the effective length of the cavity. The wider the apertures are the more the effective length of the cavity is added.

(d) Input/Output Waveguide: Wider input/output waveguide port changes the resonant pole also. This supplies a mechanism to change the band-width and Q. However, the trend of the change is in the opposite direction of that when changing the aperture width. Some optimized dimensions must exist when both the aperture width and port width are changing. The optimized band-width and Q for such single cavity.

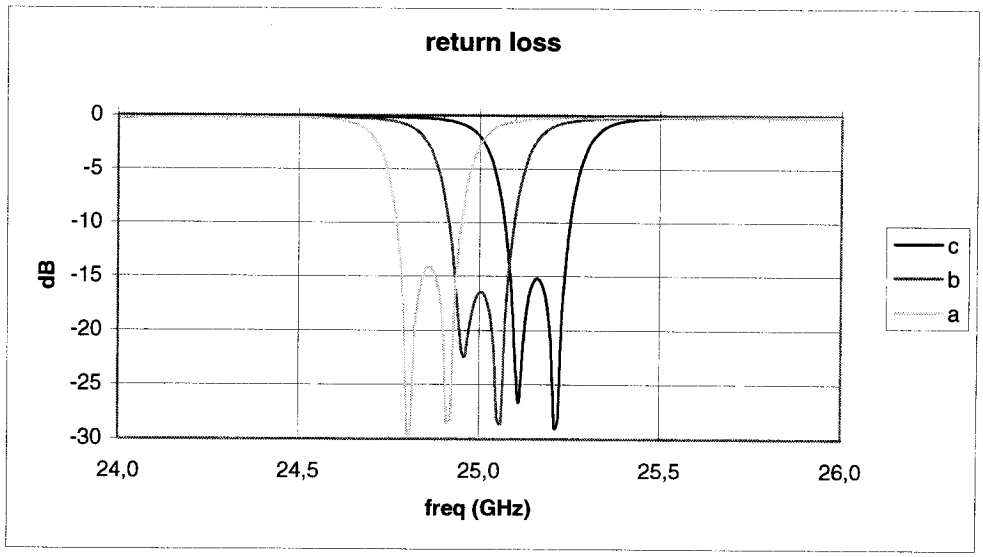

Fig. 4.3.10: Return loss versus cavity sizes $l \times a$ in mil. $\varepsilon_r = 9.9$, $h = 10mil$.

Cavity sizes: (a) 315 x 210 (b) 313 x 208.7 (c) 311 x 207.4. The same aperture size, 57 mil x 12 mil, is used. Aperture offset = 41.75 mil

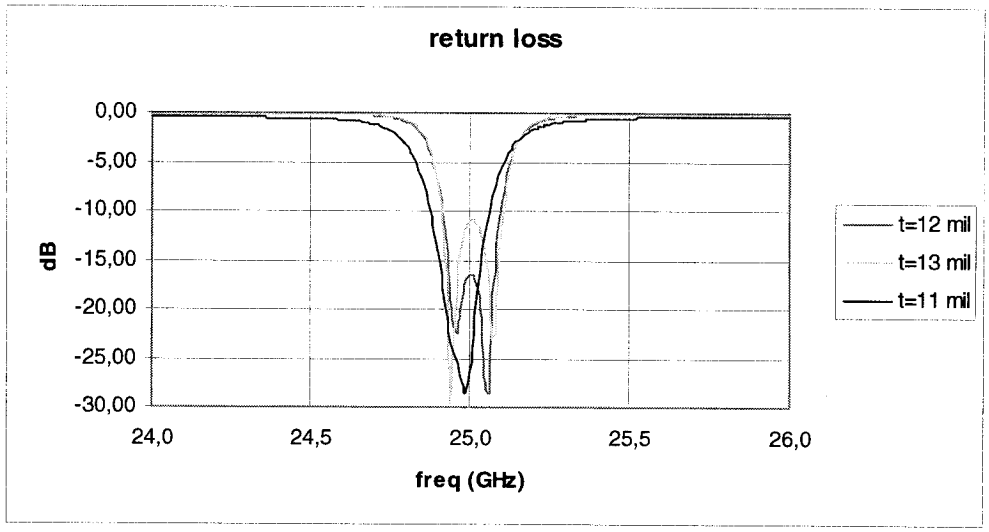

Fig. 4.3.11: Return loss versus aperture thickness t.

Cavity=$l \times a$=313 mil x 208.7 mil; apert_1 = apert_2 = 57mil x t mil, offset= 41.75 mil; port = 140 mil, h =10 mil

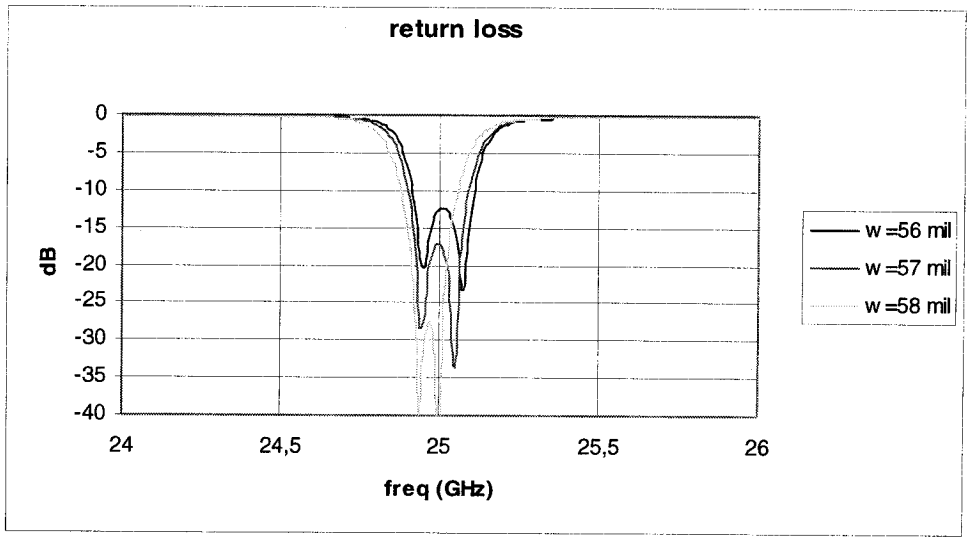

Fig. 4.3.12: Return loss versus aperture width w

Cavity=$l \times a$=313 mil x 208.7 mil; apert_1 = apert_2 = w x 12 mil,

offset= 41.75 mil; port = 140 mil, h =10 mil

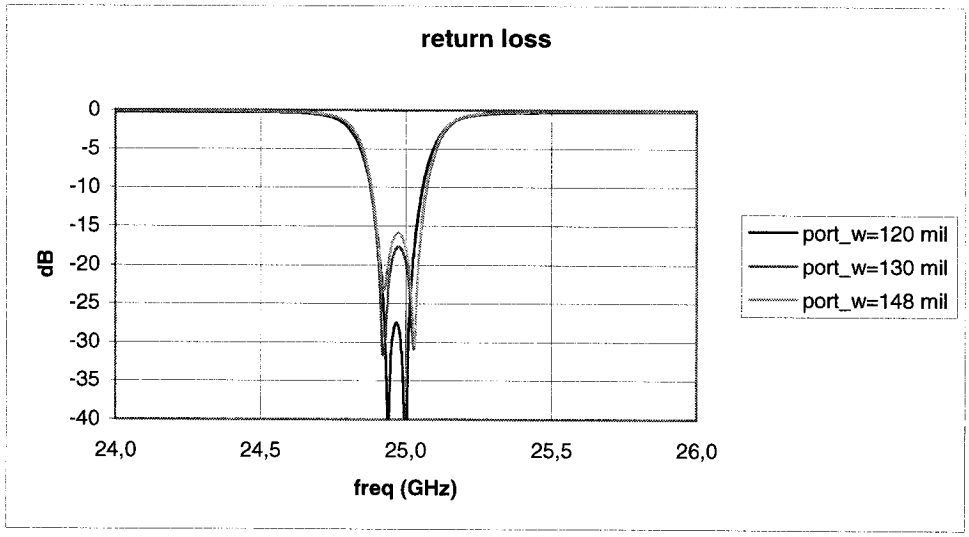

Fig. 4.3.13: Return loss versus waveguide input/output port width.

Cavity=$l \times a$=313 mil x 208.9 mil; apert_1 = apert_2 = 58 x 12 mil,

offset= 41.75 mil; h =10 mil

REFERENCES

[1] S. Darlington, "Synthesis of reactance four poles which produce prescribed insertion loss characteristics," J. Math. Phys., vol. 18, pp. 257-353, Sept. 1939.

[2] G. Reiter, "Solution of field equations for strongly coupled cavity systems," in Proc. Symp. Electromagnetic Wave Theory (Selft, The Netherlands, Sept. 1965). New York: Pergamon, 1967, pp. 357-367.

[3] A. E. Atia, and A. E. Williams, "A solution of for narrow-band coupled cavities," COMSAT Tech. Memo. CL-39-70, Sept. 22, 1970.

[4] A. E. Williams, "A four-cavity elliptic waveguide filter," IEEE Trans. Micorwave Theory Tech., vol-MTT-18, pp. 1109-1114, Dec. 1970.

[5] A. E. Atia, and A. E. Williams, "New types of waveguide bandpass filters for satellite transponders, " COMSAT Tech. Rev., vol. 1 no. 1, pp. 21-43, 1971.

[6] A. E. Atia, and A. E. Williams, "Narrow-Bandpass waveguide filters," IEEE Trans. Micorwave Theory Tech., vol-MTT-20, pp. 258-265, April, 1972.

[7] A. E. Atia, and A. E. Williams, "Nonminimum-phase optimum-amplitude band-pass waveguide filters," IEEE Trans. Micorwave Theory Tech., vol-MTT-22, pp. 425-431, April, 1974.

[8] A. E. Atia, and A. E. Williams, "Narrow-Band multiple-coupled cavity synthesis," IEEE Trans. Circuit Syst., vol-CAS-21, pp. 649-655, Sept., 1974.

[9] A. E. Atia, and A. E. Williams, "Dual-mode canonical waveguide filters," IEEE Trans. Micorwave Theory Tech., vol-MTT-25, pp. 1021-1026, December, 1977.

[10] S. Cohn, "Determination of aperture parameters by electronic tank measurements," Proc. IRE, vol. 39, pp.1416-1421, Nov. 1951.

[11] S.Cohn, "Microwave coupling by large apertures," Proc. IRE, vol. 40, pp.696-699, June 1952.

[12] G. L. Matthaei, L. Young, and E. M. T. Jones, Microwave filters, impedance

matching networks and coupling structures. New York: McGraw-Hill, 1964, ch. 8.

[13] R. M. Kurzrok, "General three-resonator filters in waveguide," IEEE Trans. Micorwave Theory Tech., MTT-14, pp.46-47, January. 1966.

[14] R. M. Kurzrok, "General four-resonator filters at microwave frequencies," IEEE Trans. Micorwave Theory Tech., MTT-12, PP-295-296, June 1966.

[15] J. D. Rhodes, "The generalized direct-coupled cavity linear-phase filter," IEEE Trans. Micorwave Theory Tech., vol- MTT-24, pp. 308-313, June. 1970.

[16] A. Morini, G. Venanzoni, and N. Iliev, "Aprototype for the design of planar waveguide filters, also containing transimission zeros, with close correspondence to the physical structure," Microwave Symposium Digest, 2004 IEEE MTT-S International, Volume 2, 6-11 June 2004 Page(s):467 - 470

[17] E. Ofli, R. Valdieck, and S. Amari, "Novel E-plane filters and diplexers with elliptic response for millimeter-wave applications," IEEE Trans. Micorwave Theory Tech., vol- MTT-53, pp. 843-851, March. 2005.

[18] G. Matthaei, L. Young, E. M. T. Jones, Microwave filters, impedance matching network, and coupling structures, New York, McGraw-Hill, 1964.

[19] M. Guglielmi, P. Jarry, E. Kerherve, O. Roquebrun, and D. Schmitt, "A new family of all-inductive dual-mode filters," IEEE Trans. Microwave Theory Tech., vol-MTT-49, pp. 1764-1769, Oct. 2001.

[20] R. E. Collin, Foundations for Microwave Engineering. IEEE Press. New York, 1992

[21] F. D. Paolo, Network and devices using planar transmission lines, CRC Press, 2000

[22] Product Note 8510-8A, "Applying the HP 8510 TRL calibration for non-coaxial measurement," Agilent.

Chapter 5 Dual Mode SIW Filters Based on H_{203} & H_{104} Resonance

5.1 Filter Employing Dual Mode Resonance of H_{203} & H_{104}

Based on the full-wave EM simulations and the tuning properties of the H_{203} & H_{104} cavities, filter configurations with two cavities and three cavities were constructed. The two cavity structure and the three cavity structure supply two TZs and four TZs respectively, since the filters are geometrically symmetric with a symmetrical aperture offset.

5.1.1 Field Polarization, Coupling and Realization of TZs

Suppose the longitudinal magnetic field amplitude of the forward H_{20} wave in the cavity is A_{20}^{+} and that of the backward H_{20} wave is A_{20}^{-}. The resulting field in the cavity consists of the superposition of the forward and backward wave. Using the boundary conditions at $z=0$ and $z=l$, when the forward wave is fully reflected, i.e. $A_{20}^{-}=-A_{20}^{+}$, the fields for the H_{203} mode may be expressed as follows [20]:

$$\begin{aligned} E_y &= \frac{-A_{20}^{+}k_{203}Z_0 a}{\pi}\sin\frac{2\pi x}{a}\sin\frac{3\pi z}{l} \\ H_x &= j\frac{3A_{20}^{+}a}{l}\sin\frac{2\pi x}{a}\cos\frac{3\pi z}{l} \\ H_z &= -2jA_{20}^{+}\cos\frac{2\pi x}{a}\sin\frac{3\pi z}{l} \\ E_x &= E_z = H_y = 0 \end{aligned} \tag{5.1.1}$$

where $k_{203}=[(\frac{2\pi}{a})^2+(\frac{3\pi}{l})^2]^{1/2}=[(\frac{2\pi}{a})^2+\beta_{20}^2]^{1/2}$, and $Z_0=\sqrt{\frac{\mu}{\varepsilon}}=\sqrt{\frac{\mu_0}{\varepsilon_0}}/\sqrt{\varepsilon_r}$.

Suppose the longitudinal magnetic field amplitude of the forward H_{10} wave in the cavity is A_{10}^{+} and that of the backward H_{10} wave is A_{10}^{-}. In the same way, the fields for the H_{104} mode may be expressed as follows:

$$\begin{aligned} E_y &= \frac{-2jA_{10}^{+}k_{104}Z_0 a}{\pi}\sin\frac{\pi x}{a}\sin\frac{4\pi z}{l} \\ H_x &= \frac{2jA_{10}^{+}a}{l}\sin\frac{\pi x}{a}\cos\frac{4\pi z}{l} \\ H_z &= -2jA_{10}^{+}\cos\frac{\pi x}{a}\sin\frac{4\pi z}{l} \\ E_x &= E_z = H_y = 0 \end{aligned} \tag{5.1.2}$$

where $k_{104} = [(\frac{\pi}{a})^2 + (\frac{4\pi}{l})^2]^{1/2} = [(\frac{\pi}{a})^2 + \beta_{10}^2]^{1/2}$, and $Z_0 = \sqrt{\frac{\mu}{\varepsilon}} = \sqrt{\frac{\mu_0}{\varepsilon_0}} / \sqrt{\varepsilon_r}$.

The phase wavelengths for the H_{203} and H_{104} modes are:

$$\lambda_{g,20} = \frac{\lambda}{\sqrt{1-(\frac{\lambda}{a})^2}}$$

$$\lambda_{g,10} = \frac{\lambda}{\sqrt{1-(\frac{\lambda}{2a})^2}}$$

respectively.

When an incident H_{10} wave is at the input and is injected through the first aperture on the left, the H_{203} mode is excited in the cavity due to the offset of the aperture, thus producing coupling M_{S1} between the source and the first resonant mode (mode 1). The H_{104} mode is also excited through the very offset aperture, producing very weak coupling M_{S2} between the source and the H_{104} mode. However, because of the dual mode property of the cavity, the excitation of H_{104} mode (mode 2) is mainly produced by coupling with the H_{203} mode in the cavity, and the relation $M_{S1} \square M_{S2}$ and $M_{12} \square M_{S2}$

hold. The polarization directions of the electric fields for the H_{203} mode and the H_{104} mode in the cavity are indicated in Fig. 5.1.1(a) and (b), respectively.

Energy is mainly coupled in mode H_{203} from cavity 1 to cavity 2 through the very offset aperture between the two cavities, thus producing M_{13} . The H_{104} mode is excited by coupling with the H_{203} mode in cavity 2, producing M_{34}. The electric field phase of the H_{104} mode near the middle coupling aperture in cavity 2 is of opposite sign with reference to the phase of the H_{203} mode near the aperture in cavity 1. The coupling between these two modes, i.e. mode 1 (H_{203}) and mode 4 (H_{104}), produces $M_{14} < 0$. Similarly, the phase reversal between mode H_{203} in cavity 2 and mode H_{104} in cavity 1 supplies the second negative coupling $M_{23} < 0$. These two negative couplings supply two TZs in the stop-band. The coupling scheme of the two cavity configuration is demonstrated in Fig. 5.1.1.

For a three cavity structure with serious offset aperture connecting cavity 3 to cavity 2, mode 5 (H_{203}) in cavity 3 couples with mode 4 (H_{104}) in cavity 2, producing $M_{45} \prec 0$, and mode 6 (H_{104}) in cavity 3 couples with mode 3 (H_{203}) in cavity 2, producing $M_{36} \prec 0$. Hence, there are four negative couplings available for such a structure and four TZs can be supplied. The field polarization directions and the coupling scheme are demonstrated in Fig. 5.1.2.

(a) Electric field directions of H_{203} mode (b) Electric field directions of H_{104} mode

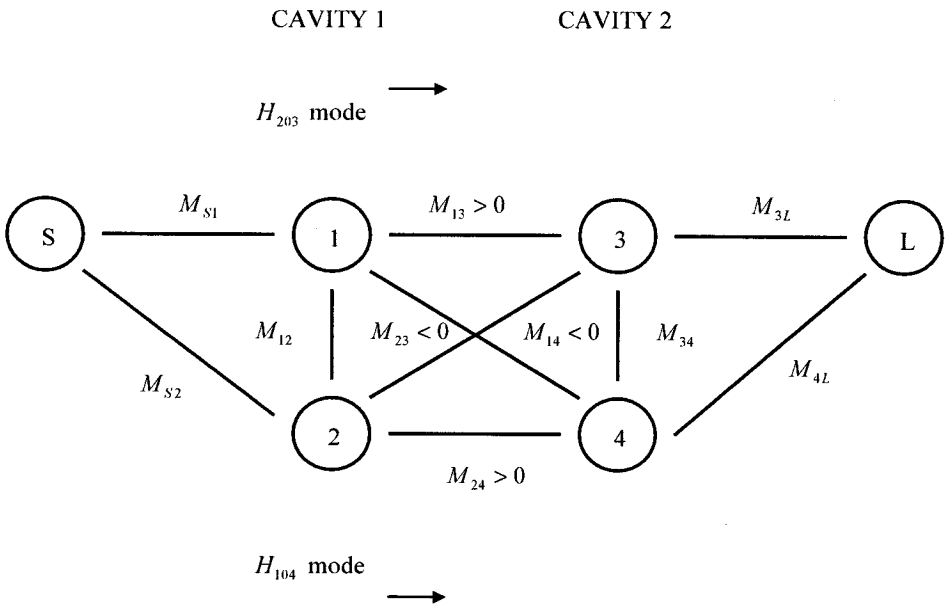

(c) Coupling and routing scheme of the two cavity structure

Fig. 5.1.1: Coupling scenario of filter with two cavities

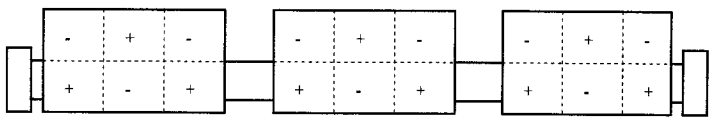

(a) Electric field directions of H_{203} mode in three cavity configuration

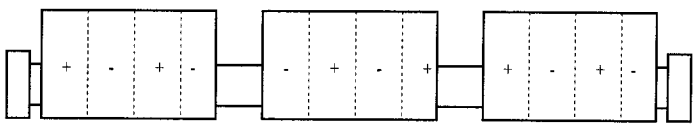

(b) Electric field directions of H_{104} mode in three cavity configuration

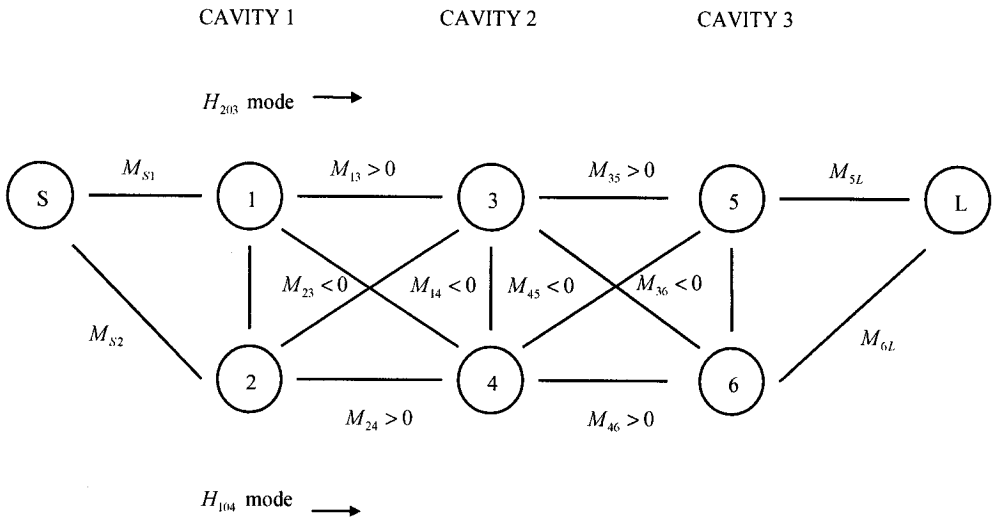

(c) Coupling and routing scheme of the three cavity structure

Fig. 5.1.2: Coupling scenario of filter with three cavities

5.1.2 Symmetrical Coupling Four-pole, Two-TZ Filter Design

According to (4.3.3) and (4.3.4), the length and width for an ideal closed H_{203} & H_{104} dual mode cavity integrated on RT/Duroid 6002, resonating at 24 GHz is $l = 614mil,\ a = 402mil$. Seeing as how the presence of two wide apertures at the ends of the cavities increase the effective length, the actually cavity length will be smaller than the above value of 614 mil, and the cavity width will be adjusted accordingly so as to maintain dual mode resonance in the cavity.

After cascading two cavities as shown in Fig. 4.3.8, the structural parameters were optimized in the Mician u-wave Wizard environment.

For a two cavity filter, the coupling coefficients are symmetrical.

$M_{3L} = M_{S1}$

$M_{4L} = M_{S2}$

$M_{34} = M_{12}$

$M_{23} = M_{14} < 0$

The geometrical parameters are symmetrical about the central line (x=219.09/2 mil in Fig.5.1.3(a)) across the middle aperture. The optimization yields the results listed in TABLE 5.1.1.

Table 5.1.1 Optimization results for a two-cavity filter on 20 mil thick RT/duroid 6002

Cav_l1	581.67	Apert_l1	43.15	Offset_apert1	59.12	WG-w	277.61
Cav_l2	581.67	Apert_l2	219.09	Offset_apert2	79.49	---	---
Cav_w1	377.21	Apert_l3	43.15	Offset_apert3	59.12	---	---
Cav_w2	377.21	Apert_w1	159.83	---	---	---	---
---	---	Apert_w2	143.17	---	---	---	---
---	---	Apert_w3	159.83	---	---	---	---

Note: unit in mil

In a u-wave environment, the four poles in the pass-band were clearly presented when the structure was optimized. The top view drawing is indicated in Fig. 5.1.3(a). The offset values listed above refer to the offset of the apertures away from the center point of the cavity. Now the y axis origin is put at the middle point of the middle aperture in Fig.5.1.3(a) and a coordinate shift in the y direction was added when this drawing was initiated. The shift distance y is 79.49 mil. All the offset values were updated with respect to this new origin in HFSS. The three rectangular apertures are drawn in heavy lines. The frequency response and the time delay of a filter integrated on 20 mil thick RT/duroid 6002 are demonstrated in Fig. 5.1.3(b), (c) and (d), respectively.

The frequency response of a two cavity filter on a 20 mil thick RT/duroid 6002 exhibits a pseudo-elliptic function response. The insertion loss at the center frequency is less than 1.7 dB and increases slightly to 2.3 dB at the pass-band edges, which are

$f_1 = 23.7GHz$ and $f_2 = 24.3GHz$, with a band-width of about 600 MHz. The time delay is approximately 62 ns at the center frequency and 80 ns at the pass-band edge.

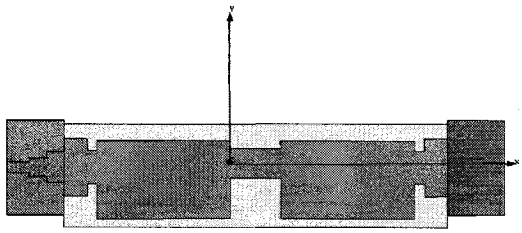

(a)Top view of the structure on 20 mil thick RT/duroid 6002

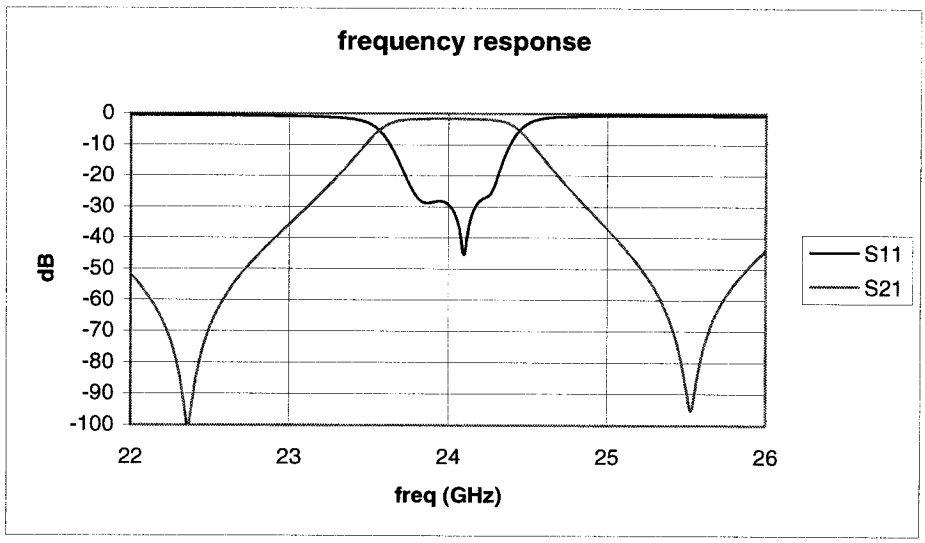

(b) Frequency response

Fig. 5.1.3: Simulation results of a four-pole, two TZ filter on 20 mil thick RT/duroid 6002

5.1.3 Symmetrical Coupling Six-Pole, Four-TZ Filter Design

For a three cavity filter,

$M_{5L} = M_{S1}$

$M_{6L} = M_{S2}$

$M_{56} = M_{12}$

$M_{45} = M_{14}$

$M_{36} = M_{23}$

$M_{14} = M_{45} < 0$

$M_{23} = M_{36} < 0$

These parameters are required for the integration of the designed filter on Rogers RT/duroid 6002 (ε_r = 2.94) laminate microwave material.

Because of the coupling symmetry, the geometrical parameters are symmetrical about the center line (x=580.97/2 mil across the middle cavity, as shown in Fig.5.1.4(a)). Optimization in the u-wave Wizard produces the results listed in Table 5.1.2.

Table 5.1.2 Optimization results for a three-cavity filter on 30 mil thick RT/duroid 6002

Cav_l1	582.21	Apert_l1	25.62	Offset_apert1	49.29	WG_w	285
Cav_l2	580.97	Apert_l2	192.67	Offset_apert2	72.47	---	---
Cav_l3	582.21	Apert_l3	192.67	Offset_apert3	72.47	---	---
Cav_w1	375.83	Apert_l4	25.62	Offset_apert4	49.29	-----	---
Cav_w2	376.58	Apert_w1	169.93	---	---	---	---
Cav_w3	375.83	Apert_w2	144.68	---	---	---	---
---	---	Apert_w3	144.68	---	---	---	---
---	---	Apert_w4	169.93	---	---	---	---

Note: unit in mil

In the u-wave environment, all six poles in the pass-band are clearly present. The top view drawing is illustrated in Fig. 5.1.4(a). The offset values listed above refer to the offset of the apertures away from the center point of the cavity width, also in the u-wave environment. Now the y axis origin is put at the central point of the middle aperture in Fig.5.1.4(a) and a coordinate shift in the y direction was added when this drawing was initiated. The shift distance y is 72.47 mil. All the offset values were updated with respect to this new origin. The four rectangular apertures are drawn in heavy lines. Frequency response and time delay are indicated in Fig. 5.1.4(b), (c) and (d), respectively.

The frequency response of such a three cavity filter is that of a pseudo-elliptic function. Two reasons cause an increase in the selectivity factor compared to that of the two cavity one. First, the band-width increases due to the additional cavity. Second, the presence of two additional TZs, which are closer to the pass-band, increases the selectivity.

The insertion loss at the center frequency is less than 2.2 dB and it increases to 3.2 dB at the pass-band edges, which are $f_1 = 23.6GHz$ and $f_2 = 24.4GHz$, with a band-width of about 800 MHz. The time delay is about 70 ns at the center frequency and 88 ns at the pass-band edge.

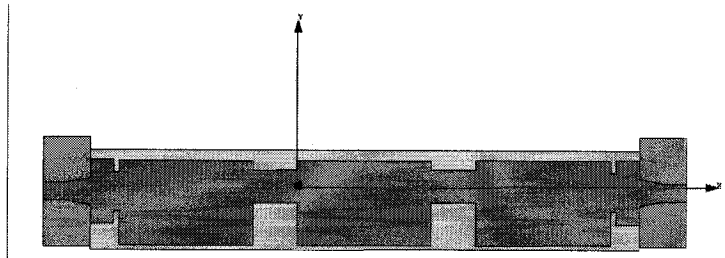

(a) Drawing of the simulated structure for 30 mil thick RT/duroid 6002

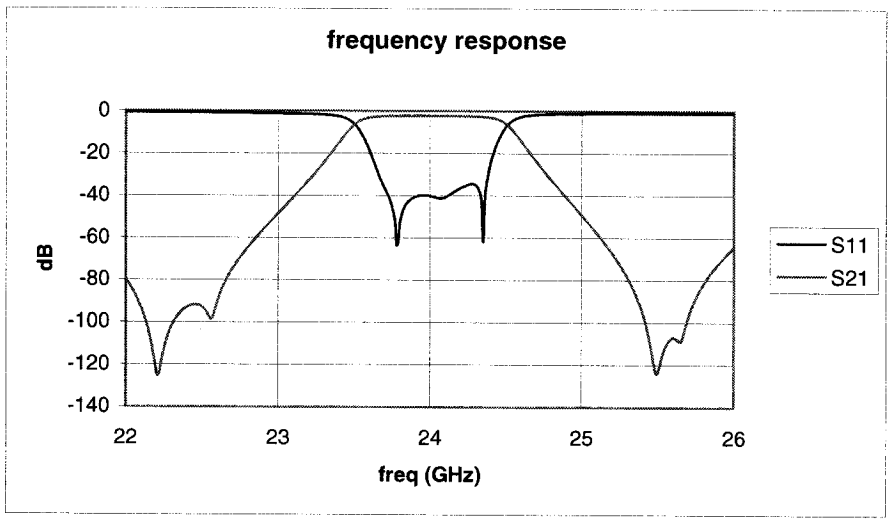

(b) Frequency response

Fig. 5.1.4: Simulation results of a six-pole, four TZ filter on 30 mil thick RT/duroid 6002 substrate

A set of parameters are obtained for the fabrication of a 3-cavity filter on TMM3 (ε_r = 3.27) laminate microwave material. These are listed in Table 5.1.3.

Table 5.1.3 Optimization results for a three-cavity filter on 20 mil thick TMM3

Cav_l1	548.9	Apert_l1	25.7	Offset_apert1	25.15	WG_w	268.8
Cav_l2	547.9	Apert_l2	173.7	Offset_apert2	63.85	---	---
Cav_l3	548.9	Apert_l3	173.7	Offset_apert3	63.85	---	---
Cav_w1	356.5	Apert_l4	25.7	Offset_apert4	25.15	----	----
Cav_w2	357.1	Apert_w1	167.3	---	---	---	---
Cav_w3	356.5	Apert_w2	139.6	---	---	---	---
---	---	Apert_w3	139.6	----	---	---	---
---	---	Apert_w4	167.3	---	---	---	---

Note: unit in mil

Fig. 5.1.5 demonstrates the simulation results in Ansoft HFSS, where a quarter wavelength transition was employed. The insertion loss at the central frequency is 2.44 dB and increases to 3.1 dB at the pass-band edges of $f_1 = 23.6GHz$ and $f_2 = 24.4GHz$. In the simulation model, only the top and bottom surfaces were set as finite conductivity walls. Hence, simulated results closer to the values for the true insertion loss are expected and can be obtained by an improved and sophisticated simulation model. The value obtained is a slighter over 2.44.

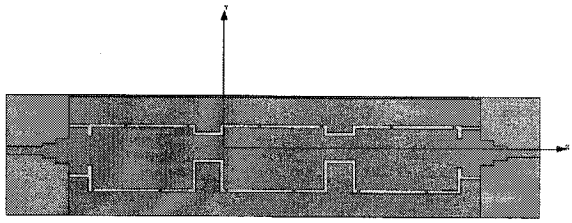

(a) The simulated structure on 20 mil Rogers TMM3 (slots were made on the substrate, as on the fabricated filter chip)

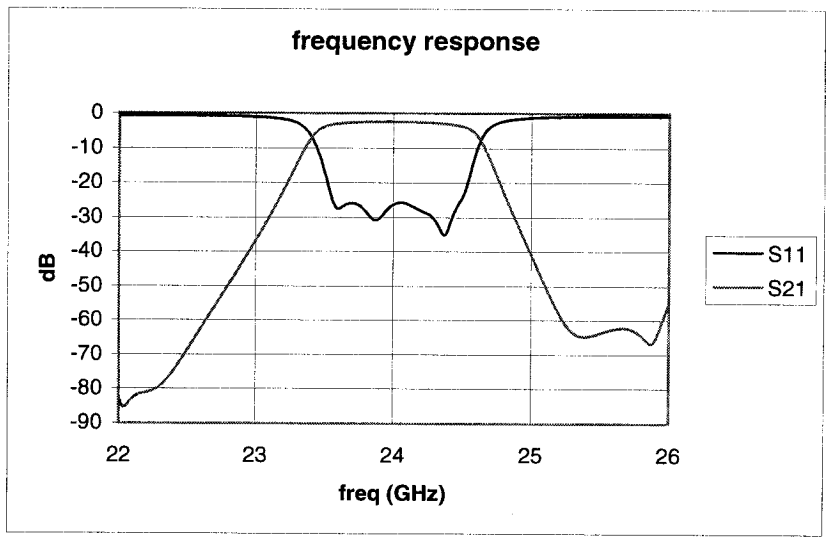

(b) Frequency response

Fig. 5.1.5: Simulation results of the six-pole, four TZ filter on 20 mil thick TMM3

5.2 Measurement of the filter integrated on 20 mil thick TMM3 substrate

The filter described in Fig. 5.1.5 was fabricated and tested.

Since the extension micro-strip line (w=47.8mil, h=20 mil) at each port is 197 mil, the TRL calibration was used for the test of the filter.

5.2.1 Defining TRL calibration standards

The measurement was carried out from $f_1 = 20GHz$ to $f_2 = 28GHz$. The frequency span is $f_2 / f_1 = 1.4:1$, which is less than 8:1. One set of TRL Cal standards is able to meet the test requirements. The reference plane was set at the quarter wavelength end connecting with the extended micro-strip. Thus, the length of THRU is:

$l_{Thru} = 2 \times 197mil = 394mil = 10.00mm$.

The effective relative permittivity of the micro-strip is [21]:

$$\varepsilon_{r,eff} = \frac{\varepsilon_r + 1}{2} + \frac{\varepsilon_r - 1}{2\sqrt{1 + \frac{12h}{w}}} \qquad (\text{w/h} > 1)$$

Taking into account the numeric values of w, h and ε_r into the above, the value of $\varepsilon_{r,eff} = 2.60$ can be obtained.

The electrical length of the phase difference between the LINE and the THRU is given by:

$$Electrical \quad Length \quad l = \frac{15}{[f_1(GHz) + f_2(GHz)]\sqrt{\varepsilon_{r,eff}}}$$

$$= \frac{0.313}{\sqrt{\varepsilon_{r,eff}}} cm = 2.0mm$$

and

$$Phase(\deg ree) = 12 \times f(GHz) \times l(cm) \times \sqrt{\varepsilon_{r,eff}}$$
$$= \begin{cases} 75^\circ & at \quad 20 \quad GHz \\ 125^\circ & at \quad 28 \quad GHz \end{cases}$$

which is in the phase range between 20 and 160 degrees required by the calibration.

Therefore, the length of the LINE is:

$$l_{Line} = 10.00 + 2.00 = 12.00mm$$
$$= 472mil$$

Both the THRU and LINE are 50 Ohm micro-strip lines fabricated on TMM3.

An open circuit acted as the REFLECT when the calibration was carried out [16].

5.2.2 Measurements

The filter was measured for a frequency band ranging from 20 to 28 GHz. The results are shown in Fig. 5.2.1.

The pass-band has a bandwidth of 760 MHz, ranging from $f_1 = 23.2GHz$ to $f_2 = 23.96GHz$. At the pass-band edge, the insertion is 5.3 dB and at the central frequency $f_0 = 23.58GHz$ the value of the insertion loss is 4.58 dB. For the entire pass-band, the return loss is better than 20 dB.

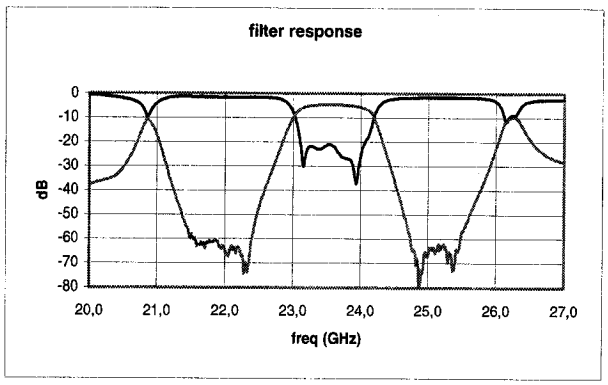

(a) The measured filter response

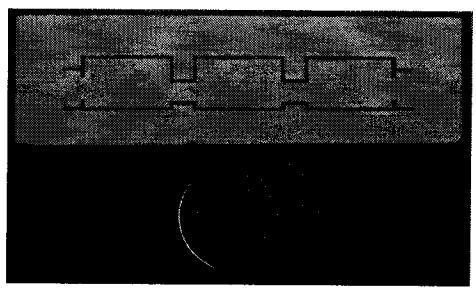

(b)The measured filter

Fig. 5.2.1: Measurement of the 3-cavity dual mode filter on 20 mil thick TMM3

The frequency shift is due to the permittivity error introduced by the Rogers TMM3 laminate material. The virtual value of relative permittivity is approximately 3.38. The simulated results with this updated dielectric constant and the measured results are demonstrated in Fig. 5.2.2. Due to the error induced by the permittivity, not all the four TZs can be presented in the test results of the fabricated filter.

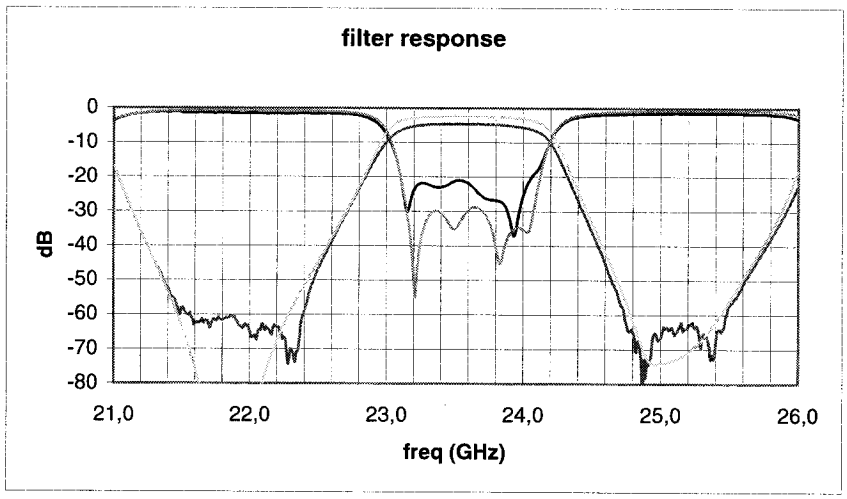

Fig. 5.2.2: Comparison between measured and simulated results

5.3 Conclusion

Using a full-wave electromagnetic simulation and optimization tool, SIW filters were designed and fabricated based on rectangular waveguide dual mode resonance. On a 20 mil thick Rogers TMM3 laminate microwave material, one 3-cavity filter of 6-poles and 4-TZs was fabricated and tested. The pass-band insertion loss reached 4.58 dB at the center frequency and 5.3 dB at the pass-band edges while the return loss was better than 20 dB over the entire band. The rejection loss at the lower frequency of 22 GHz in the stop band is -65 dB, which is 20 dB greater than the simulated value. The rejection loss at 25 GHz in the upper stop-band is -65 dB. The simulations on the design prototype show a symmetrical frequency response. Both the simulation and the measured results prove that the decrease of the rejection in the upper stop band is due to the cutting slot on the dielectric substrate. The test results agree well with the design theory.

REFERENCES

[1] S. Darlington, "Synthesis of reactance four poles which produce prescribed insertion loss characteristics," J. Math. Phys., vol. 18, pp. 257-353, Sept. 1939.

[2] G. Reiter, "Solution of field equations for strongly coupled cavity systems," in Proc. Symp. Electromagnetic Wave Theory (Selft, The Netherlands, Sept. 1965). New York: Pergamon, 1967, pp. 357-367.

[3] A. E. Atia, and A. E. Williams, "A solution of for narrow-band coupled cavities," COMSAT Tech. Memo. CL-39-70, Sept. 22, 1970.

[4] A. E. Williams, "A four-cavity elliptic waveguide filter," IEEE Trans. Microwave Theory Tech., vol-MTT-18, pp. 1109-1114, Dec. 1970.

[5] A. E. Atia, and A. E. Williams, "New types of waveguide bandpass filters for satellite transponders, " COMSAT Tech. Rev., vol. 1 no. 1, pp. 21-43, 1971.

[6] A. E. Atia, and A. E. Williams, "Narrow-Bandpass waveguide filters," IEEE Trans. Micorwave Theory Tech., vol-MTT-20, pp. 258-265, April, 1972.

[7] A. E. Atia, and A. E. Williams, "Nonminimum-phase optimum-amplitude band-pass waveguide filters," IEEE Trans. Microwave Theory Tech., vol-MTT-22, pp. 425-431, April, 1974.

[8] A. E. Atia, and A. E. Williams, "Narrow-Band multiple-coupled cavity synthesis," IEEE Trans. Circuit Syst., vol-CAS-21, pp. 649-655, Sept., 1974.

[9] A. E. Atia, and A. E. Williams, "Dual-mode canonical waveguide filters," IEEE Trans. Microwave Theory Tech., vol-MTT-25, pp. 1021-1026, December, 1977.

[10] S. Cohn, "Determination of aperture parameters by electronic tank measurements," Proc. IRE, vol. 39, pp.1416-1421, Nov. 1951.

[11] S.Cohn, "Microwave coupling by large apertures," Proc. IRE, vol. 40, pp.696-699, June 1952.

[12] G. L. Matthaei, L. Young, and E. M. T. Jones, Microwave filters, impedance

matching networks and coupling structures. New York: McGraw-Hill, 1964, ch. 8.

[13] R. M. Kurzrok, "General three-resonator filters in waveguide," IEEE Trans. Microwave Theory Tech., MTT-14, pp.46-47, January. 1966.

[14] R. M. Kurzrok, "General four-resonator filters at microwave frequencies," IEEE Trans. Microwave Theory Tech., MTT-12, PP-295-296, June 1966.

[15] J. D. Rhodes, "The generalized direct-coupled cavity linear-phase filter," IEEE Trans. Micorwave Theory Tech., vol- MTT-24, pp. 308-313, June. 1970.

[16] A. Morini, G. Venanzoni, and N. Iliev, "Aprototype for the design of planar waveguide filters, also containing transimission zeros, with close correspondence to the physical structure," Microwave Symposium Digest, 2004 IEEE MTT-S International, Volume 2, 6-11 June 2004 Page(s):467 - 470

[17] E. Ofli, R. Valdieck, and S. Amari, "Novel E-plane filters and diplexers with elliptic response for millimeter-wave applications," IEEE Trans. Microwave Theory Tech., vol- MTT-53, pp. 843-851, March. 2005.

[18] G. Matthaei, L. Young, E. M. T. Jones, Microwave filters, impedance matching network, and coupling structures, New York, McGraw-Hill, 1964.

[19] M. Guglielmi, P. Jarry, E. Kerherve, O. Roquebrun, and D. Schmitt, "A new family of all-inductive dual-mode filters," IEEE Trans. Microwave Theory Tech., vol- MTT-49, pp. 1764-1769, Oct. 2001.

[20] R. E. Collin, Foundations for Microwave Engineering. IEEE Press. New York, 1992

[21] F. D. Paolo, Network and devices using planar transmission lines, CRC Press, 2000

[22] Product Note 8510-8A, "Applying the HP 8510 TRL calibration for non-coaxial measurement," Agilent.

CONCLUSIONS AND FUTURE WORK

In this research work, four SIW filters of different structure are presented, and two methods are demonstrated for substrate integrated waveguide filter design. Those filters are classified as direct-coupled cavity filter and dual mode cavity filter, which are integrated on Rogers RT/duroid 6002 and TMM3 laminate materials, respectively.

Influences of the dielectric properties of substrate RT/duroid 6002 and alumina on insertion loss of SIW guide are investigated. Under the same metal coating condition, loss tangent of substrate dielectric and substrate thickness play major roles in determining the SIW guide loss of a given length.

The first design method employs conventional direct-coupled cavity filter synthesis based on distributed stepped impedance low-pass prototype. Square inductive discontinuities are used as coupling parts of the filters. The K inverters are calculated from the filter synthesis procedure with Levy`s modified formula, which may be extended to intermediate bandwidth filter design. Reflection coefficient of the coupling parts are obtained from numerical analysis with Wexler Model of mode matching. Hence, the dimensions of the square coupling parts are obtained inversely. Three pieces of filters with coupling part of different shape are designed, fabricated and measured. The insertion loss of one of the 4-cavity filters realized on 10 mil RT/duroid 6002 is about 3.4 dB at the center frequency of 24 GHz while keeping the return loss in the whole passband better than 17 dB. A fabrication tolerance of 0.4 mil may ensure the required filtering

performance of the component integrated on RT/duroid 6002. The measured results are in good agreement with the simulated results in both passband and stop bands.

The second design method, based on the dual mode resonance of degenerate rectangular resonant cavity, makes use of coupling apertures to cascade these cavities together. Understanding of the general synthesis theory and also production of TZs in filters yields a basis for the filter design and development. Instead of calculation of network parameter representation of a double plane waveguide junction formed by apertures, full-wave EM simulation is used after investigating the properties of each dual mode cavity in specific mode combination. Each dual mode cavity exhibits featured frequency response under the condition of wave injection through aperture connected to input port and symmetrical aperture and output port. Dual mode combinations such as H_{102} & H_{201}, H_{102} & H_{301} and H_{203} & H_{104} which exhibit two resonant poles in passband and TZ(s) in stop band can be conveniently used for filter design. The coupling scenario of the configurations using H_{203} & H_{104} is explained in diagrams. One 3-cavity filter of 6-poles and 4-TZs based on H_{203} & H_{104} resonance is designed, fabricated and measured, which is integrated on 20 mil Rogers TMM3. The pass-band insertion loss has achieved 4.58 dB at the center frequency and 5.3 dB at the pass-band edges while the return loss was better than 20 dB over the entire band. The rejection loss at the lower frequency of 22 GHz in the stop band is -65 dB, which is 20 dB greater than the simulated value. The

rejection loss at 25 GHz in the upper stop-band is -65 dB. The test results agree well with the design theory.

Filters based on other mode combination such as H_{102} & H_{201} and H_{301} & H_{102} can be developed in the future. Designing with asymmetrical network, asymmetrical apertures can be used for producing two TZs with one dual mode cavity. This may increase the stop-band response of filters employing dual mode resonance scenario. It is easy to see that, a few waveguide filter structures, e. g. those in [10] of Chapter 3 and the folded single mode structure in [17] of Chapter 5, which have two dimensional geometrical changes in H-plane and employ H_{n0} mode (n = 1, 2, 3, ...) operation can be used in the future for SIW filter design and development.